

LA-13831-MS  
Approved for public release  
Distribution is unlimited

# 70106

*Geology of the Pajarito Fault Zone  
in the Vicinity of S-Site (TA-16),  
Los Alamos National Laboratory,  
Rio Grande Rift, New Mexico*



Received by ER-RP  
SEP 14 2001  
*[Signature]*

**Los Alamos**

NATIONAL LABORATORY

Los Alamos National Laboratory is operated by the University of California under contract W-7405-ENG-36.



3672

LA-13831-MS

Issued: July 2001

*Geology of the Pajarito Fault Zone  
in the Vicinity of S-Site (TA-16),  
Los Alamos National Laboratory,  
Rio Grande Rift, New Mexico*

*Jamie N. Gardner*

*Steven L. Reneau*

*Claudia J. Lewis*

*Alexis Lavine*

*Donathan J. Krier*

*Giday WoldeGabriel*

*George D. Guthrie*

**Los Alamos**  
NATIONAL LABORATORY

Los Alamos, New Mexico 87545

2001-07-01 10:40:00

## Table of Contents

ABSTRACT .....	1
I. INTRODUCTION .....	2
II. PREVIOUS WORK .....	3
III. METHODS AND NOTES .....	4
A. <i>A Note on Units of Measure</i> .....	4
B. <i>A Note on Terminology and Names</i> .....	4
C. <i>Study Area</i> .....	5
D. <i>High-precision Bedrock Geologic Mapping</i> .....	5
E. <i>Surficial Geologic Mapping</i> .....	5
F. <i>Geochemistry</i> .....	6
G. <i>Drilling</i> .....	6
IV. GEOLOGY .....	8
A. <i>Stratigraphy</i> .....	8
1. <i>Bedrock Units of the Bandelier Tuff and Associated Deposits</i> .....	9
a. <i>Otowi Member of the Bandelier Tuff (Qbo)</i> .....	9
b. <i>Cerro Toledo Rhyolite and Interval</i> .....	10
c. <i>Tshirege Member of the Bandelier Tuff (Qbt)</i> .....	10
2. <i>Surficial Geologic Units</i> .....	11
a. <i>Older Mesa-Top Alluvial Deposits (Qoal)</i> .....	11
b. <i>Older Alluvial Fan Deposits (Qfo)</i> .....	12
c. <i>Intermediate Alluvial Fan Deposits (Qfi)</i> .....	12
d. <i>El Cajete Pumice (Qec)</i> .....	12
e. <i>Younger Alluvial Fan Deposits (Qfy)</i> .....	12
f. <i>Landslides (Qls)</i> .....	13
g. <i>Young Alluvium Along Stream Channels (Qal)</i> .....	14
h. <i>Colluvium (Qc)</i> .....	14
i. <i>Artificial Fill</i> .....	19
B. <i>Geochemistry of Bedrock Units</i> .....	19
C. <i>Structural Geology</i> .....	24
1. <i>Pajarito Fault Zone and Probable Subsidiary Faults</i> .....	26
2. <i>Northeast Trending Structures within the Eastern Parts of the Pajarito Fault Zone</i> .....	31
3. <i>Possible Deformatoin Along Cañon de Valle</i> .....	32
V. DISCUSSION AND CONCLUSIONS .....	33
A. <i>Tshirege Member Stratigraphic Units</i> .....	33
B. <i>Structural Geology</i> .....	35
1. <i>Structural Setting of S-Site</i> .....	35
2. <i>Comparison of Structure to Previous Studies</i> .....	36
3. <i>Ages of Faulting and Related Deformatoin</i> .....	36
4. <i>Potential for Seismic Surface Rupture at WETF</i> .....	37
VI. ACKNOWLEDGEMENTS .....	37
VII. REFERENCES .....	37

45119 • 100-1010 • 13

<b>APPENDIX A: Sample Locations .....</b>	<b>41</b>
<b>APPENDIX B: Whole Rock Geochemistry .....</b>	<b>48</b>
<b>APPENDIX C: Electron Microprobe Analyses of Volcanic Glasses .....</b>	<b>58</b>
<b>APPENDIX D: Total Station Survey Data .....</b>	<b>78</b>

<b>PLATE 1: MAP OF GEOLOGIC FEATURES .....</b>	<b>Inside Rear Cover</b>
--	--------------------------

2000 2001 2002

# GEOLOGY OF THE PAJARITO FAULT ZONE IN THE VICINITY OF S-SITE (TA-16), LOS ALAMOS NATIONAL LABORATORY, RIO GRANDE RIFT, NEW MEXICO

*Jamie N. Gardner, Steven L. Reneau, Claudia J. Lewis, Alexis Lavine, Donathan J. Krier, Giday WoldeGabriel, and George D. Guthrie*

## ABSTRACT

The frequency, future likelihood, and potential consequences of large earthquakes are major topics being addressed by Los Alamos National Laboratory's Seismic Hazards Program. Of obvious interest are faults that may affect new or existing facilities, particularly those that handle hazardous materials. One such facility is the Weapons Engineering Tritium Facility (WETF) at S-Site (Technical Area-16) in the southwestern corner of the Laboratory. In this report we present data that reveal the detailed geology, geomorphology, and structure of the area in and around S-Site, and discuss the potential for seismic surface rupture specifically at WETF. Data were gathered by high-precision geologic mapping of cooling units within the Bandelier Tuff, geologic mapping of surficial, post-Bandelier Tuff units, geochemical analyses of Bandelier Tuff units for correlation purposes, and borehole drilling to investigate depths to subsurface contacts.

The Laboratory is bounded on the west by the Pajarito fault zone, an active element of the Rio Grande rift. At the southwestern corner of the Laboratory, the Pajarito fault and its subsidiary faults are prominent at the western side of S-Site around West Jemez Road (NM State Road 501). S-Site lies at the base of the main, 400-foot high escarpment formed by the Pajarito fault. From the escarpment, faulting and related deformation extend at least 5000 feet to the east. However, most of the structural deformation east of the main escarpment occurs within a zone that is about 2000 feet wide. We estimate net down-to-the-west displacement of Bandelier Tuff in this zone to be greater than 100 feet at Water Canyon and about 80 to 100 feet farther north at the latitude of the S-Site administration area. WETF lies within this zone. Based on their trends, there are four clearly definable sets of structures in the vicinity of S-Site: north striking faults and one large monocline marking the main zone of deformation of the Pajarito fault zone, defining a graben in the southwestern corner of the study area; north-northeast striking faults and fissures which bound the eastern side of the probable northward continuation of that graben; northeast striking structures, dominated by two down-to-the-west monoclines; and, an east-southeast striking fault. All structures are Quaternary in that they post-date the Tshirege Member (1.2 Ma) of the Bandelier Tuff. For most structures the only other unit that is clearly faulted or deformed is the Older Mesa-top Alluvial Deposits (Qoal), which has a large age range but is in part about 1 million years old. At some localities younger units appear to be truncated by faults, but field relations are obscured by anthropogenic disturbances and we can not confirm the presence of fault contacts. Radiocarbon dates obtained from charcoal in a fissure fill sequence of borehole WETF-2C imply that a seismic event sometime prior to 8 <sup>14</sup>C ka was necessary to open the fissure and initiate sedimentation. Additionally, the fissure fill material is also faulted indicating at least one additional, younger paleoseismic event whose age is not well constrained.

Although we have identified no specific structures that directly underlie WETF, drilling revealed faults (F3 and F4, Plate 1 in pocket, rear cover) and related fissures (fis 2 and fis 3) that appear to bound the north-west and southeast sides of the facility. Additionally, WETF is surrounded by structures that account for the greatest amount of Pajarito fault zone deformation east of the main escarpment. Thus, it appears that WETF lies within the Pajarito fault zone, albeit a part of the fault zone that is dominated by subsidiary or distributed ruptures. As such, WETF is in an area of generally higher potential for seismic surface rupture, relative to locations farther removed from the Pajarito fault zone. Probabilistic analyses of surface rupture potential at S-Site by Olig et al. (2001), however, indicate that, even in consideration of 1-in-10,000 year events, seismic surface rupture only becomes a significant hazard on the principal or main trace of the Pajarito fault.

## I. INTRODUCTION

Part of the motivation for Los Alamos National Laboratory to have a program to study and evaluate potential seismic hazards is because the Laboratory and Los Alamos County are situated in the Rio Grande rift (Figure 1). The Rio Grande rift is an active and major tectonic feature of the North American continent, and it exhibits a long history of faulting, volcanism, and seismicity (for example, Riecker, 1979; Baldrige et al., 1984; and Keller, 1986). Abundant data indicate that the rift continues to be tectonically and magmatically active (for example, Sanford et al., 1991; Baldrige et al., 1995; Wolff and Gardner, 1995; Machette et al., 1998; Steck et al., 1998). In the vicinity of Los Alamos three major faults (Figure 2) have been shown to be potentially seismogenic, and paleoseismic studies indicate that each of these faults has generated multiple prehistoric earthquakes of approximate magnitude 7 (Gardner et al., 1990; Wong et al., 1995; Kelson et al., 1996; McCalpin, 1998; 1999). The frequency and future likelihood of these large earthquakes are major topics being addressed by the Laboratory's Seismic Hazards Program.

Another part of Los Alamos National Laboratory's Seismic Hazards Program is focused on evaluation of specific areas for seismic surface rupture potential through detailed studies to identify faults and gain understanding of the area's structural geology (Gardner et al., 1998a; 1999; Krier et al., 1998a and 1998b; Olig et al., 1998).

Generally, earthquakes of magnitude greater than 6 cause rupture of the host and subsidiary faults right up to the ground surface. Although most serious damage results from ground motion in such earthquakes, facilities that are situated over the ruptured faults will, in all likelihood, sustain severe damage from surface displacements. Of obvious interest to the Laboratory are faults that may affect new or existing facilities, particularly those that handle hazardous materials and have a need for maintaining containment integrity. One such facility is the Weapons Engineering Tritium Facility (WETF)

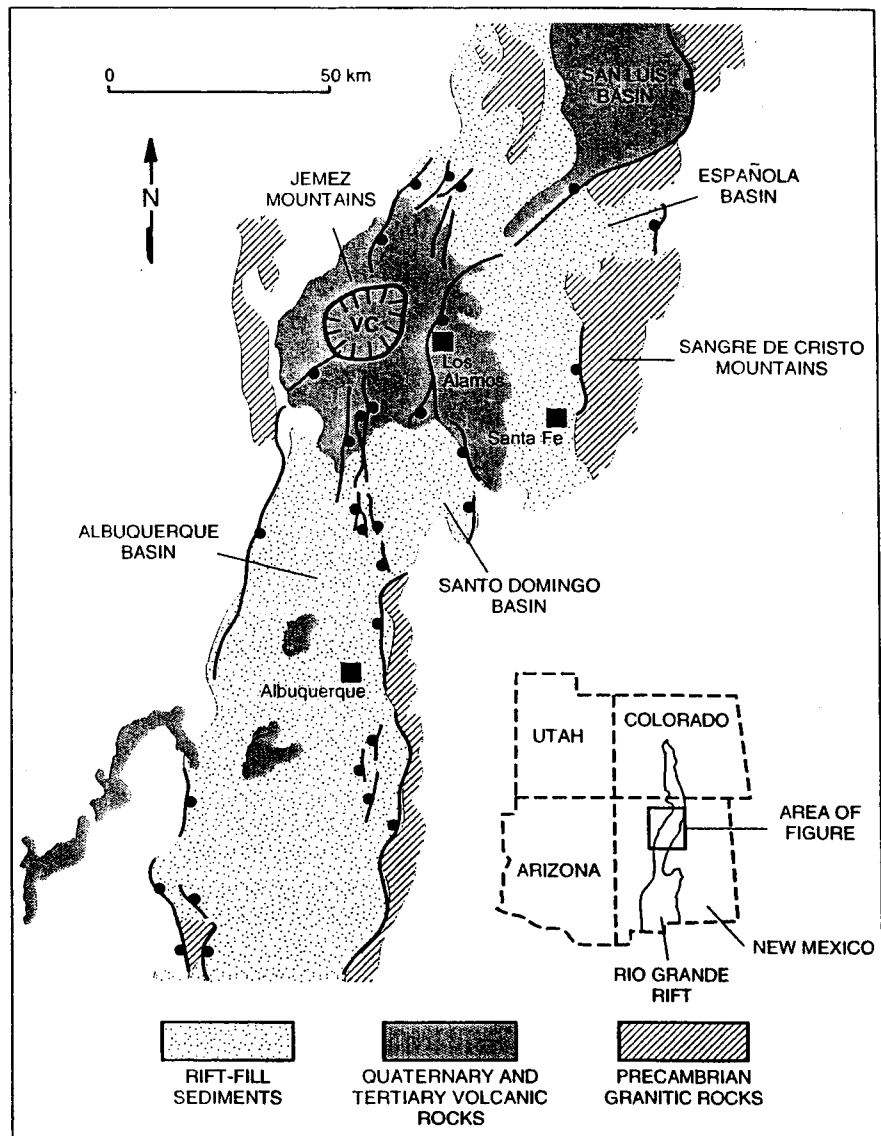


Figure 1. Map of the Rio Grande rift in northern New Mexico. Major fault systems are shown schematically (ball on downthrown side). VC is the Valles-Toledo caldera complex, the source of the Bandelier Tuff (modified from Gardner and Goff, 1984).

which is at S-Site (Technical Area 16, or TA-16) in the southwestern corner of the Laboratory (Figure 2 and Plate 1).

The Laboratory is bounded on the west by the Pajarito fault zone which is an active element of the Rio Grande rift. At the southwestern corner of the Laboratory, the Pajarito and its subsidiary faults are prominent at the western side of S-Site around West Jemez Road (also known as New Mexico 501; see Section III. B) (Figure 2 and Plate 1). WETF lies less than 2000 feet east of the 400-foot high escarpment formed by the main trace of the Pajarito fault (Plate 1). In this report we present data that reveal the detailed geology, geomorphology, and structure of the area in and around S-Site. Based on these data we discuss the potential for seismic surface rupture specifically at WETF.

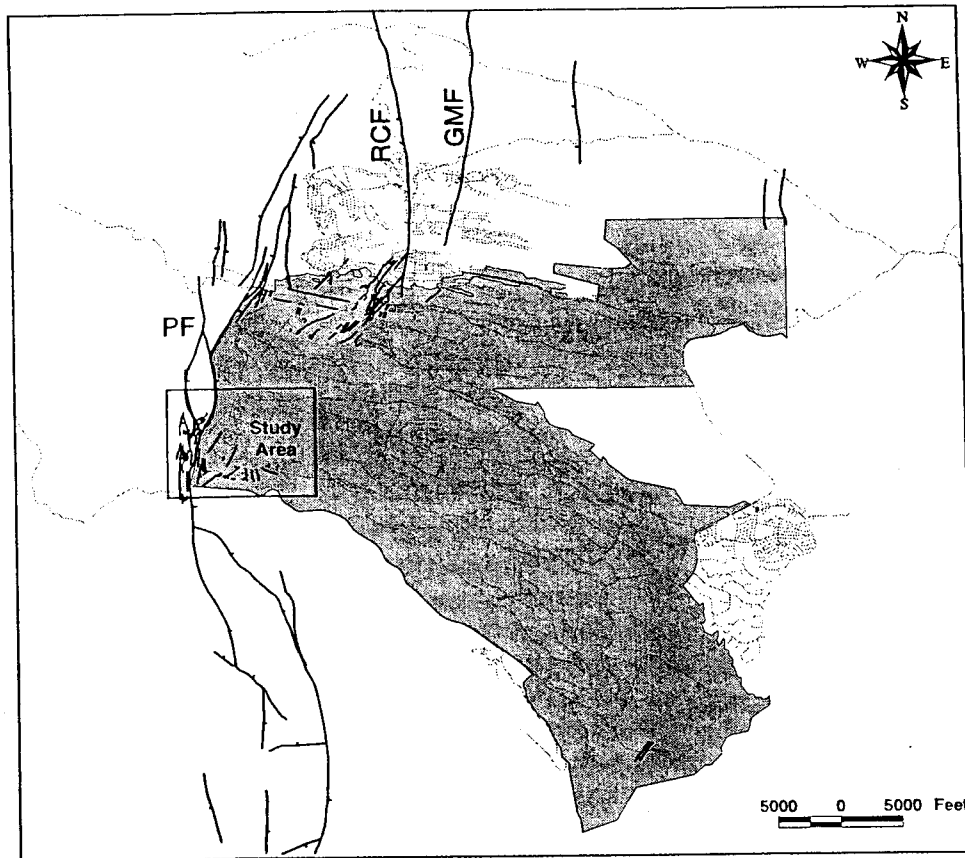


Figure 2. Map showing the study area and the main elements of the Pajarito fault system in the vicinity of Los Alamos National Laboratory. LANL is shaded gray. PF = Pajarito fault; RCF = Rendija Canyon fault; GMF = Guaje Mountain fault. Structure in the northwest portion of LANL from Gardner et al. (1999), and structure in the area between that study and this study is unmapped.

## II. PREVIOUS WORK

The area of S-Site is covered by a number of small-scale geologic maps (for example, Griggs, 1964; Smith et al., 1970; Gardner and House, 1987). The Pajarito fault zone in the vicinity of S-Site has been included in a number of studies but most of these were restricted to areas in the fault zone west of West Jemez Road. Golombek (1981) covered the Pajarito fault zone in his dissertation, but did not substantially improve the detail in the vicinity of S-Site beyond Smith et al. (1970). Wong et al. (1995) included this portion of the Pajarito fault zone in their geomorphic reconnaissance while selecting sites for paleoseismic trenching. They recognized a graben at the base of the main escarpment and speculated that it may extend as far north as Los Alamos Canyon. Wong et al. (1995) excavated at two sites (T1 and T2, Plate 1) in the Pajarito fault zone in our study area, but they failed to expose any major fault traces at either site (see also Olig et al., 1996, and Discussion and Conclusions, Section V.B.4, below). Significant advances in understanding the

nature and style of deformation in the Pajarito fault zone were provided by McCalpin (1997) with his recognition that much of the prominent portion of the Pajarito fault near S-Site is actually expressed at the surface as a large monocline. McCalpin's (1997) work, building on unpublished mapping by Reneau and Gardner, also showed that much of the main escarpment was extensively modified by mass wasting. Aspects of McCalpin (1997) and the unpublished mapping of Reneau and Gardner have been incorporated into this study and Plate 1. McCalpin (1999) excavated a paleoseismic trench (T3, Plate 1) into one strand of the Pajarito fault zone west of S-Site, beneath the hairpin curve of State Road 4 as it climbs the large escarpment. His results indicate several surface rupturing paleoearthquakes

with the most recent event likely in the Holocene, but there are large ambiguities in actual numerical age constraints (McCalpin, 1999; McCalpin, 2000). McCalpin (1999) also documented domino-style faulting in trench T3 that would appear to structurally require a down-to-the-east fault somewhere east of the trench site.

The only previous geologic mapping in the area of S-Site of sufficient detail for identification of geologic structures with respect to specific facilities was done by Rogers (1995). Rogers (1995) identified some of the major structures that we document, but for many structures we differ from Rogers (1995) in interpretation of their style of deformation and placement (see Discussion and Conclusions, Section V.B.2, below). Additionally, Rogers (1995) did not recognize many structural features that have been revealed through our use of combined high-precision bedrock and geomorphic mapping.

Budding and Purtymun (1976) show a normal fault, which they termed "the Water Canyon fault," skirting the eastern side of TA-16 and they state that

combined with topographic profiles derived from the 1:1200-scale base maps, provides geomorphic evidence for deformation in several areas. These data complement the evidence provided from bedrock mapping and, in some areas, provide information on structural deformation where bedrock data are not available.

### *III. F. Geochemistry*

Samples of Bandelier Tuff were collected for whole-rock X-ray fluorescence (XRF) analysis to further support unit identification and stratigraphic correlations (see, for example, Krier et al., 1998b; Gardner et al., 1999). In addition, because most geochemical analyses of the Bandelier Tuff have been whole rock XRF analyses, we have experimented with electron microprobe analyses of glassy pumice to determine if glass compositions can be used as a basis for correlation. Samples were taken from an outcrop depth of 2 to 4 inches to avoid obvious weathering rinds. Samples from borehole SHB-3 were collected from drill core both during the 1991 drilling and again in 1999. Samples from the WETF drill hole series were taken from the core during drilling in April, 2000. Pajarito Canyon samples were obtained in work on the Pajarito fault zone during the 1994 field season. Sample locations are shown in Appendix A.

Major and trace elements were analyzed for bulk samples using an automated Rigaku wavelength-dispersive XRF spectrometer. Samples were first crushed and homogenized in 15- to 20-gram portions in a tungsten-carbide shatterbox in accordance with Yucca Mountain Project procedure LANL-EES-DP-130—Geologic Sample Preparation. Sample splits were heated at 110°C for 4 hours, and then allowed to equilibrate with ambient atmosphere for 12 hours. One gram splits were fused at 1100°C with 9 grams of lithium tetraborate flux to obtain fusion disks. Additional one-gram splits were heated at 1000°C to obtain the loss-on-ignition (LOI) measurements. Elemental concentrations were calculated by comparing X-ray intensities for the samples to those for 21 standards of known composition, after correcting for absorption. The XRF method employed calculates the concentrations of ten major oxides (SiO<sub>2</sub>, TiO<sub>2</sub>, Al<sub>2</sub>O<sub>3</sub>, Fe<sub>2</sub>O<sub>3</sub>, MnO, MgO, CaO, Na<sub>2</sub>O, K<sub>2</sub>O, P<sub>2</sub>O<sub>5</sub>), ten trace elements (V, Cr, Ni, Zn, Rb, Sr, Y, Zr, Nb, Ba), and LOI (Appendix B). Elemental concentrations of V, Cr, and Ni in the Bandelier Tuff are generally below detection limits and are not, therefore, reported in Appendix B.

Thin sections were prepared of samples selected for petrographic and microprobe analyses for use as an additional correlation tool. Major element concentrations determined by electron microprobe analysis of glass may be useful in correlating pyroclastic deposits. Microprobe analyses were performed on carbon-coated thin sections with an automated SX50 Cameca electron microprobe using an accelerating potential of 15 kV and a fixed beam size of 10 microns. Standards used for calibrations include silicic glasses, feldspars, iron oxides, pyroxenes, and amphiboles. Between 20 and 30 analyses on glassy pumice and ash were collected from each sample. Variations in FeO, TiO<sub>2</sub>, Al<sub>2</sub>O<sub>3</sub>, and CaO are reported here in weight percent with total iron expressed as FeO.

Ninety-three samples were analyzed by whole-rock XRF, and 20 samples were analyzed by electron microprobe (Appendix B and Appendix C, respectively). Locations of samples are shown in Appendix A (Figure A-1a). Sampling sites are located in and around the TA-16 study area as follows: a section on the Pajarito fault scarp along State Road 4 (Figure A-1b); a section in Water Canyon south of WETF (Figure A-1c); a section from borehole SHB-3 (Figure A-1c); sample suites from the WETF boreholes (Figure A-1c); 430 Canyon southeast of WETF; a section on the north side of Water Canyon near building 370 (Figure A-1d); two locations along State Road 4, on Campground Mesa (Figure A-1e); a section in upper Pajarito Canyon, west of State Road 501 (Figure A-1f); and Los Alamos and Pueblo Canyons where older units of the Bandelier Tuff are exposed. Schematic sections showing the relative relationships of some sample sections are shown in Figures 3a and 3b.

### *III. G. Drilling*

The objective of the drilling program was to intercept stratigraphic contacts or marker horizons within the Tshirege Member of the Bandelier Tuff, and to evaluate if measurable stratigraphic separation or offset of those features was caused by faulting between or among drill sites. This approach was employed around the footprint of WETF (Plate 1 and Figure 4) where anthropogenic disturbances and lack of natural exposures precluded high-precision geologic mapping. Geologic cores removed from the holes were used to define and correlate the stratigraphic sequence at each drill hole to aid in identifying geologic structure. Drilling operations took place in April, 2000. The holes were continuously

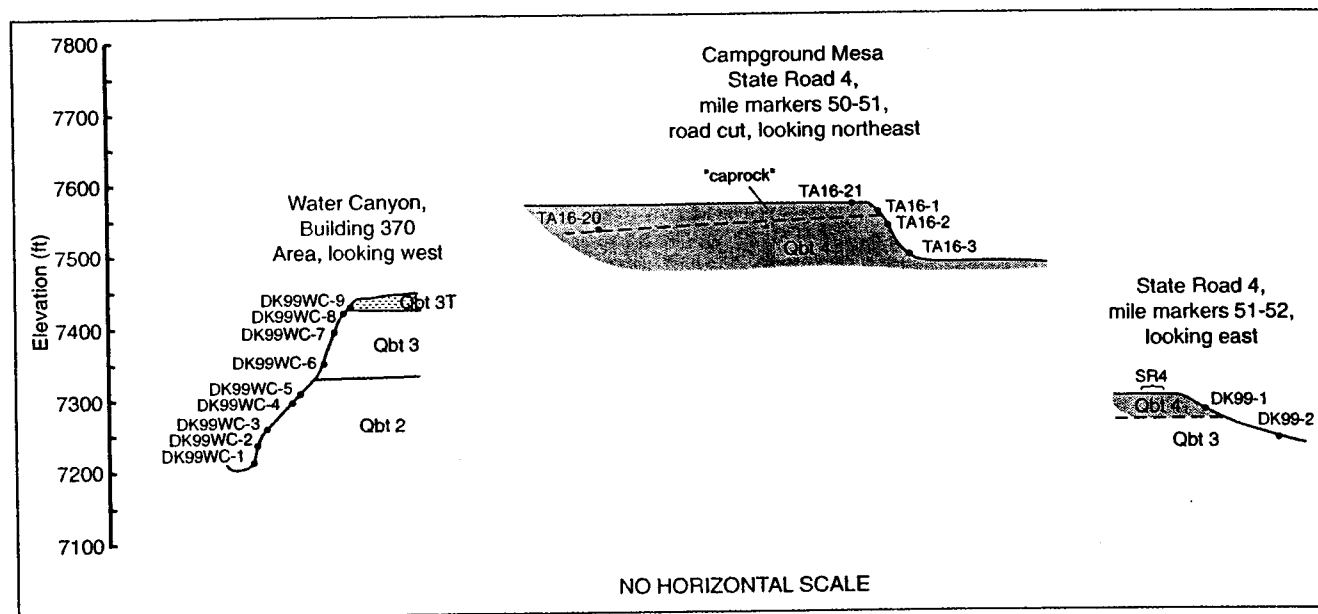
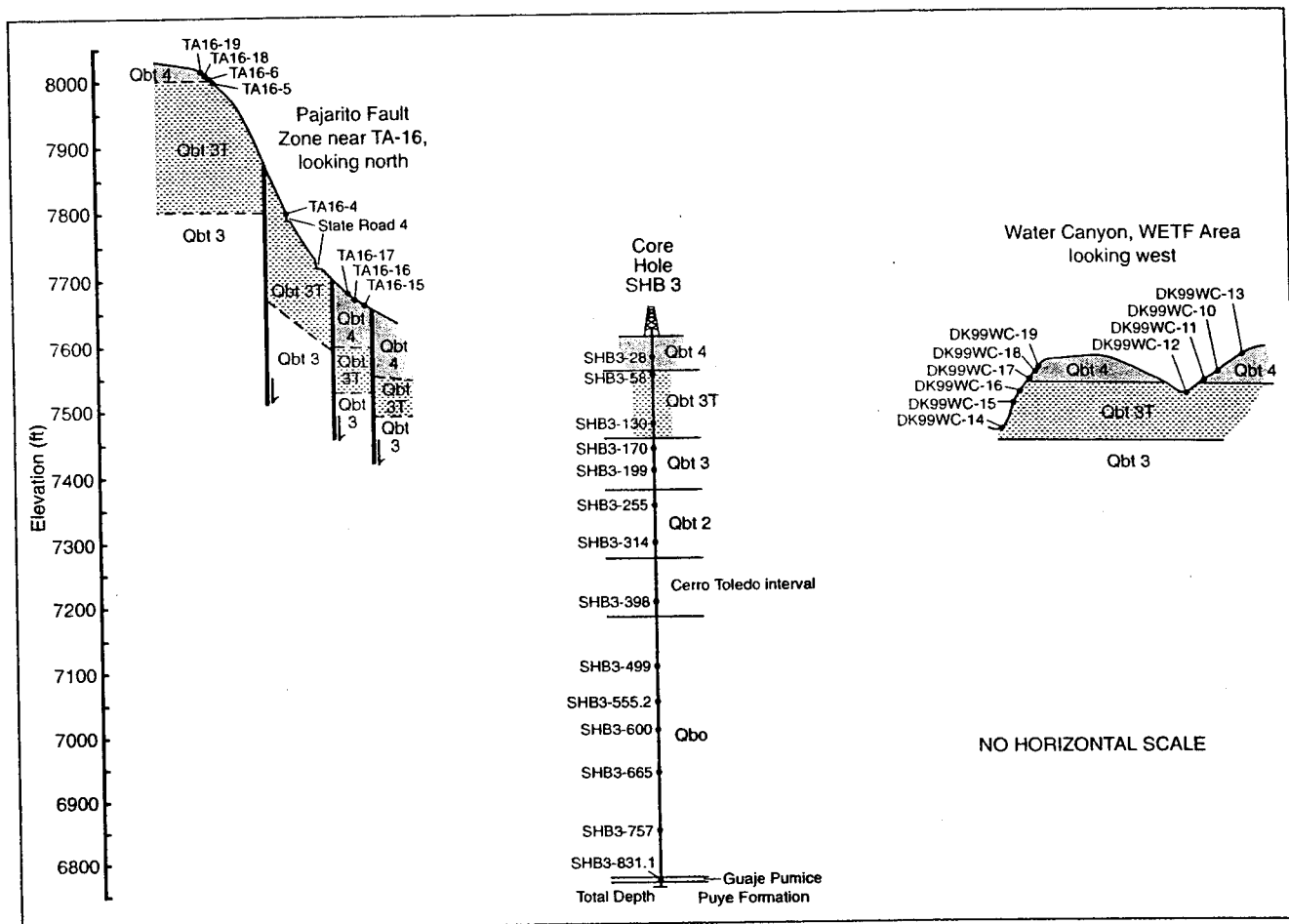


**Figure 3.** Schematic sections showing units of the Bandelier Tuff and relative sample locations. a) Pajarito fault zone, core hole SHB-3 (Gardner et al., 1993), and Water Canyon near WETF. Only selected samples from SHB-3 are plotted. b) Water Canyon near building 370, Campground Mesa, and east of Campground Mesa. See Appendix 1 for sample locations. Qbt = Tshirege Member units; Qbo = Otowi Member; see Section IV.A.1, Bedrock Units of the Bandelier Tuff and Associated Deposits. No horizontal scale.

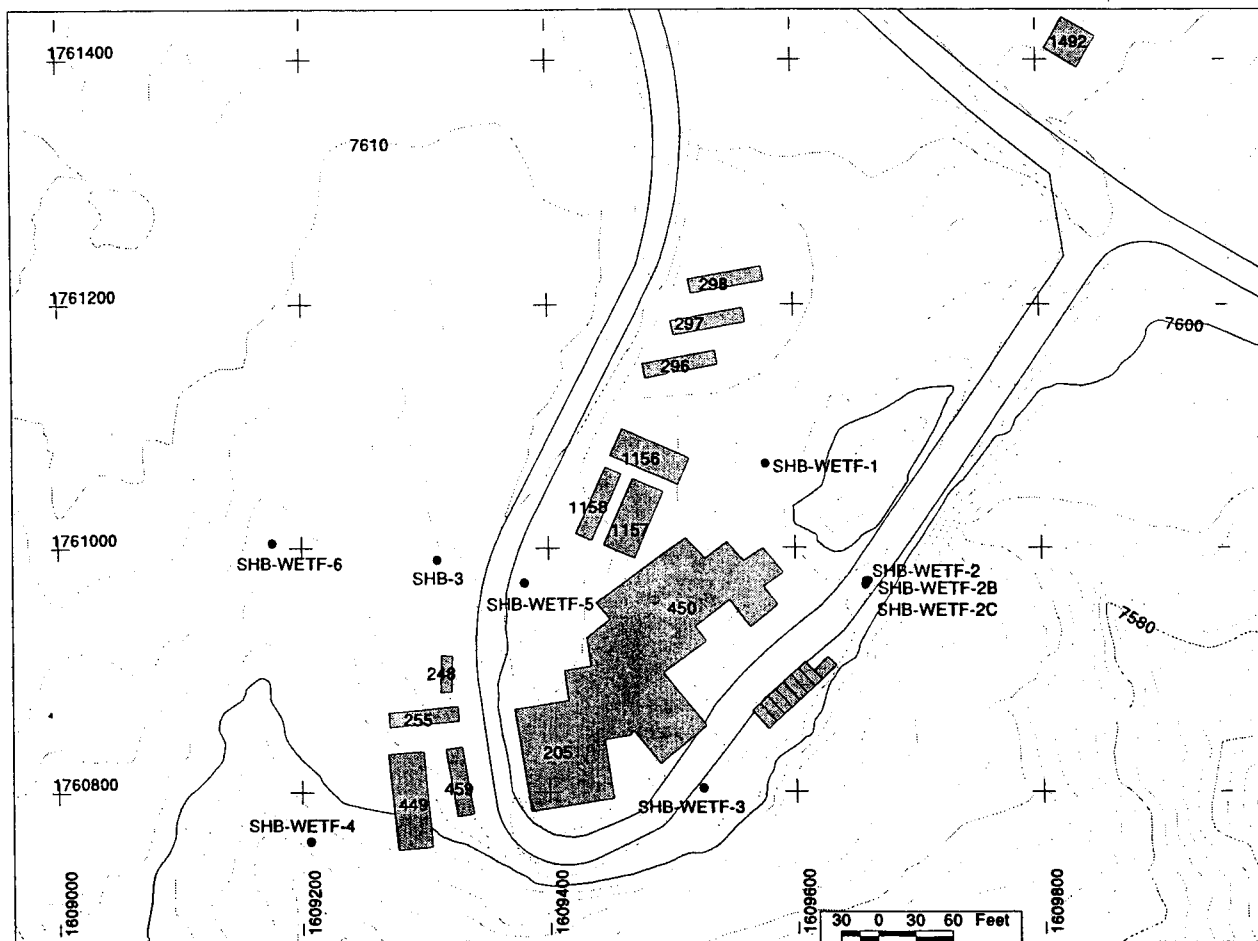


**Figure 4.** Map of facilities at WETF showing borehole SHB-3 (Gardner et al., 1993) and boreholes drilled in April 2000 (this study). The April, 2000, boreholes are officially designated SHB-WETF-n which we commonly shorten to WETF-n. Buildings numbered and shaded gray. The access road is shown by the double solid lines. The contour interval is 2 feet.

cored using either a diamond coring system with air as the circulating fluid or a hollow-stem auger with a split-spoon barrel. In some zones of particularly soft material, small diameter punch cores were taken. A total of just over 400 feet was cored in eight holes, two of which (WETF-2 and WETF-2B) had to be abandoned at shallow depths because of drilling problems.

Detailed lithologic logs were prepared for each hole at the drill sites upon retrieval of the core and supplemented with later detailed examination of key intervals at the Laboratory's Environmental Restoration Project Field Support Facility where the cores will be archived for about five years. Cores were marked and boxed at the drill sites using a procedure designed by Goff (1986) as guidance. Mapping lithologic types and checking and refining contacts against focused geochemical sampling yield contact or marker horizon elevations that are accurate to less than 1 foot in most cases. Surveying the borehole locations and depth references using the Total Station techniques discussed above allows the

borehole data to be integrated with the results of the high-precision geologic mapping.

Borehole data from previous studies in the vicinity have also been integrated with our results. Locations and stratigraphic data have been taken from Environmental Restoration Project documents and we have modified the Environmental Restoration Project's stratigraphy based on petrographic and geochemical comparisons with our field units (see Discussion and Conclusions, Tshirege Member Stratigraphic Units, Section V. A).

## IV. GEOLOGY

### IV. A. Stratigraphy

The general stratigraphic units and relations in the vicinity of S-Site are similar to those of the surrounding Jemez Mountains volcanic field (Bailey et al., 1969; Smith et al., 1970; Gardner et al., 1986; Goff et al., 1990). Volcanism forming the Jemez Mountains had begun by about 16.5 Ma just 5 miles

1000  
 900  
 800  
 700  
 600  
 500  
 400  
 300  
 200  
 100  
 0

south of S-Site (Gardner et al., 1986), and volcanic activity continued up through the most recent eruptions in the volcanic field, the El Cajete Member of the Valles Rhyolite, at about 50 to 60 ka (Reneau et al., 1996b). Several independent lines of evidence indicate that future volcanism in the Jemez Mountains is likely (Wolff and Gardner, 1995; Reneau et al., 1996b; Steck et al., 1998). The oldest exposed and very widespread unit in the study area is the Bandelier Tuff which forms the local, near-surface bedrock. Overlying the Bandelier Tuff is a variety of mostly volcanoclastic surficial units which notably includes El Cajete tephra deposits.

**IV. A. 1. Bedrock Units of the Bandelier Tuff and Associated Deposits**

The shallow bedrock in the vicinity of S-Site is the Bandelier Tuff (Griggs, 1964; Smith et al., 1970). The Bandelier Tuff consists of two members that were erupted as a series of ash-flows during enormous, caldera-forming volcanic events at about 1.2 Ma and 1.6 Ma (Izett and Obradovich, 1994). The younger member, the Tshirege, is the unit exposed in the S-Site area, whereas the older member, the Otowi, has been encountered in two relatively deep drill holes in the study area (SHB-3 and R-25, Plate 1). Figure 5 shows a generalized stratigraphy of the Bandelier Tuff and associated deposits. Beneath the Otowi in both wells that penetrated through the Bandelier Tuff are sands and coarse gravels of the Puye Formation (Gardner et al., 1993; Environmental Restoration Project, in prep.) which ranges in age from about 7 Ma to about 1.6 Ma (Bailey et al., 1969; Gardner et al., 1986).

**a. Otowi Member of the Bandelier Tuff (Qbo).** Although not exposed in the study area, the Otowi Member of the Bandelier Tuff will provide additional data on the subsurface structure of S-Site and the Laboratory with information derived from planned deep drilling. Consequently, we have begun to develop petrographic and geochemical data on the Otowi in the vicinity of S-Site mostly from core hole SHB-3 (Gardner et al., 1993). Ash-flows of the Otowi Member were erupted and

emplaced during the volcanic and structural events that formed the Toledo caldera at about 1.6 Ma (Smith and Bailey, 1966; Izett and Obradovich, 1994). In SHB-3, the Otowi Member consists of about 400 feet of mostly nonwelded ignimbrite. Within the upper 75 feet, however, Gardner et al. (1993) report a zone about 25 feet thick that exhibits a moderate degree of welding, overlying a zone with prominent vapor-phase altered pumices. Other than the Otowi's general lack of welding on the Pajarito Plateau, even in thick sequences relatively close to the caldera source, it is petrographically similar to the Tshirege Member. Quartz, commonly in bipyramidal form, and sanidine are the most conspicuous phenocryst phases in the Otowi. In contrast to the Tshirege, the Otowi tends to be a bit more lithic rich, and Precambrian lithologies are more prominent among the lithic population. At this time data are insufficient to allow further subdivision of the Otowi Member ignimbrites.

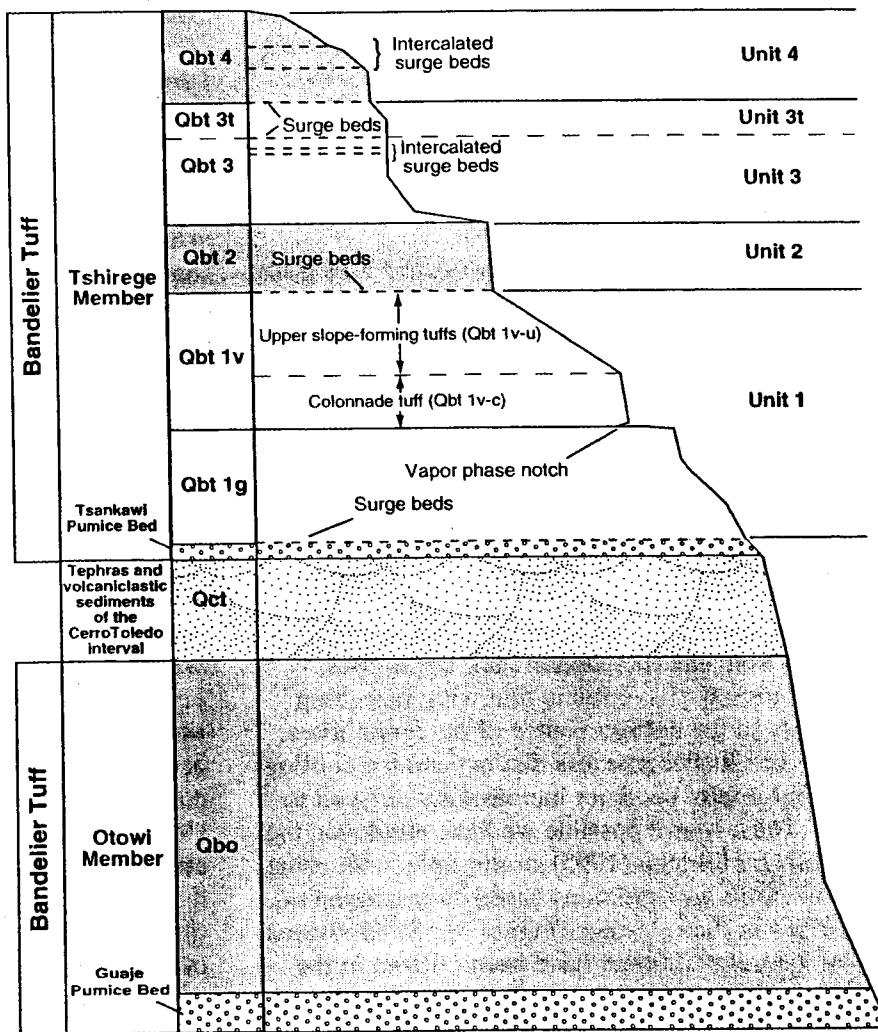


Figure 5. Generalized stratigraphy of the Bandelier Tuff and associated deposits (modified from Broxton and Reneau, 1995).

### ***b. Cerro Toledo Rhyolite and Interval.***

Following the eruption of the Otowi Member ash flows, intracauldron volcanism in the Toledo caldera began almost immediately at about 1.6 Ma and continued up to 1.2 Ma, just prior to the eruption of the Tshirege Member (Spell et al., 1996). On the Pajarito Plateau these intracauldron eruptions are marked by fallout deposits of the Cerro Toledo Rhyolite (for example, Smith et al., 1970; Heiken et al., 1986). Gardner et al. (1993) reported a thick sequence of volcanoclastic sands and gravels, with interbedded fallout tephra of the Cerro Toledo Rhyolite, in the interval between the Otowi and Tshirege members of the Bandelier Tuff in core hole SHB-3. Broxton and Reneau (1995) refer to all volcanoclastic and Cerro Toledo Rhyolite deposits stratigraphically between the Otowi and Tshirege members as the Cerro Toledo Interval. In SHB-3 and R-25 the Cerro Toledo Interval is about 100 feet thick. With motivations similar to those for beginning to develop petrographic and geochemical data for the Otowi, we have sampled and analyzed the Cerro Toledo tephra from SHB-3. In SHB-3, the Cerro Toledo Rhyolite appears to be represented by several thin layers of white, very fine ash or pumice lapilli. The ash layers are generally devoid of visible crystals and contain rare, coarse sand-sized pieces of obsidian.

### ***c. Tshirege Member of the Bandelier Tuff (Qbt).***

The stratigraphy for the Tshirege Member of the Bandelier Tuff that we employ is largely based on that presented by Broxton and Reneau (1995). The Broxton and Reneau (1995) stratigraphy is based on cooling units within the Tshirege Member in the central and eastern parts of the Laboratory, but as we have mapped from central to more western portions of the Laboratory (Gardner et al., 1999), we have discovered that, although the Tshirege units defined by Broxton and Reneau (1995) are laterally continuous, there are a number of other mappable Tshirege units not included in their definitions. Furthermore, we have found that with increasing proximity to the caldera source of the ignimbrites, cooling breaks become less distinct and the cooling unit stratigraphy becomes increasingly difficult to apply. Thus, where possible we have employed the Broxton and Reneau (1995) stratigraphy with some modifications and additions based on petrographic variations in the sequence (Figure 5). Subdivisions of the Tshirege Member have been utilized in the vicinity of Water Canyon and in the boreholes. Additionally, a few Tshirege units have been identified and broken out on the main escarpment of the Pajarito fault, but for many areas on Plate 1, Qbt represents undivided Tshirege Member of the

Bandelier Tuff. These areas are mainly on mesa tops where no soil or only thin and patchy soil was present, or on steep slopes, such as canyon walls or the Pajarito fault escarpment, where colluvial cover and units of the tuff were not practical to map separately. The lowest stratigraphic unit of the Tshirege Member exposed in the study area is Unit 2 and the descriptions that follow begin with it. Unit 1 is absent from the lower portion of the Tshirege Member in borehole SHB-3 (see Structural Geology, Section IV.C.1. below).

Unit 2: greater than 40 feet thick in Water Canyon and greater than 80 feet thick in borehole SHB-3, but the base is not exposed. Unit 2 is recognized in the field as a prominent cliff-forming, strongly welded unit. Well-exposed in Water Canyon in the eastern part of the map area, the unit disappears, as one moves west, beneath younger units. Additionally, the Unit 2-Unit 3 contact is covered with dense vegetation in Water Canyon. Accidental lithic fragments are rare (<1%), and the welded tuff is moderately porphyritic (15%–20% phenocrysts of subequal amounts of sanidine and quartz). Pumices tend to be relatively sparse (5%–10%), but can be difficult to distinguish because of the densely welded nature of the unit.

Unit 3: 80 to 130 feet thick. The boundary between Unit 2 and the overlying Unit 3 is marked by an abrupt change in welding characteristics, from densely welded Unit 2 to nonwelded Unit 3, in the eastern third of the area mapped in Water Canyon. Moving west in Water Canyon, this contact is hidden beneath dense vegetation and younger units; however, the Unit 2-Unit 3 contact is marked by a welding break in borehole SHB-3. In most of the western part of the map area, the base of Unit 3 is not exposed, and the higher portions of the unit achieve a moderate to dense degree of welding. The top of Unit 3 can be marked by a crystal-rich surge deposit, and, in a few locations, we have mapped surges within Unit 3. The surge deposits are commonly crystal-rich (up to 90%), ash-poor, and composed of sand-sized grains of crystals and both cognate and accidental lithic fragments. In outcrop, and even in core, these deposits can exhibit sedimentary structures that include plane beds and low-angle crossbeds. Unit 3 is more pumice rich (about 30%) than Unit 2, and contains relatively abundant (locally up to 5%) accidental lithic fragments, most of which are around 5 cm in diameter. In contrast to other units, Unit 3 is more porphyritic, with at least 30% phenocrysts. Again, quartz and sanidine occur in subequal amounts, but, fairly distinctive of the phenocryst population of Unit 3 is the relatively coarse crystal size, with most phenocrysts 4 to 6 mm



are present within the mesa-top alluvial deposits at several sites on the Pajarito Plateau, including the map area, and geochemical fingerprinting of the pumice indicates that the primary source is the Cerro del Medio dome complex in the Valles caldera (D. Broxton, unpublished data, 1996; see Reneau and McDonald, 1996, p. 90-91). Cerro del Medio lavas have yielded  $^{40}\text{Ar}/^{39}\text{Ar}$  ages of 1.207 to 1.095 Ma (Spell and Harrison, 1993; Izett and Obradovich, 1994; Spell and Harrison, 1993, argue, however, that the most "reliable age" of all these dates is 1.133 Ma), indicating an early Pleistocene age for the mesa-top alluvium associated with these pumice beds. Elsewhere, these gravels may be younger, but no younger than the ca. 50 to 60 ka El Cajete pumice (see Qfi below). Qoal has a gradient that is gentler than the modern stream channels in Cañon de Valle (Figures 6a and 6b) and Water Canyon, apparently roughly parallel to the original upper surface of the Tshirege Member of the Bandelier Tuff. Along Cañon de Valle near MDA P, a unit Qoal2 is distinguished which is topographically lower than other nearby gravels to the west.

**b. Older Alluvial Fan Deposits (Qfo).** Unit Qfo consists of relatively old dacite-rich alluvial deposits which are typically inset below the top of the Tshirege Member of the Bandelier Tuff along major canyons in the western Pajarito Plateau; thus, these deposits postdate initial canyon incision. Stratigraphic relations indicate that these deposits are younger than nearby deposits of Qoal and older than intermediate-age fan deposits (Qfi); however, the age range of Qfo is unknown and these deposits may overlap in age with Qoal and Qfi. In the map area Qfo occurs as several distinct fan segments near Cañon de Valle, inset about 20 feet below the top of Qoal with an apparent gradient roughly parallel to Qoal (Figures 6a and 6b). Qfo has an estimated maximum thickness in the map area of greater than 10 feet.

**c. Intermediate Alluvial Fan Deposits (Qfi).** Unit Qfi consists of intermediate-age alluvial fan deposits that predate the ca. 50-60 ka El Cajete pumice (Qec). Qfi includes abundant dacite gravel along the main drainages that head in the Sierra de los Valles, but largely contains Bandelier Tuff clasts along smaller drainages. Qfi is locally buried beneath younger alluvial fans (Qfy) or colluvium (Qc), as well as Qec (e.g., Figures 7 and 8). Qfi probably includes deposits with a wide range in age. As exposed in a 1999 gas line trench in TA-9 north of Cañon de Valle (Plate 1), the youngest Qfi deposits are apparently only slightly older than the El Cajete pumice, being separated by a weakly developed soil. The maximum age of Qfi is uncertain. The distinction

between Qfi and Qfo is based entirely on local topographic relations and may not be consistent across the map area. Near Cañon de Valle, Qfi includes multiple distinct fan lobes, some of which appear to have gradients roughly parallel to Qfy (see below) and others which appear to have gradients roughly parallel to Qfo, supporting the inference that Qfi may span a considerable period of time.

**d. El Cajete Pumice (Qec).** Unit Qec consists of the El Cajete pumice, derived from the youngest major eruptions from the Valles caldera and dated at ca. 50 to 60 ka (age from Toyoda et al., 1995, and Reneau et al., 1996b). In the formal stratigraphy of the volcanic field, this unit is the El Cajete Member of the Valles Rhyolite (Bailey et al., 1969; Gardner et al., 1986). Commonly, Qec consists of primary fallout deposits of dominantly pumice lapilli that directly overlie the preeruption soil, but some locations on the main escarpment of the Pajarito fault provide evidence for local reworking. Trench exposures in nearby areas (Kolbe et al., 1994; Reneau et al., 1995) have shown that deposits of undisturbed pumice can be very discontinuous, and that the pumice is often highly disrupted by burrowing animals and other forms of bioturbation. The pumice beds are also typically overlain by colluvial, alluvial, or eolian deposits (Figures 7 and 8; see also Kolbe et al., 1994; Reneau et al., 1995, 1996a, 1996b; Wong et al., 1995; Reneau and McDonald, 1996). In the map area, the existence of Qec below the surface soil can often be inferred from the presence of abundant pumice in mounds adjacent to animal burrows. We made, however, no attempt on Plate 1 to separate Qec from overlying colluvium and eolian deposits. Instead, a composite "Qec + Qc" map unit is employed that indicates that Qec is at least locally present in the shallow subsurface. Importantly, previous trench studies (Kolbe et al., 1994; Reneau et al., 1995) have shown that even where no undisturbed pumice remains, the top of the pre-El Cajete soil can often still be recognized in such areas and used as a key stratigraphic horizon in paleoseismic studies. The maximum observed thickness of primary fallout El Cajete pumice in the map area is about 6.5 feet, along a northern tributary to Water Canyon (Figure 7), similar to the maximum thickness observed to date within the Laboratory area of about 7 feet, on Frijoles Mesa about 3 miles east of the map area (Reneau and McDonald, 1996, pp. 73-75).

**e. Younger Alluvial Fan Deposits (Qfy).** Unit Qfy consists of relatively young alluvial fan deposits that postdate the El Cajete pumice. Qfy is locally subdivided into adjacent deposits of differing relative ages, although these subdivisions are not intended to

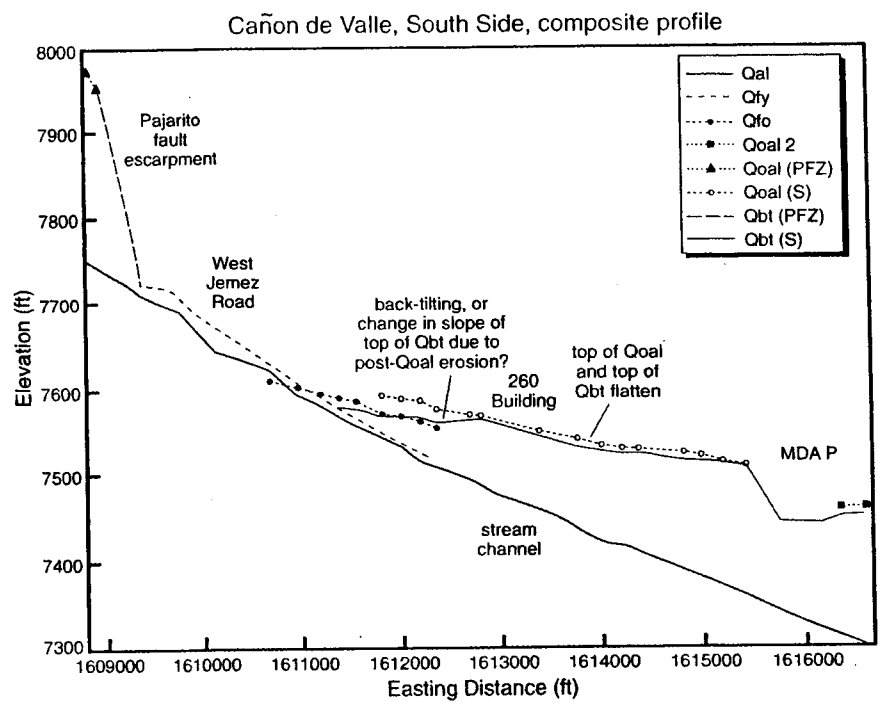
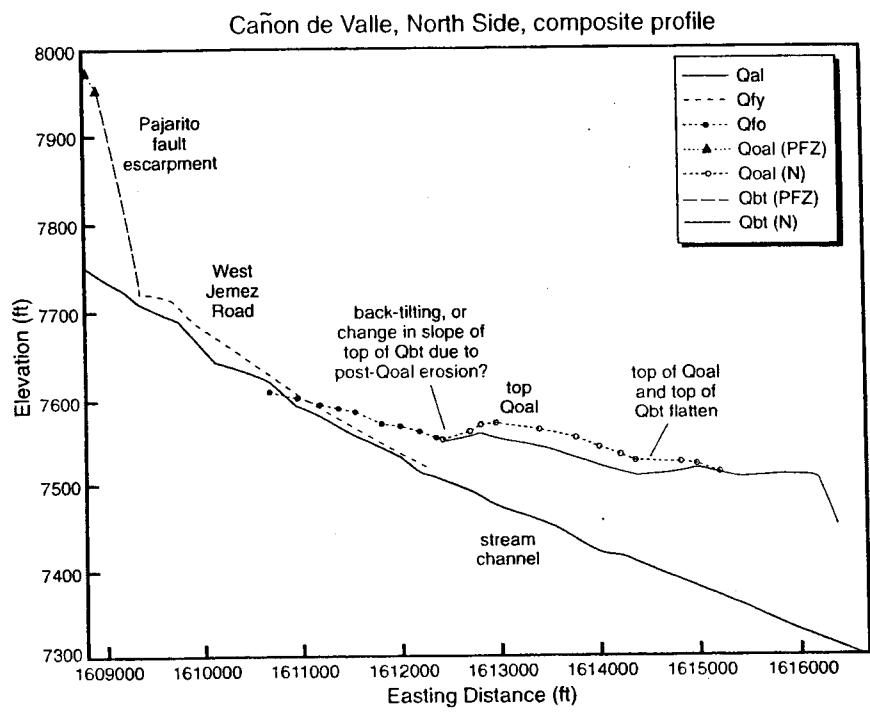


Figure 6. Composite longitudinal profiles along Cañon de Valle, projected into an east-west plane, showing the tops of Qal, Qfy, Qfo, Qoal, and Qbt relative to the modern stream channel. a) North side of canyon. b) South side of canyon. In this and subsequent figures, see text for description of units. PFZ, Pajarito fault zone; N, north side of canyon; S, south side of canyon.

be consistent between drainages (for example, the oldest fan unit mapped along one drainage as Qfy1 may be latest Pleistocene or early Holocene in age, whereas Qfy1 on another fan from a different drainage may include significantly older deposits).

incision. Gentler gradients develop after a subsequent decrease in sediment supply and incision.

f. *Landslides (Qls)*. Extensive areas on the Pajarito fault escarpment show evidence of large-

In some areas where there is no age control, the distinction between Qfy and Qfi is arbitrary and will probably require revision. Qfy includes stream terraces along some drainages, as the distinction between fan and terrace is also often arbitrary. The thickness of Qfy is unknown in most areas, although it is 20 feet thick at one site north of Water Canyon (Figure 7).

Age control has been obtained from Qfy at several sites in the map area. Radiocarbon dates on detrital charcoal of ca. 9.3 to 9.6 ka were obtained from the upper part of the 20-ft thick section mentioned above (Figure 7, Table 1), and probably closely constrains the end of fan deposition at this site. Soils exposed in a pit in Qfy along Cañon de Valle (Reneau and McDonald, 1996, p. 93-95) suggest a similar age for that fan unit, and a Qfy stream terrace along Water Canyon that was trenched by Wong et al. (1995) may be of similar age (T2 on Plate 1; see also Reneau and McDonald, 1996, p. 82). Along Cañon de Valle, Qfy has a gradient that is slightly steeper than the modern stream channel, being about 20 feet higher than the channel at the base of the Pajarito fault escarpment but converging with the channel about 3000 feet to the east (Figure 6). This difference in gradient is consistent with Qfy recording a period of aggradation associated with an increase in sediment yield from the upper watershed, causing a steepening of the stream channel that was followed by

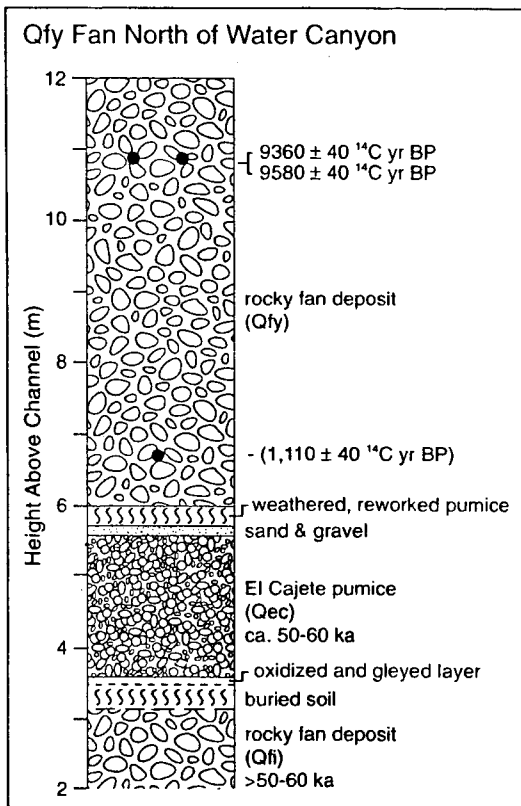


**Figure 7.** Stratigraphic section showing units beneath Qfy surface along unnamed tributary to Water Canyon, west of West Jemez Road (locations C3 and C4 on Plate 1 and in Table 1). Radiocarbon dates were obtained from charcoal fragments collected from stream bank and from soil pit WJR-8 (Reneau and McDonald, 1996). The ca. 9.3-9.6 ka dates provide a good estimate of the end of fan deposition at this location. The date in parentheses probably represents young charcoal introduced by bioturbation into the section. Modified from Figure 2-11 of Reneau and McDonald, 1996).

scale mass wasting and were mapped as Qls. Although distinct slump blocks can occasionally be recognized and partially delineated, more typically the specific nature of the landsliding and the margins of individual slide blocks cannot be reliably determined. Areas mapped as Qls also include extensive deposits of colluvium cover that were not mapped in detail. Because we have used this unit somewhat generally for areas of extensive mass wasting, it is possible that some areas mapped as Qls include *in situ* Qbt on the escarpment. We expect that the history of landsliding on the Pajarito fault escarpment is closely related to faulting, with landsliding triggered by earthquakes and with some landslide blocks being bounded by fault traces. Available data, however, are

insufficient to allow correlation of the landslide and paleoseismic histories.

**g. Young Alluvium Along Stream Channels (Qal).** Unit Qal consists of relatively young alluvium along stream channels, and includes presently active channels and adjacent floodplains, low terraces, and associated colluvium. Qal also includes active channels with little or no alluvium in some areas. A unit Qal2 is mapped in some areas to identify Holocene terraces, but these were not consistently distinguished within the map area. Radiocarbon dates indicate a middle Holocene age for a buried Qal terrace in one area in Cañon de Valle, near MDA P (Table 1, Figure 9).

**h. Colluvium (Qc).** Unit Qc includes deposits with a wide range in texture, origin, and age which were not practical to subdivide in this investigation. The term "colluvium" is used in this report to include both deposits on steep slopes that record primarily gravity-driven transport, and deposits on gentle slopes that record deposition by dispersed overland flow. As used in this context, the

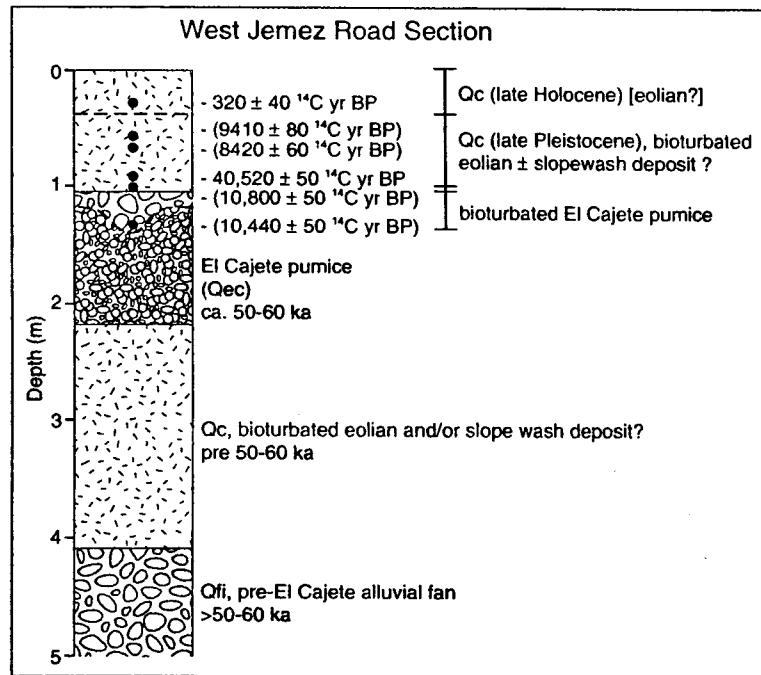


**Figure 8.** Stratigraphic section showing units beneath Qec+Qc surface along West Jemez Road north of Water Canyon (location C2 on Plate 1 and in Table 1). Radiocarbon dates were obtained from charcoal fragments collected from soil pit WJR-9 and from road cut (Reneau and McDonald, 1996). Dates in parentheses probably represent young charcoal introduced into post-El Cajete colluvium or eolian deposits by bioturbation in the latest Pleistocene or early Holocene. Both soil development and cosmogenic  $^{21}\text{Ne}$  analyses indicate that the ca. 40 ka date is a reasonable minimum-limiting age estimate for the post-Qec deposits (Phillips et al., 1998). The ca. 0.3 ka date was obtained from a possible latest Holocene eolian deposit and may be accurate. Soils below this surface are described in Reneau and McDonald (1996) and McDonald et al. (1996a).

**Table 1. Radiocarbon Analyses From TA-16 and Vicinity**

Field Number	Laboratory Number *	<sup>14</sup> C Date (yr B.P.)	δ <sup>13</sup> C (o/oo)	Depth (m)	Source**	Location on Plate 1	Notes
<b>West Jemez Road, TA-16, north of Water Canyon, deposit above El Cajete pumice (Qc)</b>							
<b>roadcut</b>							
F-28	Beta-84724	8,420 ± 60	-24.1	0.65	1	c1	post-El Cajete deposit; date believed to be younger than deposit due to bioturbation (AMS analysis)
<b>soil pit WJR-9</b>							
WJR-17	Beta-108397	320 ± 40	-24.8	0.3	1	c2	upper silt-rich unit; possible eolian or reworked eolian deposit
WJR-12	Beta-108396	9,410 ± 80	-24.4	0.6	1	c2	Bt horizon; date believed to be younger than deposit due to bioturbation (AMS analysis)
WJR-10	Beta-108395	40,520 ± 1200	-23.8	0.95	1	c2	0.2 m above primary El Cajete pumice; date close to limit of method and may be too young due to contamination (AMS analysis)
WJR-23	Beta-113027	10,800 ± 50	-22.7	1.0	2	c2	single charcoal fragment in lower part of pumice-poor slope wash deposit; date believed to be younger than deposit due to bioturbation (AMS analysis)
WJR-24	Beta-113028	10,440 ± 50	-24.5	1.35	2	c2	single charcoal fragment in uppermost bioturbated El Cajete pumice; probably records period of bioturbation and not age of overlying deposit (AMS analysis)
<b>West Jemez Road, north of Water Canyon, Qfy fan deposits overlying El Cajete pumice</b>							
<b>stream bank exposure</b>							
WJR-6	Beta-93951	1,110 ± 40	-25.6	5.5	2	c3	0.5 m above base of fan gravels; believed to be too young due to bioturbation (AMS analysis)
<b>soil pit WJR-8</b>							
WJR-8	Beta-107270	9,360 ± 40	-24.9	1.15	2	c4	sand beds in coarse gravel (AMS analysis)
WJR-9	Beta-107271	9,580 ± 40	-24.2	1.15	2	c4	coarser gravelly layer than WJR-8 (AMS analysis)

**Table 1 (cont.). Radiocarbon Dates From TA-16 and Vicinity (continued)**

Field Number	Laboratory Number *	<sup>14</sup> C Date (yr B.P.)	δ <sup>13</sup> C (o/oo)	Depth (m)	Source**	Location on Plate 1	Notes
<b><u>Water Canyon, soil pit WCSP2, colluvium overlying Qfy terrace</u></b>							
WCSP2-1	TO-3415	8,060 ± 160	na	1.0	3	c5	silty sand; stratigraphic reversal from WCSP2-2 suggests bioturbation or contamination of sample
WCSP2-2	Beta-55318	9,490 ± 110	na	0.5	3	c5	silty sand (AMS analysis)
<b><u>Cañon del Valle near MDA P, colluvium</u></b>							
<b>section 1, colluvium overlying mid-Holocene terrace deposits</b>							
CDV-1	Beta-84479	3,650 ± 40	-25.6	0.9	2	c6	thin buried soil in colluvium (AMS analysis)
CDV-3	Beta-84480	4,000 ± 60	-23.2	1.3	2	c6	buried soil in colluvium (AMS analysis)
CDV-5	Beta-84481	4,390 ± 40	-24.1	1.9	2	c6	buried soil in colluvium, 0.1 m above stream sands (AMS analysis)
<b>section 2, colluvium overlying mid-Holocene terrace deposits</b>							
CDV-7	Beta-84483	2,290 ± 40	-22.4	0.5	2	c7	colluvium (AMS analysis)
CDV-9	Beta-84484	3,610 ± 40	-22.5	1.1	2	c7	colluvium (AMS analysis)
CDV-6	Beta-84482	3,770 ± 40	-24.2	1.9	2	c7	buried soil in colluvium, 0.3 m above stream sands (AMS analysis)
<b>colluvium on hillslope</b>							
CDV-10	Beta-84485	520 ± 30	-24.2	0.3	2	c8	colluvium, north-facing hillslope (AMS analysis)
CDV-12	Beta-84487	640 ± 30	-24.3	0.8	2	c9	colluvium, south-facing hillslope (AMS analysis)
CDV-11	Beta-84486	3,840 ± 40	-23.9	1.2	2	c10	colluvium, base of south-facing hillslope (AMS analysis)

**Table 1 (cont.). Radiocarbon Dates From TA-16 and Vicinity (continued)**

Field Number	Laboratory Number *	<sup>14</sup> C Date (yr B.P.)	δ <sup>13</sup> C (o/oo)	Depth (m)	Source**	Location on Plate 1	Notes
<b><u>Water Tanks trenches WTT1 and WTT2, colluvium above and below El Cajete pumice</u></b>							
WTT1-4	Beta-56176	1,120 ± 80	na	0.25	3	c11	uppermost silt-rich unit; possible eolian or reworked eolian deposit
WTT1-6	TO-3414	5,840 ± 90	na	0.65	3	c11	post-El Cajete colluvial soil; charcoal possibly bioturbated
WTT2-1	na	22,420 ± 690	na	1.05	3	c12	pre-El Cajete colluvium; date is too young and represents contamination of deposit or charcoal with young carbon
WTT1-5	TO-3413	19,070 ± 160	na	1.45	3	c11	pre-El Cajete colluvium; date is too young and represents contamination of deposit or charcoal with young carbon
WTT1-1D	Beta-55313	>47,500	na	1.8	3	c11	pre-El Cajete colluvium (AMS analysis)
<b><u>1998 Trench 6, Pajarito fault escarpment south of Water Canyon, colluvium</u></b>							
98T6-1	Beta-122653	2,370 ± 50	-24.0	0.25	4	c13	colluvium; Pinus charcoal (AMS analysis)
<b><u>1998 Trench 4, post-El Cajete alluvial fan (Qfy) along western trace of Pajarito fault zone north of Cañon de Valle</u></b>							
98T4-5	Beta-122649	1,420 ± 50	-24.0	0.35	4	***	post-El Cajete colluvium; Pinus charcoal (AMS analysis)
98T4-6	Beta-122650	840 ± 50	-25.1	0.6	4	***	post-El Cajete colluvium; conifer charcoal (AMS analysis)
98T4-7	Beta-122651	17,940 ± 100	-24.9	2.2	4	***	pebble gravel layer in post-El Cajete alluvial fan; conifer charcoal (AMS analysis)
98T4-3	Beta-122087	29,570 ± 150	-22.9	2.6	4	***	silty sand in post-El Cajete alluvial fan (AMS analysis)
98T4-2	Beta-122086	30,910 ± 180	-23.0	3.9	4	***	pebbly sand in post-El Cajete alluvial fan (AMS analysis)
98T4-4	Beta-122088	43,660 ± 750	-25.7	4.2	4	***	gravelly sand in post-El Cajete alluvial fan (AMS analysis)

**Table 1 (cont.). Radiocarbon Dates From TA-16 and Vicinity (continued)**

Field Number	Laboratory Number *	<sup>14</sup> C Date (yr B.P.)	δ <sup>13</sup> C (o/oo)	Depth (m)	Source**	Location on Plate 1	Notes
<b>WETF-2c Drill Hole</b>							
wetf2c-46.5	Beta-143830	6,330 ± 50	-22.0	14.3	5	c14	gravelly sands and laminated fine-grained sand in fissure (AMS analysis)
wetf2c-49.0	Beta-143831	7,540 ± 50	-22.8	15.0	5	c14	gravelly sands and laminated fine-grained sand in fissure (AMS analysis)
wetf2c-56.5	Beta-143831	8,070 ± 50	-22.5	17.3	5	c14	clay in fissure (AMS analysis)

**Notes:**

\* Laboratory designations. Beta: Beta Analytic, Inc.; TO: Toronto

\*\* Source. 1: Philips et al., 1998; 2: S. Reneau, unpublished; 3: Wong et al., 1995; 4: McCalpin, 1999; 5: this report

\*\*\* outside map area

na: not available

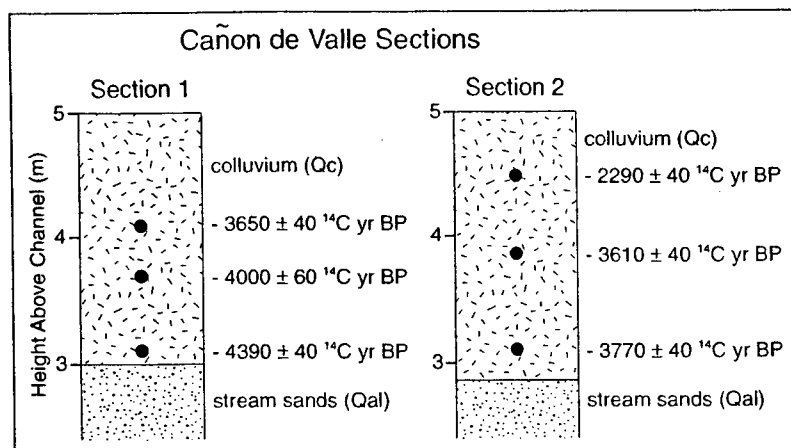


**Figure 9.** Stratigraphic sections showing locations of radiocarbon dates on charcoal collected from colluvium overlying middle Holocene alluvium (Qal) along Cañon de Valle near MDA P (Section 1 and Section 2 are locations C6 and C7, respectively, on Plate 1). The soil stratigraphic context indicates that Qal here is similar in age to the overlying colluvium, or middle Holocene in age, and that the channel was several meters higher at that time. Soils at these sections are described by McDonald et al. (1996b).

distinction between colluvium and alluvium is somewhat arbitrary and is made solely for convenience in mapping. In addition, Qc includes fine-grained deposits that are probably dominated by eolian sediment, although this eolian sediment may be locally reworked by overland flow and/or mixed with other material by bioturbation. Qc includes deposits that range in age from >50-60 ka (pre-Qec) to present (for example, Figures 8 and 9). Evidence for the eolian origin of some early Holocene and late Holocene deposits on Pajarito Mesa, northeast of the map area, is presented in Reneau et al. (1995, 1996a), and eolian deposits of similar age may be widespread in the TA-16 area. On Plate 1, Qc is often included in other map units and not broken out separately. Where possible, the unit directly underlying Qc is noted in the map designation to aid in interpreting the distribution of different units; for example, "Qc/Qbt" indicates that thin colluvium overlies tuff.

**i. Artificial Fill.** Artificial fill and anthropogenic disturbances are widespread in the map area. On Plate 1 this unit locally includes highly disturbed areas such as roads, parking lots, and borrow pits. Many areas that include patchy or thin fill were mapped instead as the underlying geomorphic unit.

#### IV. B. Geochemistry of Bedrock Units

Geochemical compositions of samples obtained in this study are similar to compositions of Tshirege Member samples from previous studies on the Pajarito Plateau (Broxton et al., 1996; Warren et al., 1997; Stimac et al., 1998; Gardner et al., 1998a;

Krier et al., 1998a and b; Gardner et al., 1999). Silica (SiO<sub>2</sub>), titania (TiO<sub>2</sub>), zirconium (Zr), strontium (Sr), rubidium (Rb) and barium (Ba) concentrations are each strongly zoned with respect to stratigraphy, and have been shown to effectively differentiate among units within the Tshirege Member of the Bandelier Tuff (Broxton et al., 1996; Warren et al., 1997; Stimac et al., 1998; Gardner et al., 1998a; Krier et al., 1998a and b; Gardner et al., 1999). Among several discriminators, titania is the single, most useful major element oxide used for unit identification throughout the Tshirege Member. Figure 10 shows the distribution of SiO<sub>2</sub> and TiO<sub>2</sub> versus elevation in four geographic areas investigated as part of this study.

Comparison of geochemical data from measured, intact stratigraphic sections with faulted sections shows the utility of geochemical analyses in identifying obscure geologic structures.

Eighteen samples of the Tshirege Member were collected west of the intersection of State Road 4 and West Jemez Road (Appendix A, Figures A-1a and A-1b) to determine the stratigraphic separation of the Bandelier Tuff on the Pajarito fault in the vicinity of the WETF and to understand the distribution of chemical units where more uniform welding throughout the sequence can obscure identifying characteristics. Unit 4 is repeated in the sequence by 3 fault strands along the main escarpment (Pajarito fault zone section, Figure 10).

The Pajarito Canyon section (Appendix A, Figure A-1a, and Figure 10) is also within the main escarpment zone of the Pajarito fault. This section was measured and analyzed in 1994 to determine stratigraphic separation on the Bandelier Tuff across the Pajarito fault. We present these data here for comparison to the sample suite in the main part of the fault zone near the intersection of State Road 4 and West Jemez Road. The Pajarito Canyon section crossed three fault strands, resulting in the repetition of stratigraphic units with increasing elevation.

SHB-3, located northwest of and adjacent to the WETF (Figure 4, Plate 1, and Appendix A, Figure A-1c), was drilled in 1991 to a depth of about 850 ft (Gardner et al., 1993). Samples were collected from the Tshirege Member, the Cerro Toledo Rhyolite, and the Otowi Member of the Bandelier Tuff to constrain elevations of contacts. Variation diagrams of elevation in the borehole versus selected major elements obtained by whole rock analysis are shown in Figure 11. Generally the

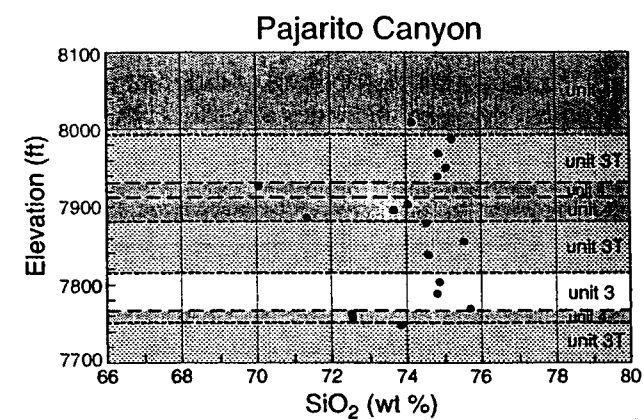
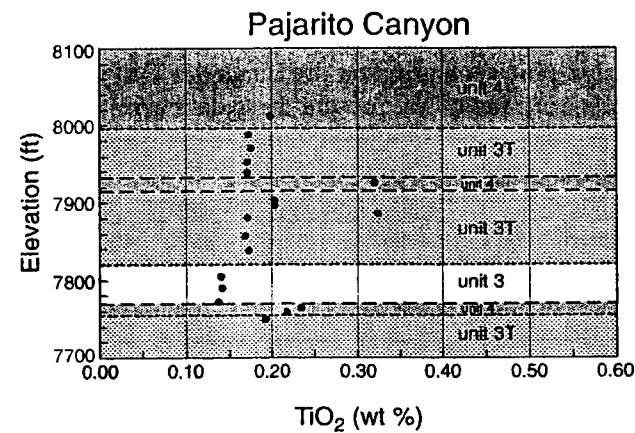
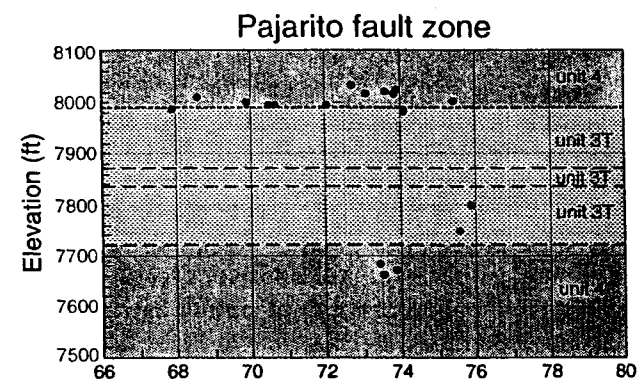
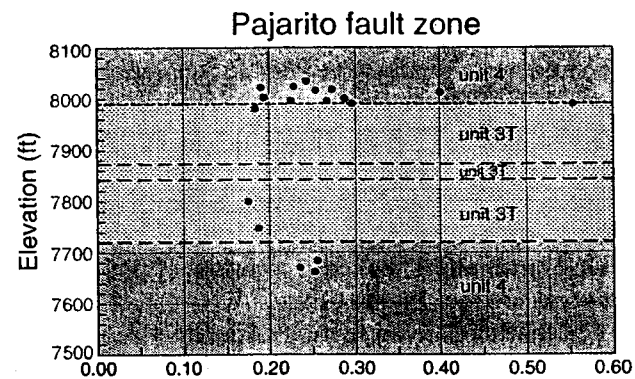
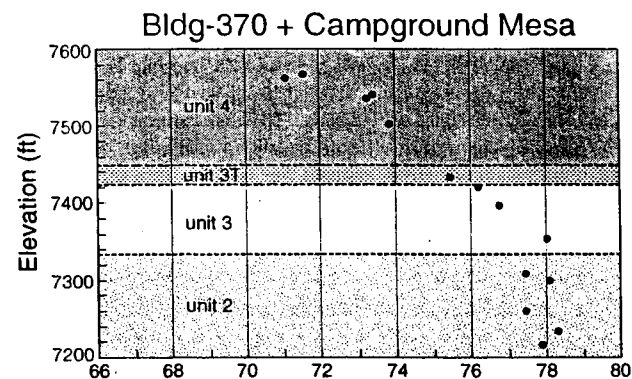
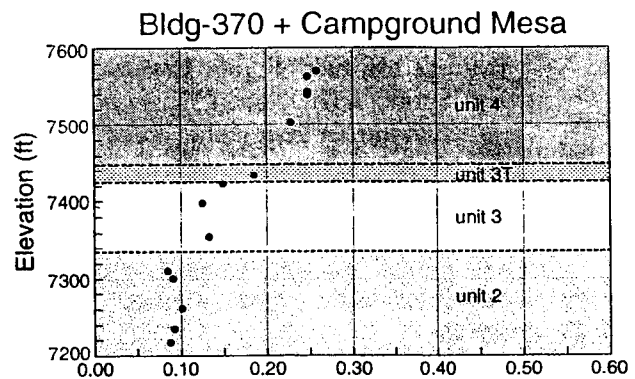
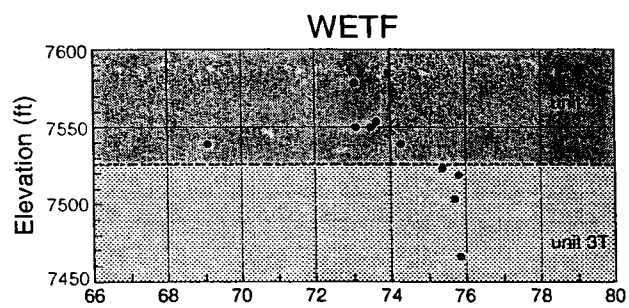
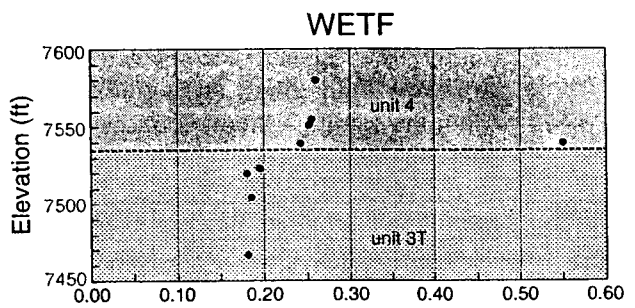


**Figure 10.** a) Variation in  $\text{TiO}_2$  with respect to elevation for samples from WETF, Building 370 and Campground Mesa, Pajarito fault zone, and Pajarito Canyon (see figures of Appendix A for locations). b) Variation in  $\text{SiO}_2$  for samples from same sites. The long dashes represent faults.

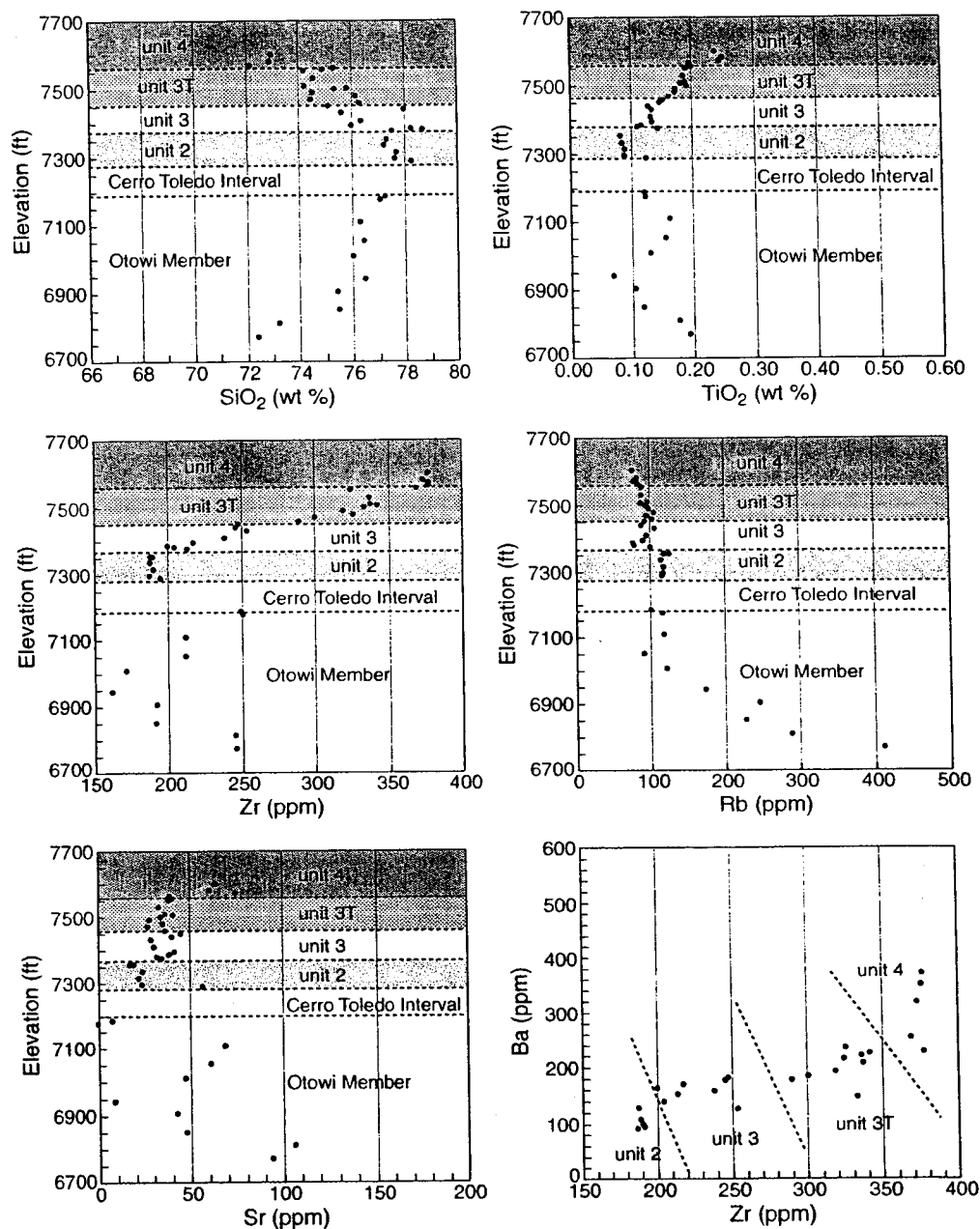


Figure 11. Chemical variation with respect to stratigraphy and elevation for samples from core hole SHB-3 (Figure 4 and Plate 1).

concentrations of  $\text{SiO}_2$  increase and Rb decrease up section in the Otowi, although the Otowi Member samples reveal a reversal of chemical trends with respect to stratigraphic position and concentrations of  $\text{TiO}_2$ , Zr, and Sr. Tshirege Member samples show systematic variations from a high silica to a slightly lower silica end member toward the top of the section. Trace element plots show similar trends for the upper Otowi and Tshirege members (Figure 11). Unit 1 of the Tshirege Member is absent from SHB-3. Unit 1, however, is present in borehole R-25 about 1.3 miles to the northeast and at borehole 49-2-700-1 at TA-49 about 3 miles to the southeast (Figure 12;

ically complete hole that has only a thin surge separating the two units, and shows a fairly exact correlation of the stratigraphic picks based on petrography with the geochemistry.

The geochemical data reveal an unusual component of Unit 4. The stratigraphic sequence exposed on the north side of Water Canyon (south of the WETF) includes three subunits of Unit 4, as discussed above (Section IV.A.1.c.). At this locality the basal subunit of Unit 4 is a slightly welded ash flow, which is about 3 feet thick. This thin basal ash flow contains 68.6 wt %  $\text{SiO}_2$  (mean of two analyses), compared with 73.5 wt % (5 samples;

see Structural Geology, Pajarito Fault Zone and Probable Subsidiary Faults, Section IV. C.1. below).

The geochemistry of samples from the WETF boreholes shows some interesting details. In most of the boreholes, the complete stratigraphic exposure afforded by continuous core reveals a sequence of bedded ashes and crystal-rich surges in a ten foot-interval separating what are petrographically obvious Unit 4, with conspicuous crystal clots, and Unit 3T (Figure 13). The ash and surge sequence does not exhibit hand specimen petrographic characteristics typical of either Unit 4 or 3T, whereas it has variable geochemical affinities. For example, in WETF-1 the entire ash and surge sequence has the geochemical traits of Unit 4; however, in WETF-4 the geochemical boundary between Units 3T and 4 occurs about 3 feet above the base of the sequence. WETF-6 is the only stratigraphic-

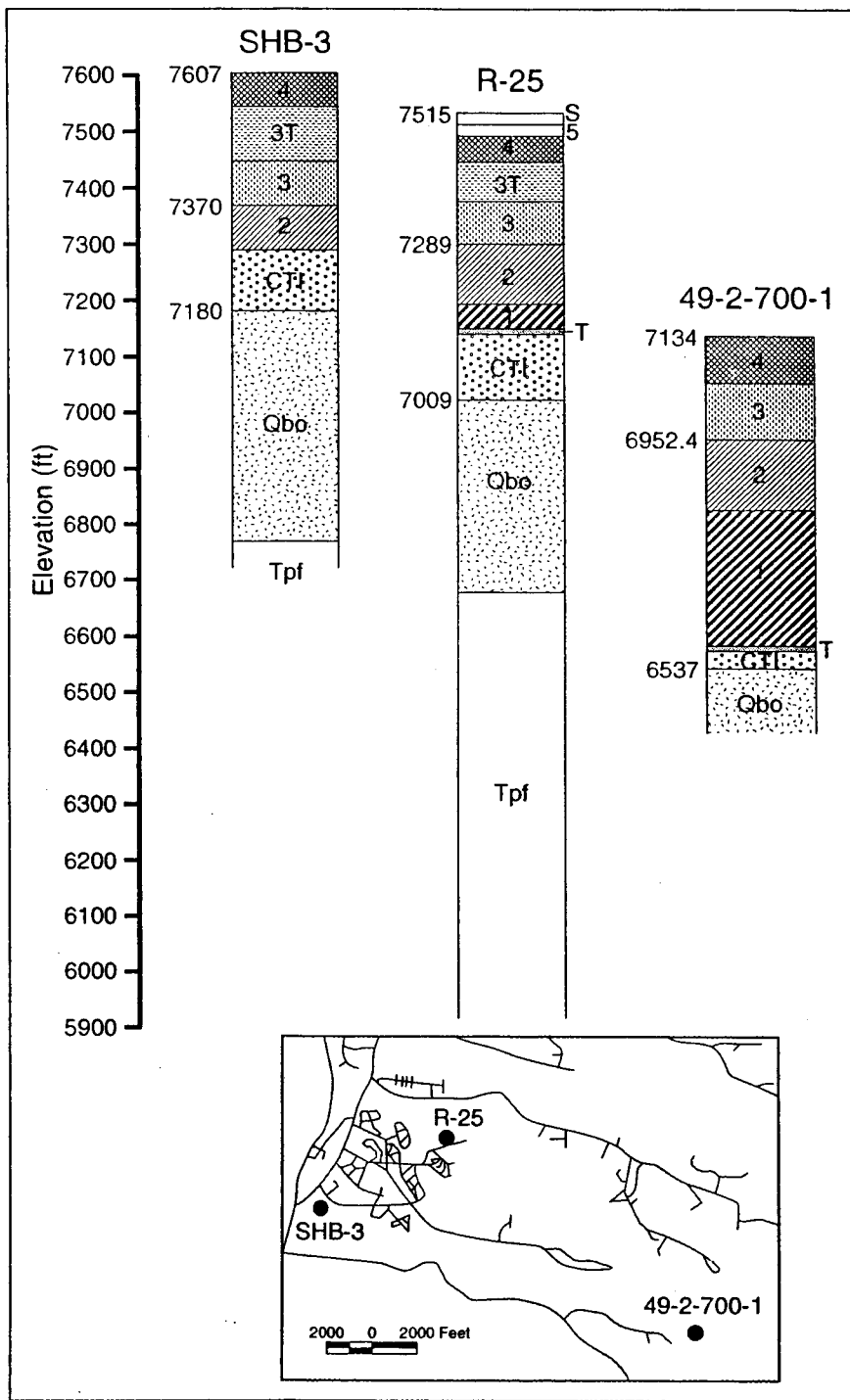


**Figure 12.** Stratigraphy of boreholes SHB-3 (Gardner et al., 1993, and this report), R-25 (Environmental Restoration Project, in preparation), and 49-2-700-1 (Stimac et al., 1998). Units labeled 1, 2, 3, 3T, 4, and 5 are within Tshirege Member (see text for discussion). Other symbols: Tpf, Puye Formation; Qbo, Otowi Member of Bandelier Tuff; CTI, Cerro Toledo interval; T, Tsankawi pumice; S, soil. The inset map shows locations.

s.d. = 0.5) for the rest of the overlying Unit 4 samples, and has distinctively high titanium ( $\text{TiO}_2$  greater than 0.5 wt %) and barium concentrations (450 to 600 ppm). Data are preliminary, but similar chemical anomalies, highlighted by unusually high

titanium for the Bandelier Tuff (generally greater than about 0.3 wt %), were captured at the base of Unit 4 in the Pajarito fault zone section (Figure 10) as well as in the bedded ash and surge sequence at the base of Unit 4 in most of the WETF boreholes (Figure 14). Thus, it appears that basal portions of Unit 4 can exhibit dacitic whole rock chemistry; however, it is problematic that we do not see this chemical anomaly everywhere, and that it has been detected in variable lithologies.

Microprobe analyses for major elements (normalized to 100 total wt % oxides) were obtained on glass from twenty samples of ash and pumice from the Otowi Member, the Cerro Toledo Rhyolite, and the Tshirege Member in Pueblo and Los Alamos canyons, borehole SHB-3, and the south side of Water Canyon on Campground Mesa (Appendix C). Most samples from the Otowi Member and the Cerro Toledo Rhyolite plot in distinct clusters with respect to CaO, FeO, and  $\text{Al}_2\text{O}_3$  but are scattered with respect to  $\text{TiO}_2$  (Figures 15a and 15b). The sample of Guaje pumice has distinctly higher  $\text{SiO}_2$  than glasses from other units in the Otowi Member and the Cerro Toledo Rhyolite. Two samples from the middle and uppermost tephra layers of the Cerro Toledo Rhyolite (Figure 15b) are particularly distinctive. Microprobe analyses of glass, therefore, appear to be useful in distinguishing pumice units within the Cerro Toledo Rhyolite and in differentiating Guaje Pumice from other pumice beds with which it might be confused.

Samples from the Tshirege Member (three samples of Unit 4, and one sample each of Unit 1g and the basal Tsankawi pumice bed) show scatter with respect to CaO, FeO,  $\text{Al}_2\text{O}_3$ , and  $\text{TiO}_2$  (Figure 15c). Samples from a road cut along State Road 4 on Campground Mesa between mile markers 50 and 51, and from

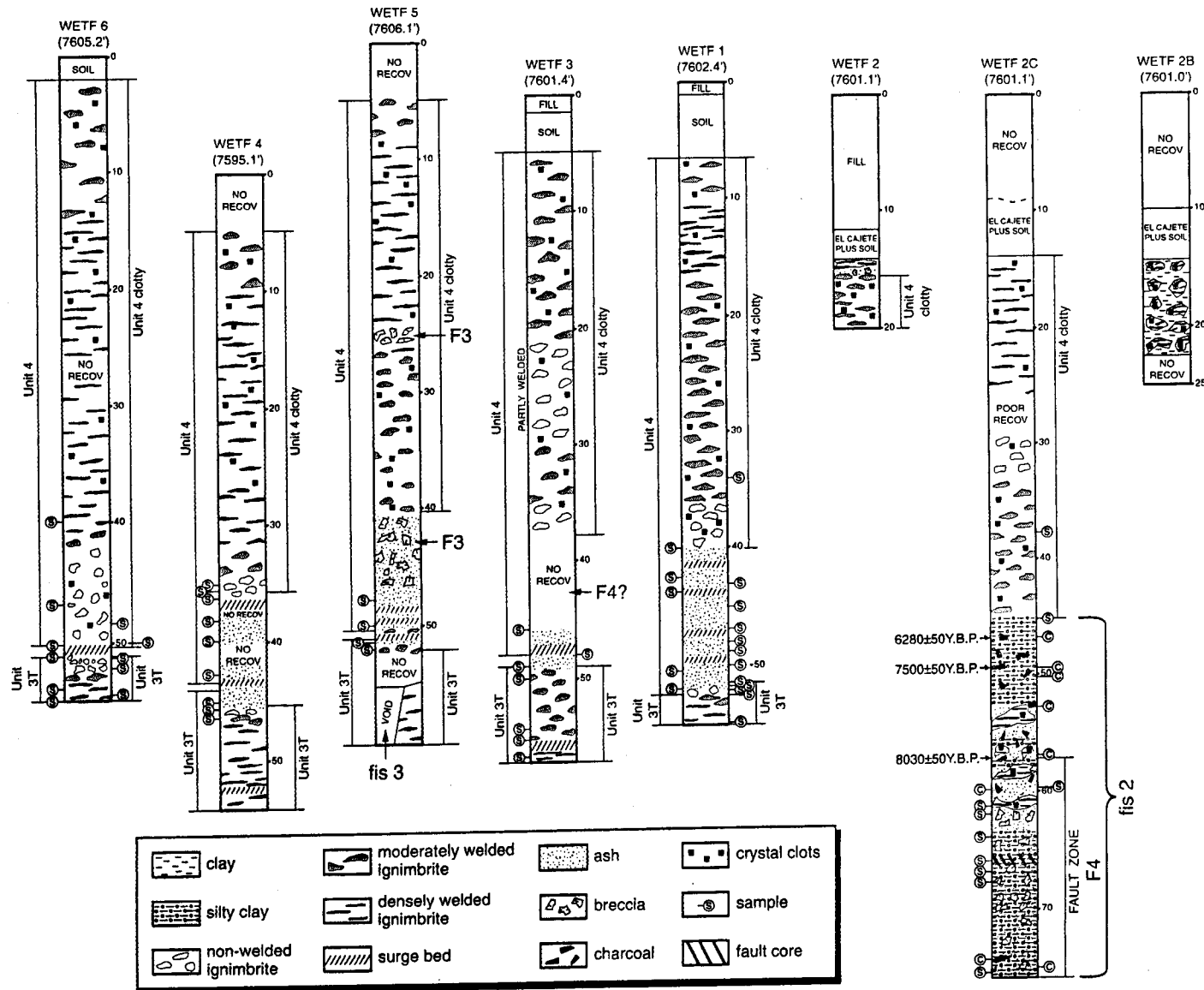


Figure 13. Stratigraphy of boreholes at WETF (locations in Figure 4). Boreholes projected into an east-west line of section and aligned vertically by elevation at top of borehole. The Qbt unit labels on the right side of each column are based on hand specimen petrography, whereas those on the left side are based on geochemical data. C = charcoal sample; S = geochemistry sample; fault and fissure symbols as on Plate 1.

### SHB-WETF Boreholes

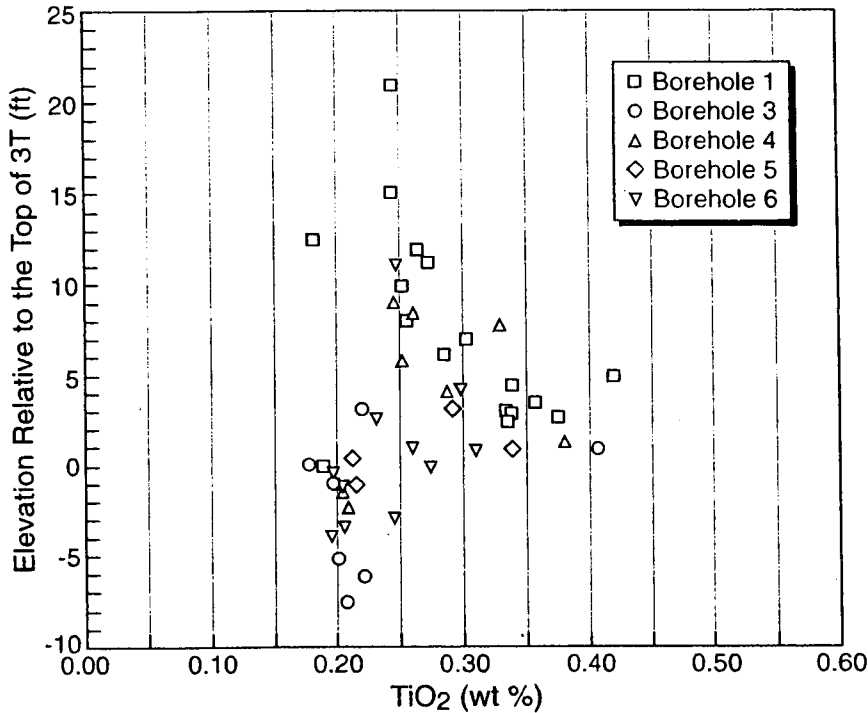


Figure 14. Variation in TiO<sub>2</sub> with respect to normalized elevation in WETF boreholes. Samples are plotted by elevation with respect to the top of unit 3T. Thus samples within unit 3T plot below 0 ft elevation, and samples within unit 4 plot above 0 ft.

exposures between mile posts 51 and 52 (Appendix A) were analyzed for whole-rock and glass compositions to examine the variety of Tshirege Member Unit 4 subunits (Figure 15c). Unit 4 exposed at the road cut consists of a white to beige, vitric, nonwelded ash-flow tuff (sample TA-16-303), overlain by a crystal-rich, dark pink, densely welded, devitrified ash-flow tuff, containing 5% to 10% dark brown to red fiamme with large (up to 2 cm) clots of quartz and feldspar. The top eastern tip of the road cut is marked by a wedge of vitric, densely welded tuff with large, black glassy fiamme with more abundant crystal clots (sample TA-16-302). Glass chemistry of pumice clasts from the nonwelded ignimbrite and the wedge of densely welded, vitric fiamme ignimbrite at the road cut and another coarse-pumice dominated ignimbrite unit (sample TA-16-304), from about 500 feet south of the road cut were obtained with the electron microprobe. The two flow units from the road cut have similar glass chemistry; however, the coarse-pumice ignimbrite has a glass composition distinct from the other two (Figure 15c).

CaO and Al<sub>2</sub>O<sub>3</sub> concentrations in Tshirege Member Unit 4 glass are generally lower than in whole rock analyses. Petrographic examination of samples of Unit 4 shows abundant feldspar crystal

clots, cored with plagioclase, which contribute to the higher concentrations of CaO and Al<sub>2</sub>O<sub>3</sub> in whole-rock XRF analyses. Similarly, FeO and TiO<sub>2</sub> concentrations in Unit 4 glass are lower than in whole rock analyses, suggesting that at least some of the FeO and TiO<sub>2</sub> reside in phenocrystic ferromagnesian minerals and possibly lithic fragments. However, titania concentrations in glass samples analyzed using the electron microprobe are quite variable, spanning in some cases most of the range of variability identified by whole rock XRF analyses (Figure 15c and Figure 10).

Glass compositions hold promise for correlation purposes particularly in the fallout tephra of the Otowi Member and the Cerro Toledo Rhyolite. Hampering application of glass composition as a correlation tool for units of the Tshirege Member is widespread devitrification. For the most part, primary glass appears to be only

preserved in the lower portions of Unit 1 and in Unit 4. Nevertheless, there is some indication that different subunits of Unit 4 have distinct glass geochemistry. Thus, microprobe analyses may prove useful in correlating subunits within Unit 4.

#### IV. C. Structural Geology

The area of TA-16 is structurally complex. Units of nonuniform thickness, commonly subtle expressions of deformation, and nonplanar contacts complicate interpretations; furthermore, these factors make extrapolations of structures into areas of no useful bedrock exposure difficult. Generally, the structural geology of TA-16 is dominated by the Pajarito fault zone. While some structures are related to the Pajarito fault zone more clearly than others, it can be argued that virtually every structure that we have identified is part of a broad zone of deformation related to the Pajarito fault zone. North-trending faults with clear Pajarito fault zone affiliation have been mapped to within about 700 feet west of WETF (F1, Plate 1). These faults exhibit down-to-the-west sense of displacement and form a broad zone of deformation bounding the eastern side of a graben (G1, Plate 1) at the base of the main escarpment. Two north-northeast trending structures, a concealed fault (F2) and a lineament

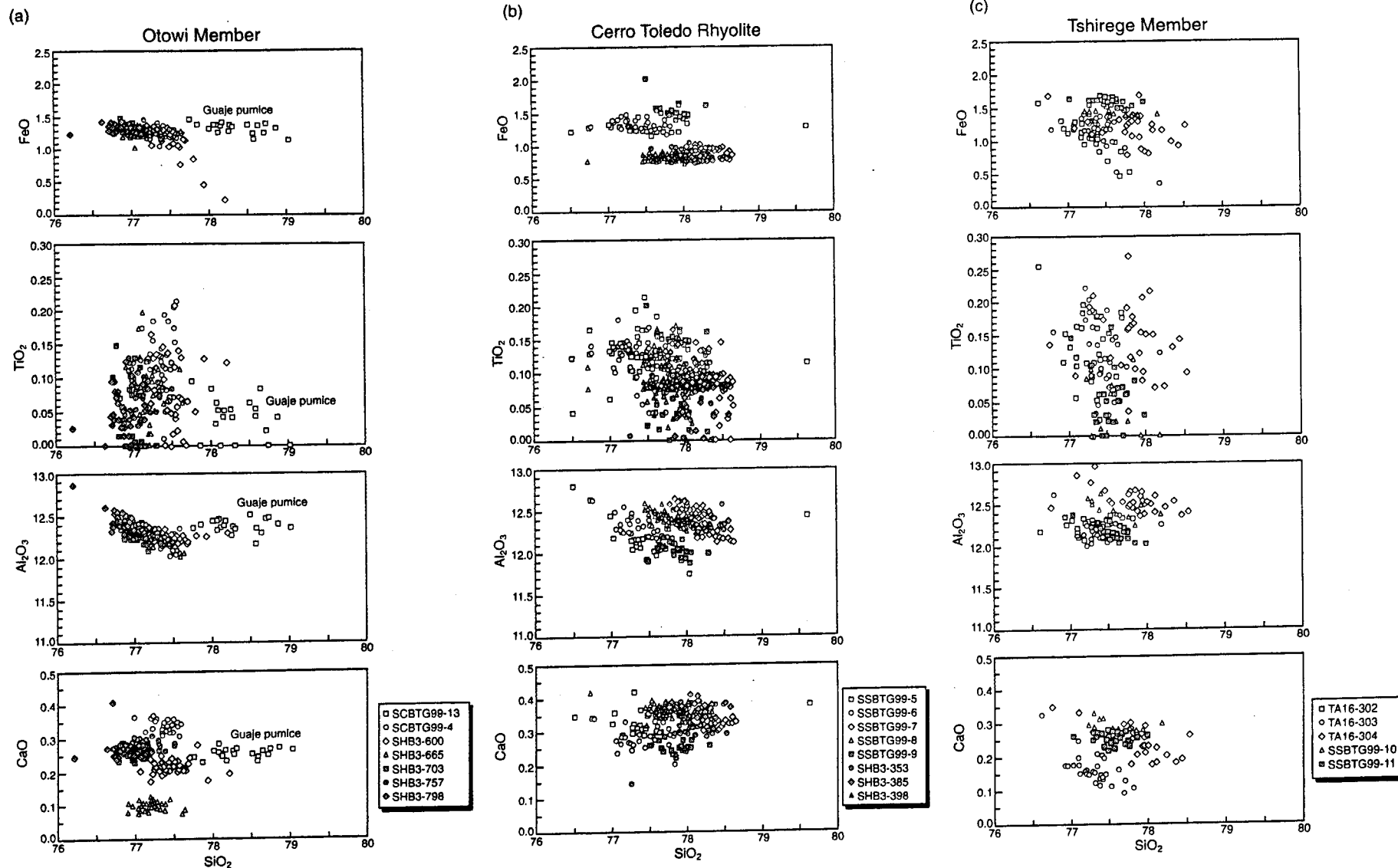


Figure 15. Major element variation diagrams for glasses from a) the Otowi Member, b) the Cerro Toledo Rhyolite, and c) the Tshirege Member. Samples numbered as follows: SCBTG99-n and SSBTG99-n from Pueblo Canyon; SHB3-n from borehole SHB3 (Gardner et al., 1993), where n is depth (ft) in borehole; and TA-16-x from Campground Mesa, where x is a sequential sample number.

with discontinuous, open fissures (fis 1, Plate 1), probably define the broad eastern side of the northward continuation of this graben (G2). Within this broad zone of deformation that appears to bound the eastern side of graben G2, drilling identified two faults (F3 and F4) and two more fissures (fis 2 and fis 3) near WETF. Another set of major structures trends northeast and is expressed in the bedrock as three larger displacement (generally greater than 20 feet on Bandelier Tuff) monoclines (M1, M2, and M3) and one relatively small displacement fault (F5). The relations of these northeast-trending structures to the Pajarito or other structures to the north and east are unclear, but proximity to the Pajarito fault may imply that they are an integral part of the same fault system. One small fault zone (F6) that exhibits a somewhat unusual west-northwestern trend cuts bedrock in the small drainage that separates buildings 410 and 370. A series of small faults (for example, F7) with strikes nearly parallel to the north rim of Water Canyon are likely related to mass wasting of large blocks of bedrock.

#### *IV. C. 1. Pajarito Fault Zone and Probable Subsidiary Faults*

The most obvious part of the Pajarito fault zone in the vicinity of S-Site is the greater than 400 foot-high escarpment formed by a large, north-trending, faulted monocline (M4, Plate 1) that exhibits a down-to-the-east displacement of the Tshirege Member of the Bandelier Tuff of magnitude comparable to the scarp height. Elements of the monocline are evident in the road cuts along State Road 4 where, as one climbs the scarp, tilted and toppled blocks of densely welded Bandelier Tuff are exposed on the steep limb of the fold. At the top of the scarp along the highway road cuts, a large (15 to 25 feet wide) filled tensional fissure (fis 4) is exposed, marking the upper hinge zone of the monocline. The steep limb of the monocline is cut by small faults. McCalpin (1999) excavated a trench (T3, Plate 1) on one of these small faults near the lower hinge zone of the monocline beneath the sharp hairpin turn in State Road 4. The trench revealed a complex zone of faults but structural relations in the trench indicate that there must be additional down-to-the-east faults east of the trench site that are apparently buried by young fan deposits. North of Water Canyon the main escarpment of the Pajarito fault zone has been extensively modified by mass wasting. Landslides, including block slides and nested slides, in this area are cut by very strong aerial photograph lineaments and other linear features which, for a variety of reasons, cannot be identified as faults with certainty.

Geochemical correlations of Bandelier Tuff units across the main escarpment of the Pajarito fault zone (Figure 3), indicate that stratigraphic separation on the tuff exceeds 400 feet. Similar correlations to Tshirege Member tuff units in SHB-3 and Water Canyon, south of WETF, suggest apparent net stratigraphic separations of about 460 to 470 feet, based on contact elevations relative to those of units at the top of the main escarpment. Along strike to the north, where the fault zone crosses upper Pajarito Canyon (north of the map area), stratigraphic separation on the Tshirege Member of the Bandelier Tuff is about 260 feet across the main escarpment.

East of West Jemez Road, several down-to-the-west faults (for example, F1 and F8, Plate 1) are about 500 to 1500 feet east of the base of the main Pajarito fault escarpment. These faults are antithetic to the main portion of the Pajarito zone, and form the eastern side of a graben (G1). The maximum offset on one of these north trending antithetic faults (F8) occurs immediately south of Water Canyon, where the base of Qoal is apparently offset 60 feet or more (Plate 1). At this location the fault is not exposed, but lies concealed beneath young alluvium in a north trending drainage. On strike with this drainage immediately north of Water Canyon, the base of Qoal is offset approximately 20 to 25 feet, suggesting that the amount of offset decreases rapidly to the north. However, it is notable that West Jemez Road here is located in a major north-south drainage that truncates both the Bandelier Tuff and an intermediate-age fan (Qfi), and the drainage and road could conceal an additional fault trace (F9) with a similar amount of displacement. Additional down-to-the-west faults (for example, F1) with a maximum of 4 feet of displacement on bedrock and Qoal occur in this area both north and south of Water Canyon, documenting a relatively broad zone of deformation associated with the eastern margin of graben G1. Net down-to-the-west deformation of the Qoal-Qbt contact into the graben across these faults, together with contributions from monoclines M1 and M2 (discussed below, Section IV.C.2), is likely greater than 100 feet (Figure 16).

An additional relatively large-displacement down-to-the west fault, fault F2 on Plate 1, is inferred as part of the northward continuation of the eastern side of this graben. The fault is mostly concealed beneath anthropogenic works, but it is marked by an abrupt disappearance of exposed bedrock at the surface, a substantial thickness of post-Bandelier sediments west of its trace, and a topographic anomaly at its northern end. About 500 feet east of the former steam plant this fault lies concealed beneath colluvium. Local topography and exposures

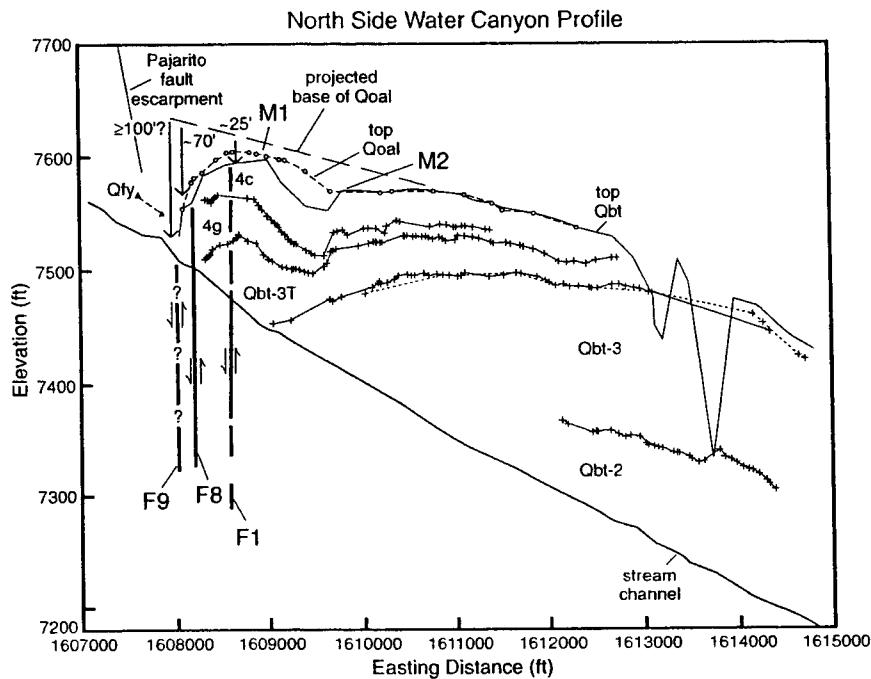


**Figure 16.** Composite profile along north side of Water Canyon, projected to an east-west plane. The surveyed bedrock contacts are shown with other data from topographic maps and surficial mapping. Inferred minimum amounts of net deformation east and west of the down-to-the-west faults and monoclines use the base of Qoal as an approximate datum. Structural features are labeled as in Plate 1. Qbt-n = Tshirege Member unit; 4g = fines depleted ignimbrite of Unit 4; 4c = crystal clot rich ash-flow tuff of Unit 4.

of Qoal to the east and west indicate that this area consists of an ancient fan derived from Cañon de Valle before development of the main Pajarito fault escarpment, which has been subsequently buried by colluvium and pumice. Evidence for faulting consists of an anomalous low saddle interrupting the slope, and a topographic profile across this saddle suggests a minimum of about 30 feet of offset here (Figure 17 and Plate 1). Because the area west of the saddle probably continued to accumulate colluvium after faulting, the actual total offset here likely exceeds 30 feet. West and north of WETF, Unit 4 of the Bandelier Tuff is exposed at the surface with spotty, thin colluvial cover. Farther west, exposed bedrock vanishes along a north-northeast trending line that is on strike with the low saddle near the steam plant and is coincidentally covered by a road. Geotechnical reports for buildings

in and around the administration area of S-Site (S-Site Admin area, Plate 1) describe more than 50 feet of alluvial material filling a "graben" immediately west of this road; thus, there must be an eastern boundary fault for the graben that has a down-to-the-west sense of displacement somewhere close to the line defined by the disappearance of bedrock.

Parallel to fault F2 and about 1700 feet east of it, there is a prominent north-northeast trending fissured lineament (fis 1) that extends for about 2500 feet through TA-16. It is marked by a drainage that is roughly perpendicular to most other drainages in the area and by a series of open fissures in bedrock and closed depressions. One active sinkhole in colluvium that lies along the lineament is inferred to be generated by the loss of material into another open subsurface fissure. This feature projects south to near the northern end of one of the faulted

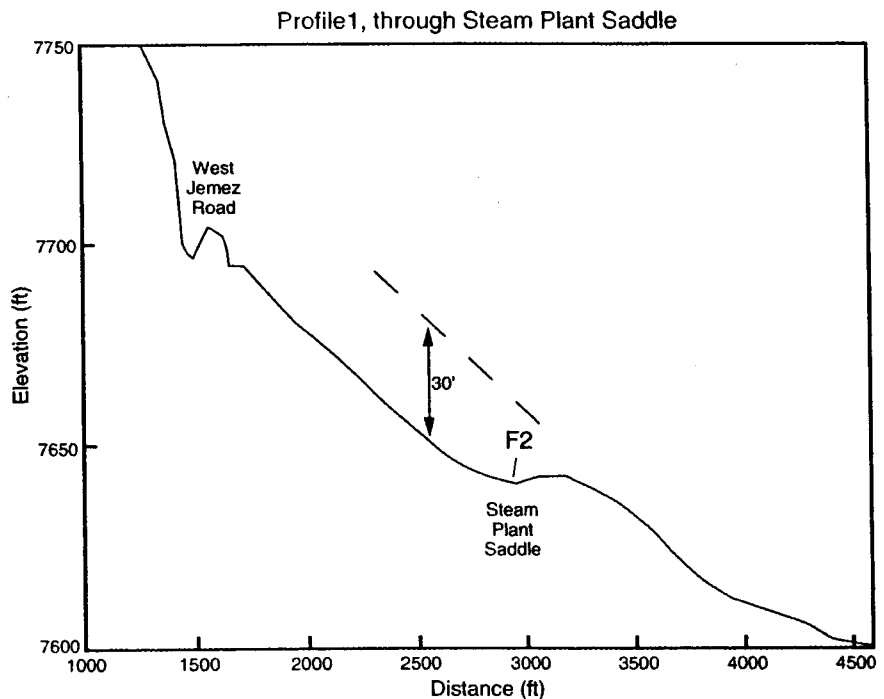


**Figure 17.** Topographic profile across a Qoal fan surface east of the steam plant. The saddle in the topography suggests that the surface is cut by a concealed down-to-the-west fault that has been buried by an unknown thickness of colluvium. The profile indicates minimum fault displacement of the topographic surface, projected from the east as a dashed line, of about 30 feet down-to-the-west. The line of profile is plotted on Plate 1.

monoclines (M2) in Water Canyon about 1000 feet southeast of WETF, and may represent a northern extension of the same zone of deformation; however, the strikes of the two structures differ by about 30° and field evidence indicates no clear connection of the structures. We have not been able to document displacement of bedrock across the southern portions of the fissured lineament, but, at a minimum, flexural deformation has been of sufficient magnitude to interrupt the normal east-southeast drainage pattern and divert surface runoff to the south-southwest. A topographic profile across the northern part of the fissured lineament suggests about 7 feet of net down-to-the-west deformation of the contact between Qoal and Qbt at that location (Figure 18 and Plate 1). Rogers (1995) mapped this feature as a down-to-the-east fault, but, as mentioned above, we can only infer down-to-the-west displacements across it. Significantly, however, the fissured lineament is parallel to the local trend of the Pajarito fault escarpment and to the trend of fault F2, discussed above, and may locally mark an eastern margin of the zone of young deformation associated with the Pajarito fault.

Parallel to both the fis 1 fissured lineament and the F2 fault is a 400-foot long down-to-the-east step (F10) in tuff northeast of WETF about 700 feet. This feature may also represent a concealed fault, although exposures are poor and confirmation would require subsurface exploration.

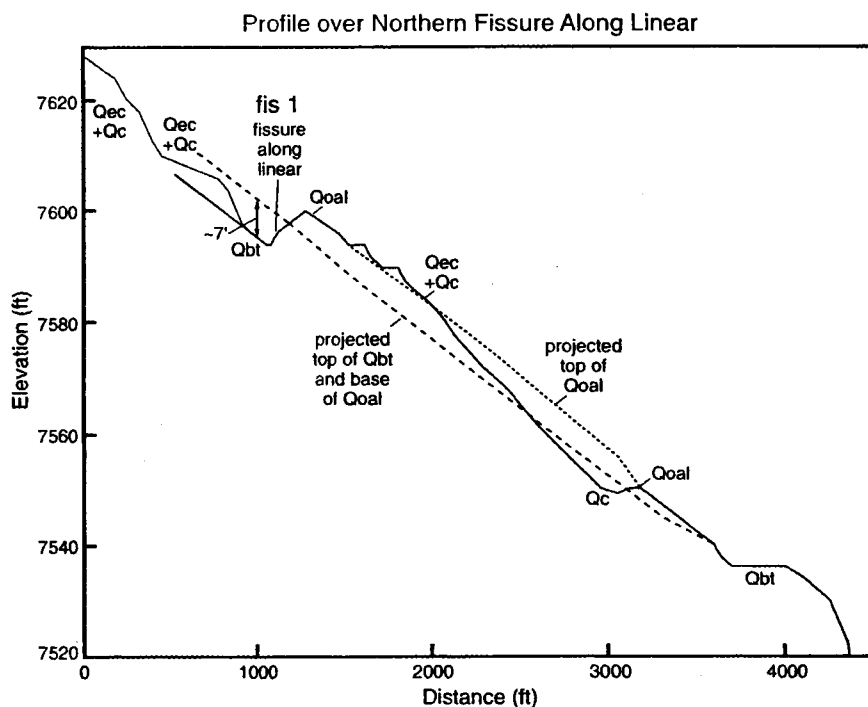


Figure 18. Topographic profile across the fissured lineament (fis 1 on Plate 1). The inferred amount of net deformation across the lineament uses the base of Qoal as an approximate datum. The line of profile is plotted on Plate 1.

Stratigraphy and structure logged in the WETF boreholes (Figure 13) indicates general eastward dips on the Unit 3T-Unit 4 contact and the presence of at least two normal faults and two fissures (faults F3 and F4, fissures fis 2 and fis 3 on Plate 1), all of which intersect boreholes. As constrained by relations among the boreholes, both faults strike north-northeast. The western fault (F3, Plate 1), likely two parallel faults or splays of one fault, intersects borehole WETF-5 in two places as shown by zones of cataclastic breccia at about 25 and 41 to 47 feet deep. The contact of Units 3T and 4 is below these fault intercepts and is, assuming F3 to be a normal fault, on the upthrown or footwall block of the fault in WETF-5. In boreholes WETF-4 and SHB-3 the Unit 3T-Unit 4 contact is at approximately the same elevation, but lower than in WETF-5. These relations indicate that the contact in WETF-4 and SHB-3 is on the downthrown or hanging wall fault block. The Unit 3T-Unit 4 contact in borehole WETF-6 is also likely on the same hanging wall block, but slightly updip. Fault F3, therefore, displaces the Unit 3T-Unit 4 contact about 4 feet down-to-the-west, and, if it is a normal fault, which is highly likely, it dips to the west. There are some features of SHB-3 that are important to consider in evaluating the potential magnitude of displacement on fault F3: 1) the absence of Unit 1, which is about 40 feet thick in borehole R-25, from the base of the Tshirege sequence (Figure 12); 2) the unusual thickness of Unit 3T, by at least 30 feet (Figure 19), compared to exposed thicknesses in surrounding canyons; and 3) the low elevation of the top of Unit 3, by about 30 or more feet, compared to its updip projection from exposures to the east (Figure 20). Projecting fault F3 at a reasonable dip of 70 to 80 degrees to the west causes it to intersect SHB-3 at the base of Unit 2, where there was poor core recovery, which suggests that the absence of Unit 1 in SHB-3 may be due to faulting. Faulting the Tshirege section in SHB-3 by about 30 feet of down-to-the-west movement could also accommodate the low elevation of the top of Unit 3. The thickness of Unit 3T in SHB-3 implies that the hole was drilled into a paleohill formed by more source-proximal deposition of flow units. Thus, downfaulting the paleohill by about 30 feet on fault

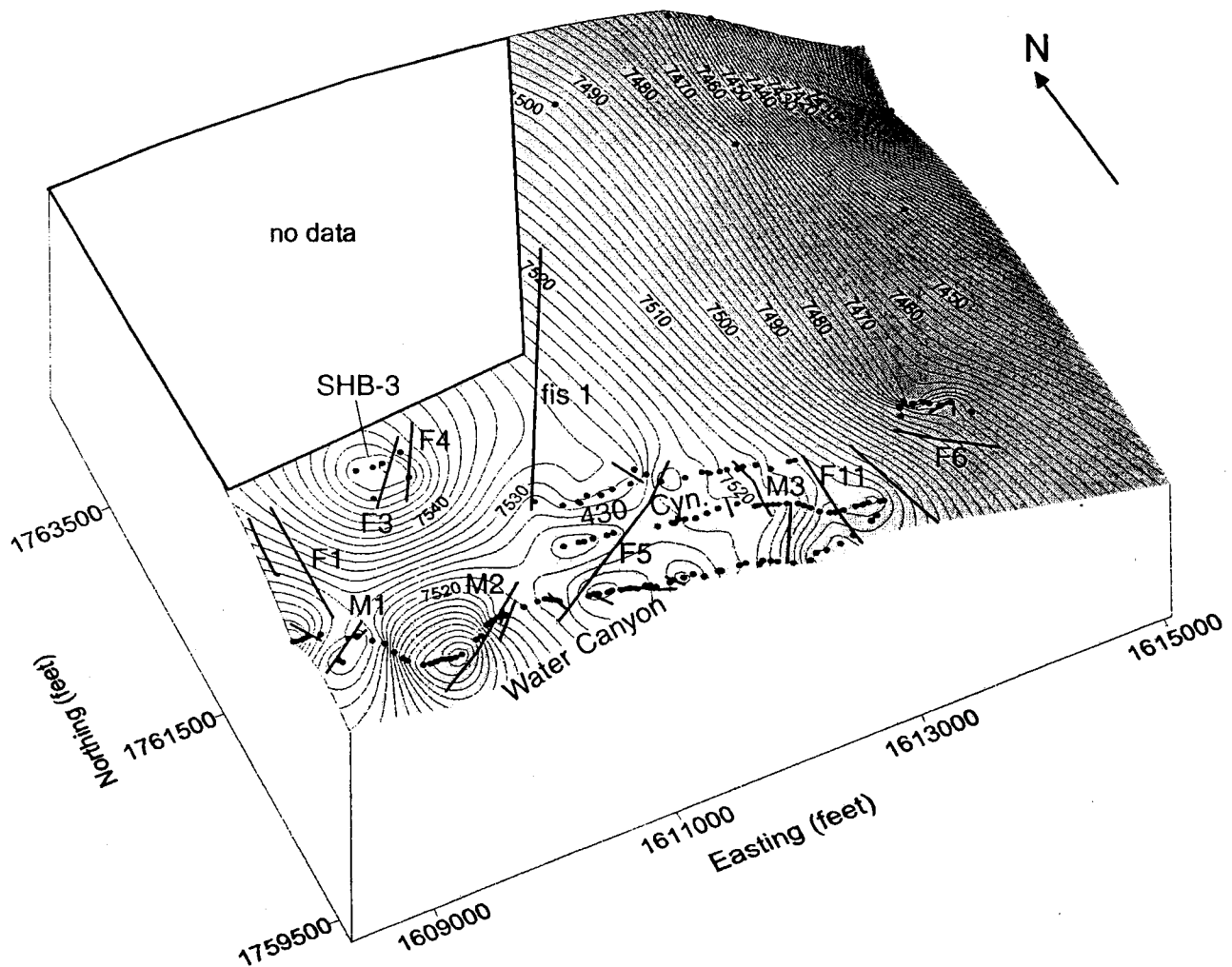


Figure 19. Oblique 3-dimensional view of contoured upper surface of Unit 3T. Note the high on the surface caused by thickening of Unit 3T in the vicinity of borehole SHB-3 (see text for discussion). The contour interval is 10 feet. The filled circles are surveyed points on the Unit 3T-Unit 4 contact. Faults, fissures, and monoclines are as labeled on Plate 1.

F3 yields an apparent displacement of the Unit 3T-Unit 4 contact of only about 4 feet.

WETF-5 also encountered an open fissure (fis 3) in the bottom 7 feet of the hole. The open fissure network was extensive enough to emanate subterranean winds and cause difficulties in backfilling the borehole. During attempts to bridge the fissure to facilitate backfilling, it was noted that low density objects dropped into the borehole, such as empty soda cans, were consistently wafted out of downhole sight in a N35E direction. This trend is very similar to the strike of surrounding faults and fissures (for example, F2 and fis 1) and probably represents the strike of WETF-5's open fissure.

Borehole WETF-2C also intersected a fissure and a fault (fissure fis 2 and fault F4 on Plate 1).

WETF-2C first penetrated about 45 ft of Unit 4 of the Tshirege Member of the Bandelier Tuff. At this depth in the core, tuff is underlain by finely bedded sands, silts, and clays with abundant charcoal (Figure 13). The contact between tuff and sands is horizontal, and no disruption of layering in the bedded sediments is evident. Radiocarbon dates obtained from charcoal in this interval give internally stratigraphically consistent dates of  $8030 \pm 50$ ,  $7500 \pm 50$ , and  $6280 \pm 50$  radiocarbon years BP at depths of 56.5, 49.0, and 46.5 ft, respectively. We interpret these laminated sediments as deposits of streams and standing water (ponds) in an open fissure (fis 2, Plate 1) created by offset and opening on a high angle normal fault. It is clear that the fissure fill was deposited after the fissure-opening

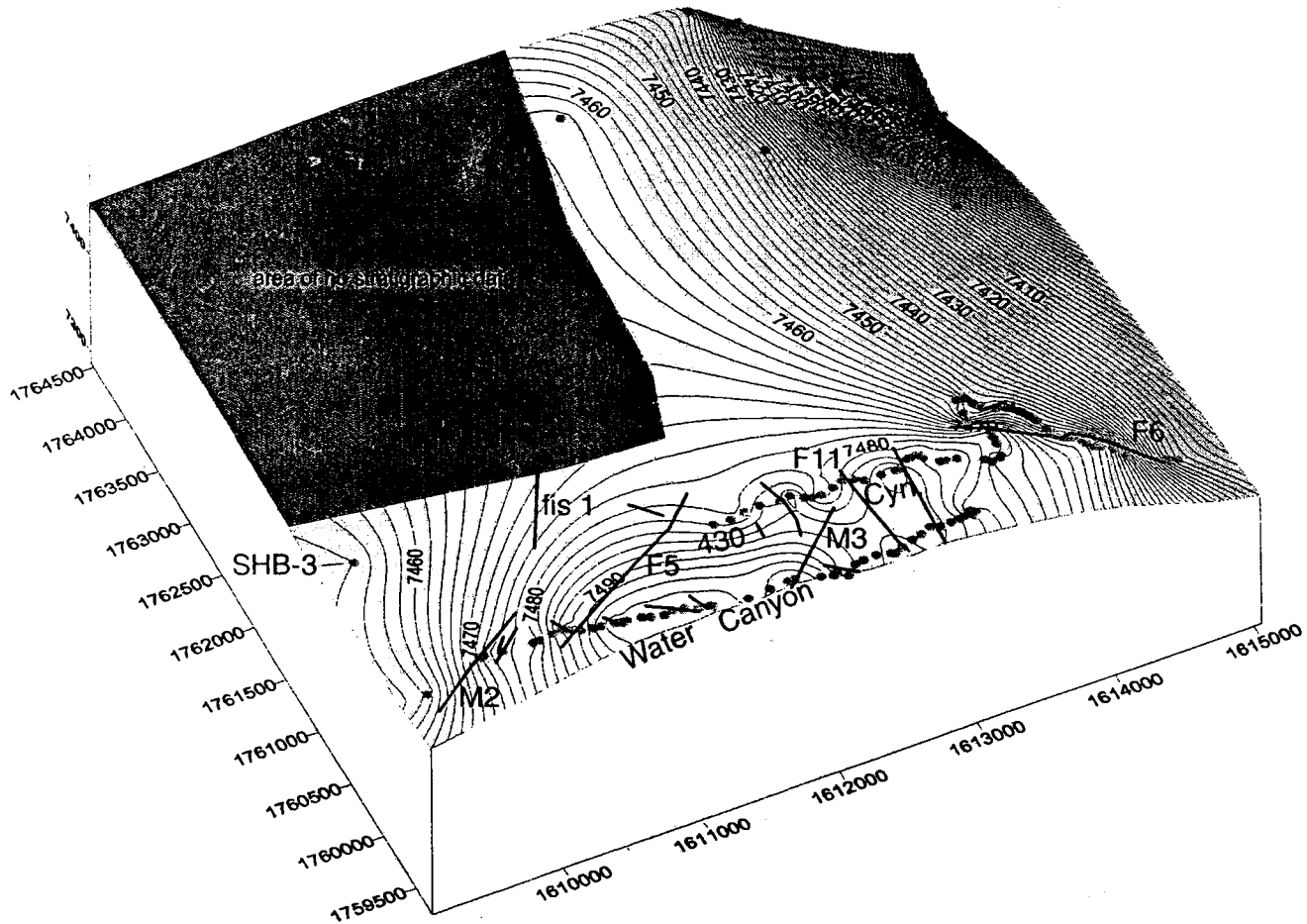


**Figure 20.** Oblique 3-dimensional view of contoured upper surface of Unit 3. Note the anomalously low elevation of the top of Unit 3 in borehole SHB-3 (see text for discussion). The contour interval is 10 feet. The filled circles are surveyed points on the Unit 3-Unit 3T contact. Faults, fissures, and monoclines are labeled on Plate 1.

rupture occurred on a fault that underlies the laminated sediments and that the fissure fill sediments were also faulted in at least one younger rupture (see below).

Fault F4 (Plate 1), the eastern fault at WETF, intersects borehole WETF-2C as a zone of cataclastic deformation between depths of about 57 feet and 77.5 feet (total depth of the borehole) and deforms fissure fill sediments discussed above (Figure 13). Clay-rich sediments at about 65 feet exhibit foliated clays which dip at about  $60^\circ$  (Figure 21). These foliated clays, examined by petrographic and scanning electron microscopy, show evidence for cataclasis, including weak dimensional preferred orientations of sand-sized grains, well-developed preferred orientations of clay minerals, as well as parallel grooves in clay (Figure 22). Cataclastic lineations are subparallel to the presumed slip direction. Laminated sediments are deformed above the foliated clays to a depth of 57 ft and below them to total depth of the borehole. The deepest  $^{14}\text{C}$  date obtained from laminated sediments in WETF-2C lies 0.5 ft above the highest occurrence of sediments

deformed by fault F4. Thus, available data do not constrain the paleoseismic history very well. A fissure-opening rupture or ruptures occurred sometime prior to  $8^{14}\text{C}$  ka. The fissure fill sediments may have been faulted in a paleoseismic event or events after deposition of the entire sequence (since  $\sim 6^{14}\text{C}$  ka), during deposition of the dated sequence (6 to  $8^{14}\text{C}$  ka), or immediately before deposition of the dated part of the sequence (prior to  $\sim 8^{14}\text{C}$  ka).

The elevation of the Unit 3T-Unit 4 contact is very similar among boreholes WETF-1, WETF-3, and WETF-5, implying that the contact is within the same fault block in all three holes. These relations suggest that fault F4 is an east-dipping normal fault that intersects WETF-3 above the Unit 3T-Unit 4 contact. Between depths of about 37 feet and 46 feet in WETF-3 is a zone of no core recovery that produced enough water to cause drilling difficulties with the air-circulating fluid and cuttings. Poor core recovery and water saturation are common in faults characterized by rubble breccia, and, thus, we interpret this zone in WETF-3 as the fault intercept. We have no good stratigraphic markers on either

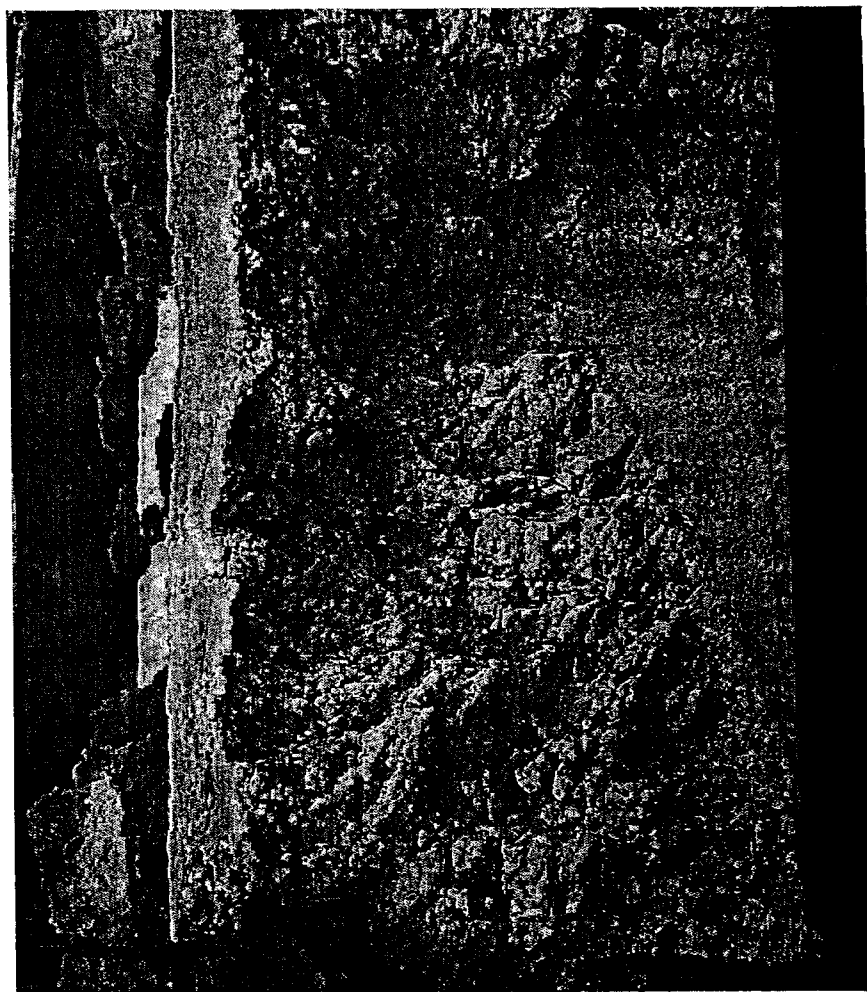


Figure 21. Photograph of steeply dipping, foliated silty clays from 65.6 ft depth in borehole SHB-WETF-2C (location on Figure 4). Intensity of cataclasis suggests that the interval from 65 to 66 ft is the core of a fault. The core diameter is 3.5 inches (about 9 cm).

upthrown and downthrown sides of this fault on which to base estimates of magnitude of displacement on fault F4. Comparing the elevation of the base of Unit 4 in WETF-1 with the lowest recovered intact Unit 4 from WETF-2C suggests at least 6 feet of down-to-the-east movement.

Several small (less than 5 feet of displacement on Bandelier Tuff) north-trending faults cut through both Water and 430 canyons, between Building 430 and Building 410. These faults lie about 4000 to 5000 feet east of the main escarpment of the Pajarito fault zone, and most of them exhibit down-to-the-west senses of displacement. One of these small faults (F11, Plate 1) is a high angle reverse fault at its southern end, based on the trend of its surface trace with respect to topography in Water Canyon, and it appears to truncate one of the northeast trending monoclines (M3, discussed below, Section IV.C.2).

#### IV. C. 2. Northeast Trending Structures within the Eastern Parts of the Pajarito Fault Zone

The bedrock mapping in Water and 430 canyons indicates that there is a broad zone of deformation that extends at least 5000 feet east of graben G1 at the base of the main escarpment of the Pajarito fault zone (Plate 1, Figure 23). The major structures in this broad zone are two northeast trending, down-to-the-west faulted monoclines (M1 and M2) just east of the G1 graben, a northeast trending normal fault (F5) with 6 feet of down-to-the-west displacement on bedrock units, and a northeast trending monocline (M3) with down-to-the-east displacement of about 10 feet on bedrock units. The most prominent of these features are the two faulted monoclines (M1 and M2) near the graben. These structures each offset bedrock contacts more than 20 feet down-to-the-west, but this deformation also includes apparent widespread tilting of the tuff both westward and eastward. The distribution of post-Bandelier deposits and the topography reflect the deformation associated with the eastern of these two monoclines (M2), but provide less

precise definition of the deformation than the bedrock units because of erosional modification (Figure 16). In particular, the topographic expression of the monocline M2 has been subdued by preferential preservation of thick Qoal to the west and erosion to the east. The apparent offset of the base of Qoal across monocline M2 is similar to that indicated by the bedrock contacts, suggesting that most or all of the deformation postdates Qoal. An estimate of the minimum net post-Qoal deformation across monocline M2 of about 25 feet can be made by assuming that the base of Qoal provides an approximately planar datum, and that the eastern occurrences of Qoal are east of the primary deformation (Figure 16). In addition, total down-to-the-west displacement of Qoal across both of the monoclines (M1 and M2) and into the graben at the base of the main escarpment is at least 70, if not greater than 100, feet (Figure 16). The magnitude of

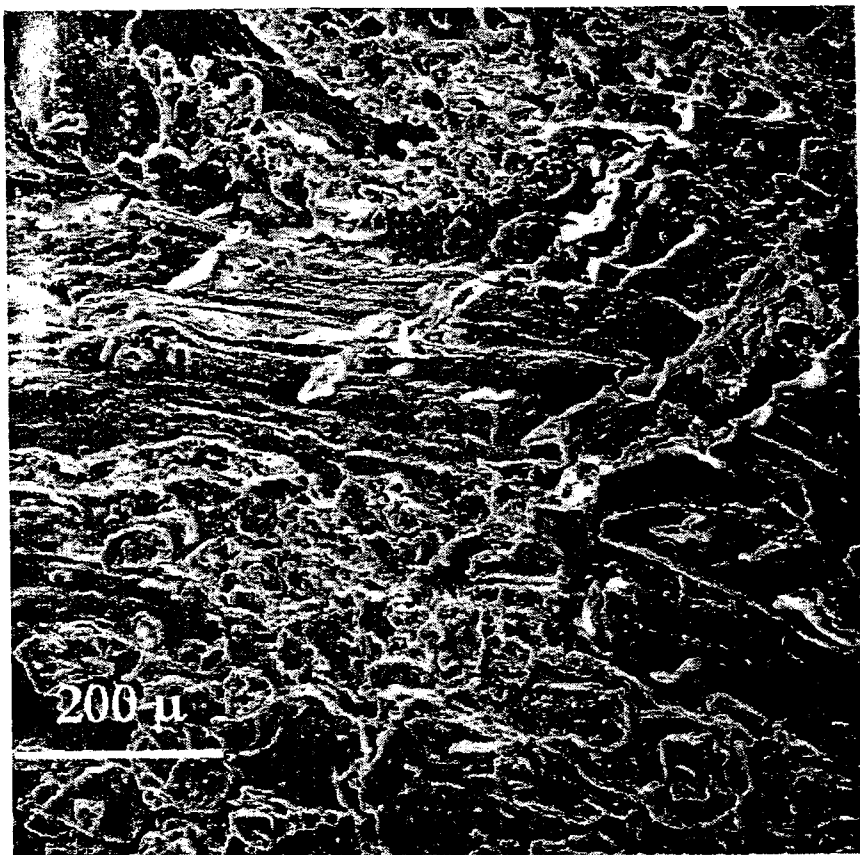


Figure 22. Scanning electron microscope image of clay from 65-66 ft depth in borehole WETF-2C. Lineations and grooves on surface of clay are likely produced by plowing of silt grains during cataclasis.

the deformation in this area could be significantly greater for two reasons. First, the base of Qoal may approximate the original top of the Bandelier Tuff, which in turn may steepen westward because of the thickening of individual units evident in Figure 16, invalidating the assumption of a planar datum. Second, there is some indication in the surveyed bedrock contacts that dips steepen to the east, and that all of the Qoal locations may be within an area of deformed tuff. Both of these conditions would result in an underestimate of the original gradient of the base of Qoal, which in turn would result in an underestimate of total net deformation.

The zone of deformation is less well defined on the south side of Water Canyon than on the north side due to poor exposures of both bedrock and surficial geologic units. However, the available exposures of the tops of both Qoal and the Tshirege Member suggest a flattening to the west that is consistent with westward tilting of an originally eastward dipping surface (Figure 24), similar to that present on the north side of the canyon. This flattening is equivalent to about 20 feet of net down-to-the-west deformation, although this estimate is a minimum because of the same uncertainties

discussed above. Deformation in this area is also suggested by a decrease of about 25 feet in elevation of the mesa top to a prominent low saddle along State Road 4, although there are no exposures to reveal what units underlie the mesa top here and the precise nature of the deformation is uncertain. It is noteworthy, however, that the topographic high at the eastern side of this saddle lies on strike with the upper hinge zone of monocline M2. Similar to relations on the north of Water Canyon, net down-to-the-west displacement of Qoal across this zone of deformation, presumably caused largely by monocline M2, and across fault F8 into graben G1 exceeds 80 feet (Figure 24).

#### IV. C. 3. Possible Deformation Along Cañon de Valle

Profiles of the top of post-Bandelier Tuff alluvial units and Qbt along Cañon de Valle suggest the possibility of deformation about 1000 feet east of Building 260. In this area there is a strong inflection in the upper surface of Qoal and underlying Qbt on both

sides of Cañon de Valle, with gradients abruptly becoming gentler to the east (Figures 6a and 6b). This suggests an area of westward tilting of originally east-dipping units, which is supported by a west-dipping surge exposed in a roadcut on R-Site Road, a short distance to the northeast of the map area. This deformation may be related to a zone of faulting, but further definition of the nature of this deformation will require more detailed data on the Tshirege Member units.

Other anomalies on the top of the Bandelier Tuff occur just west of Building 260, where available exposures indicate a drop in elevation of the tuff surface to the west on both sides of Cañon de Valle, suggesting down-to-the-west tilting (Figures 6a and 6b). The mesa top north of Cañon de Valle also drops rapidly in a similar sense in this area. However, there is no corresponding change in the gradient of the top of Qoal south of Cañon de Valle, and interpretation of possible deformation in this area is hindered by poor exposures and by uncertainties related to local erosion and deposition. South of Cañon de Valle, Qoal appears to thicken to the west (Figure 6b), which would be consistent with

North side Water Canyon

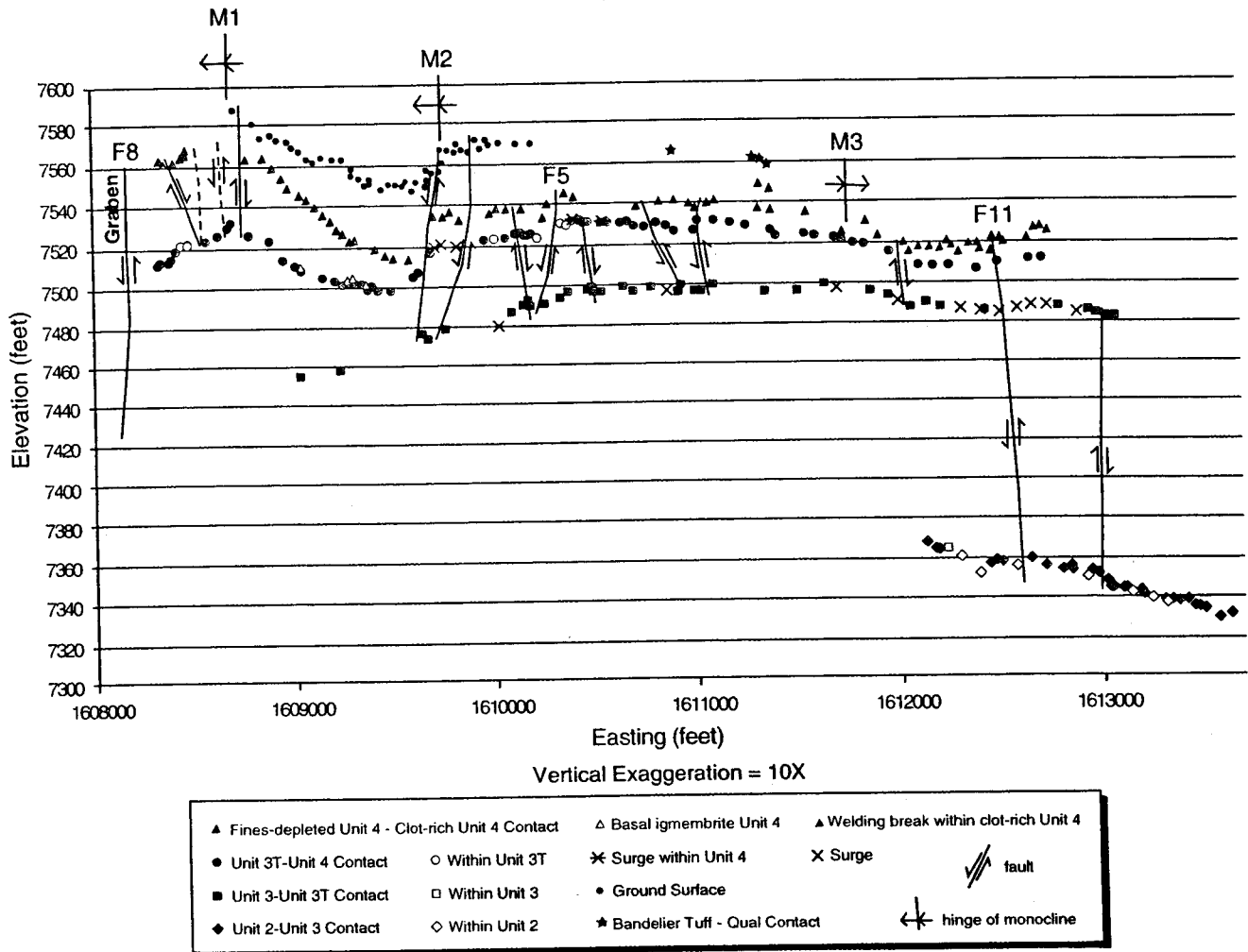


**Figure 23.** East-west profile of surveyed points on bedrock contacts and stratigraphic features on the north wall of Water Canyon. The eastern margin of the graben at the base of the main escarpment of the Pajarito fault zone is at the left end of the profile. Bedrock units are faulted, folded, and tilted throughout a zone that extends at least 5000 feet east of the graben. Faults and monoclines as on Plate 1.

differential preservation of Qoal on a west-tilted or down-dropped block. North of Cañon de Valle, however, Qoal is thickest to the east (Figure 6a). This east thickening would appear to be inconsistent with down-to-the-west deformation, but probable Qfo deposits may have a westward dip in the TA-9 gas pipeline trench. On both sides of Cañon de Valle the apparent westward drops in the top of Qbt are geographically associated with Qfo deposits, suggesting that the variations on the tuff surface could partly reflect local erosion and truncation of Qoal deposits during Qfo time. This apparent deformation may be related to a zone of faulting, but because of uncertainties, additional studies involving mapping of Qbt contacts, drilling, and/or trenching are necessary to define the deformation in this area.

## V. DISCUSSION AND CONCLUSIONS

### V.A. Tshirege Member Stratigraphic Units

A number of other workers have also subdivided the Tshirege Member of the Bandelier Tuff in or near our study area into map units (Rogers, 1995) or into petrologic units based on detailed petrographic, microprobe, and geochemical studies of samples from measured sections and boreholes (Warren et al., 1997; Environmental Restoration Project, 1998). Some discussion of how our units relate is therefore warranted. Most of our Tshirege Member units correlate well with Rogers' (1995) map units in the study area: her units C, D, E, and F correspond to our units 2, 3, 3T, and most of 4, respectively, although there are some differences in actual placement of contacts. We note, however, that the close

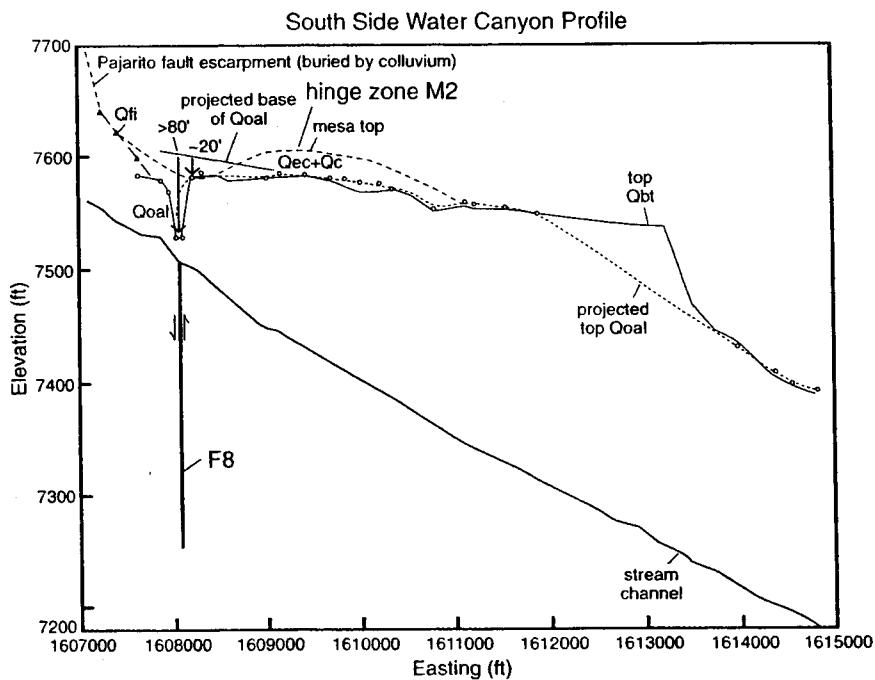


Figure 24. Composite profile along the south side of Water Canyon projected to an east-west plane. The inferred minimum net deformation east and west of the down-to-the-west fault F8 and monocline M2 uses the base of Goal as an approximate datum.

correspondence of our Unit 3T with Rogers' (1995) Unit E does not hold in parts of the Laboratory north of this study area (Gardner et al., 1999).

Some descriptions (Warren et al., 1997; Environmental Restoration Project, 1998) of Unit 3T are not entirely consistent with our usage. Unit 3T was described by Warren et al. (1997) as "chemically indistinguishable from [the underlying] Unit 3, but contain[ing] a much lower content of quartz phenocrysts." Environmental Restoration Project (1998) identified Unit 3T by its lower quartz abundance than underlying Unit 3 but about 5% more quartz than overlying Unit 4T. We, however, require criteria that can be applied in the field later to be supported with geochemical data. Small variations of quartz, for example, on the order of 5%, cannot be distinguished reliably in hand samples. We define Unit 3T, therefore, based on its welding characteristics and the nature of its phenocryst population.

In Water Canyon as well as areas mapped farther north (Gardner et al., 1999), Unit 3T appears in some localities to have lower and upper parts most commonly separated by a surge bed. The lower part is distinguished by platy weathering and the upper part by the round-edged platform it forms directly beneath Unit 4. This differential weathering may correspond to slight differences in chemistry noted in Warren et al. (1997), Stimac et al. (1998), Krier et al. (1998a, 1998b), and this study, which suggest that

Unit 4T of Warren et al. (1997) and Environmental Restoration Project (1998) is chemically more similar to underlying Unit 3T than to overlying Unit 4. Warren et al. (1997) defined Unit 4T as "petrographically indistinguishable from Unit 4, but chemically intermediate between units 3 and 4." However, the absence of a clear welding break within 3T dictated our decision to map this tuff as a single unit. In incorporating data from boreholes at MDA P (Environmental Restoration Project, 1998), we have accordingly included Unit 4T of Warren et al. (1997) in Unit 3T. We emphasize that our use of Unit 3T is petrographically and chemically consistent over the significant areas mapped in this study and by Gardner et al. (1999).

While we acknowledge that most of what we have included in our Unit 4 at S-Site is petrographically distinct from the Unit 4 of Gardner et al. (1999) farther north, the two units bear strong geochemical affinities and occupy the same stratigraphic position. It is likely that the moderately welded ignimbrite with conspicuous crystal clots of our Unit 4 is the same as Warren et al.'s (1997) Unit 5 and Rogers' (1995) Unit F. Unit 5 was defined informally by Warren et al. (1997) as the caprock above a prominent surge near the top of Broxton and Reneau's (1995) Unit 4. We have learned, however, that surges, while useful locally as stratigraphic markers, can only be applied as a stratigraphic criterion for identification of units above and below with a great deal of caution and supporting petrologic data; surges can appear at virtually any horizon in the sequence of tuffs (e.g., Gardner et al., 1999). In addition, Environmental Restoration Project (1998) identified the contact between Units 4 and 5 by a sharp rise, just above the contact, in ferromagnesian phenocryst abundance and, in some localities, an increase in quartz abundance. As discussed above, criteria such as these are difficult to apply to hand samples. We await, therefore, designation of a separate Unit 5 until the area between this study area and that of Gardner et al. (1999) has been mapped, revealing the stratigraphic relations among the various units near the top of the Tshirege Member.

Microprobe analyses on glass are useful in distinguishing among ash and pumice units of the

Otowi Member and Cerro Toledo Rhyolite. However, SiO<sub>2</sub>, TiO<sub>2</sub>, and Ba/Zr variation determined by whole rock XRF analysis provide a more widely useful, and less expensive, method for distinguishing among various units of the Tshirege Member. Widespread devitrification limits the utility of microprobe glass analyses for correlations among Tshirege Member units. Fresh glass appears to be preserved only in the lower portions of Unit 1 and in the various subunits of Unit 4.

The complexities of the upper Tshirege Member stratigraphy in the larger picture notwithstanding, we have been able to apply an internally consistent tuff stratigraphy over the map area. Most mapped contacts have been walked in their entirety and, together with more local stratigraphic markers, have provided a strong basis for interpretations of geologic structures, their spatial relations, and the nature of deformation. Furthermore, the bedrock constraints, when combined with geomorphic data, provide a detailed and accurate view of the structural geology of the Pajarito fault zone in the vicinity of S-Site.

## V. B. Structural Geology

### V. B. 1. Structural Setting of S-Site

S-Site lies at the base of the main escarpment formed by the Pajarito fault. Stratigraphic separation on the Tshirege Member of the Bandelier Tuff exceeds 400 feet across the main escarpment. From the escarpment, faulting and related deformation extend at least 5000 feet to the east. Although it may be argued that all structures we have mapped are part of a 5000 foot-wide zone of the Pajarito fault system, the structures in the western third of the area at Water Canyon accommodate most of the structural deformation that we document east of the main escarpment. We estimate net down-to-the-west displacement of Bandelier Tuff and the base of Qoal to be greater than 100 feet in the western third of the map area at Water Canyon (Figure 16). Farther north at the latitude of the S-Site administration area this zone of greatest deformation, east of the main escarpment, occupies about the western half of the study area with an estimated 80 to 100 feet of net down-to-the-west displacement on Bandelier Tuff. WETF lies within this zone.

Based on their trends, there are four clearly definable sets of structures in the vicinity of S-Site: north trending faults (F1, F8, and F9, Plate 1) and one large monocline (M4) marking the main zone of deformation of the Pajarito fault zone, defining a graben (G1) in the southwestern corner of the study area; north-northeast trending faults (F2, F3, F4, and

F10) and fissures (fis 1, fis 2, and fis 3) which bound the eastern side of graben G2, the probable northward continuation of graben G1; northeast trending structures, dominated by two down-to-the-west monoclines (M1 and M2), but including fault F5 and monocline M3; and, the east-southeast trending fault (F6) near Buildings 410 and 370. These are very similar structural elements to those identified and mapped farther north along the Pajarito fault system by Gardner et al. (1999) (see below). In addition, we recognize similar variable styles of deformation on structures as reported by Gardner et al. (1999), and, following their arguments, we interpret all structures in the study area to be related to deeper seated normal faulting.

In general, the structural setting of S-Site appears similar in many respects to the setting of TA-3 to the north (Gardner et al., 1999). At both locations a relatively narrow graben, about 1000 feet wide, lies at the base of and parallel to the main escarpment of the Pajarito fault. Structure to the east of the narrow graben is dominated by north-northeast and northeast trending normal faults and monoclines all of which show significant net down-to-the-west displacements on Bandelier Tuff. At TA-3, however, the north-northeast and northeast trending structures are caused by convergence of the Rendija Canyon fault with the Pajarito fault, forming the southern end of the large 12,000 foot-wide Diamond Drive graben (Gardner et al., 1999). It is possible that the patterns of structures at S-Site are the result of an analogous convergence of structures, but, if this is the case, the fault analogous to the Rendija Canyon fault must lie outside of the study area to the east and north. Alternatively, some of the different sets of structures at S-Site may represent different generations of deformation within a locally varying stress field; however, the age constraints on deformation that we have (see below) do not permit evaluation of this hypothesis.

In contrast to the structural geology east of the main escarpment of the Pajarito fault at TA-3, however, at S-Site we have found several north-northeast trending open fissure networks (fis 1, fis 2, and fis 3, Plate 1). Most commonly, we have observed such open fissures in the tensional upper hinge zones of monoclines (for example, fis 4) or as open framework fissure fill breccias developed at fault surfaces (Wong et al., 1995, McCalpin, 1997, 1998; Gardner et al., 1998b). Stratigraphic contacts are nearly horizontal in the WETF boreholes and at the southern end of the fissured lineament (fis 1) which would appear to argue against creation of the open fissures in the hinge zone of monoclines. On the other hand, the proximity of fis 2 and fis 3 to

documented faulting in the WETF boreholes may imply their direct relations to opening and brecciation on fault surfaces, and suggestions from geomorphic arguments imply that at least part of the fissured lineament of fis 1 is also caused by faulting.

### *V. B. 2. Comparison of Structure to Previous Studies*

Rogers (1995) recognized many of the larger structures that we have mapped, but we differ in placement and interpretation of the style of deformation. Rogers (1995) recognized one of the graben bounding faults (F8, Plate 1) but depicted one of our northeast-trending monoclines (M2) as a down-to-the-west fault. The trend of the structure is the same in both interpretations, and the distinction here is largely semantic in that the deformation responsible for what can be observed at the surface is deeper seated normal faulting (Gardner et al., 1999). Rogers (1995) also recognized the north-northeast-trending fissured lineament (fis 1) but shows it as a down-to-the-east fault. As discussed above, any displacements that we might infer on this structure would be down-to-the-west. A major structure, by virtue of its length, on Rogers' (1995) maps is the Water Canyon Arch. From this study we cannot address the Water Canyon Arch in its depicted entirety, but in Water Canyon the apparent arching of bedrock units is caused by the east-southeast-trending fault zone (F6) that cuts the small drainage between Buildings 410 and 370. When viewed from the south side of Water Canyon, this fault, which displaces units down-to-the-north, appears to form an arch. Rogers (1995) also recognized fault F6, but shows it with a different trend, running west up 430 Canyon. The high-precision mapping data clearly do not allow this trend and run. A north-trending anticline is shown on Rogers' (1995) maps running from State Road 4 across Water Canyon. Examination of the profile of bedrock data of Figure 16 reveals a broad arching of contacts through this area. We have chosen to not show this feature as an anticline because it is caused by regional dip on the tuff to the east and west-side-down structural displacements across the northeast-trending monoclines to the west. Rogers (1995) shows a number of west-trending faults in the northern part of our study area for which we have found no evidence. We note that for these structures, and for many similar ones north of the study area, Rogers (1995) shows no offset, at the scale of 1:4800, where the faults cross contacts.

Budding and Purtymun (1976) show the Water Canyon fault skirting the east side of our study area. It is difficult from their map to discern the precise placement of this fault but it appears to run from the

topographic step at the east end of Campground Mesa, through the small drainage between Buildings 410 and 370, and along an aerial photograph linear that Gardner and House (1987) show on their maps. Our work suggests that the step and linear are erosional features, perhaps formed near a flow front within Unit 4. High-precision mapping data show no such structure in the small drainage, and do not reveal displacements of 30 feet anywhere in this portion of Water Canyon, as reported by Budding and Purtymun (1976). As mentioned above, however, it is plausible that such a structure may lie east of our study area.

### *V. B. 3. Ages of Faulting and Related Deformation*

Bounds on the timing of the structural deformation in the study area are not particularly robust. All structures are Quaternary in that they postdate the Tshirege Member (1.2 Ma) of the Bandelier Tuff. For most structures (F1, F2, F8, M1, M2, and possibly fis 1) the only other unit that is clearly faulted or deformed is Qoal, which is in part about 1 million years old. At a number of localities younger units such as Qec (for fault F2) and Qfi (for fault F9) appear to be truncated by the faults, but field relations are equivocal and we cannot confirm the presence of fault contacts. The complex of extensive mass wasting on the main scarp of the Pajarito exhibits many strong linears on the landslides. This may imply that some faulting postdates the landslides, but the age is not well constrained.

From trenches within the main escarpment zone of the Pajarito fault in the study area (for example T1, Plate 1) Olig et al. (1996) report a paleoseismic event just before 50 to 60 ka; however, they state that their trenches provided an ambiguous and probably incomplete paleoseismic record because they never exposed a major fault trace. Farther north in the fault system McCalpin (1998) reported the most recent surface rupturing paleoearthquake occurred between about 1.3 and 2.3 ka, but he later revised this estimate to roughly 3 to 7 ka (McCalpin, 2000). Similarly, McCalpin (1999) reported most recent paleoseismic events within the main Pajarito escarpment in the western part of our study area (T3, Plate 1), and immediately north of it, to have occurred between 2-3 and 12-20 ka, but later revised his age estimate of this event to between 8-10 and 18-24 ka (McCalpin, 2000). Clearly, more paleoseismic investigations are necessary within the Pajarito fault system to better constrain the timing of surface rupturing paleoseismic events. In parallel to this project, Reneau and Gardner (1999) evaluated sites for potential future paleoseismic trenching. Among other sites elsewhere in the fault system,

they identified nine sites with potential for yielding paleoseismic data in and around this study area.

Radiocarbon dates obtained from charcoal in the fissure fill sequence of borehole WETF-2C give internally stratigraphically consistent dates of  $8030 \pm 50$ ,  $7500 \pm 50$ , and  $6280 \pm 50$  radiocarbon years BP, with the deepest  $^{14}\text{C}$  date (56.5 feet) about 0.5 ft above the shallowest sediments recognized to be deformed by fault F4. Thus, a seismic event sometime prior to 8  $^{14}\text{C}$  ka is necessary to open the fissure and initiate sedimentation. Additionally, the fissure fill material is also faulted indicating at least one additional, younger paleoseismic event whose age is not well constrained.

#### ***V. B. 4. Potential for Seismic Surface Rupture at WETF***

While we have identified no specific structures that directly underlie WETF, drilling revealed faults (F3 and F4, Plate 1) and related fissures (fis 2 and fis 3) that appear to bound the northwest and southeast sides of the facility, and are probably similar in trend and structural character to the north-northeast trending structures (F2, F10, and fis 1) observed nearby in the course of mapping. Direct evidence in the core for faulting was found as cataclastic breccias and zones of gouge in boreholes WETF-2C and WETF-5. Additional evidence for these faults is inferred from differences in the elevation of the Unit 3T-Unit 4 contact among the boreholes, stratigraphy in SHB-3, and from a water saturated zone of no core recovery, common in faults characterized by rubble breccia, in WETF-3. Our analyses of the drilling data indicate the western fault at WETF (F3) has at least 4 and more likely greater than 30 feet of down-to-the-west displacement on Bandelier Tuff. The eastern fault at WETF (F4) exhibits at least 6 feet of down-to-the-east displacement on Bandelier Tuff and deforms possible Holocene fissure-fill deposits. In spite of complications imparted by tuff units that thicken westward, WETF is surrounded by structures that account for the greatest amount of Pajarito fault zone deformation east of the main escarpment. Thus, it appears that WETF lies within the Pajarito fault zone, albeit a part of the fault zone that is dominated by subsidiary or distributed ruptures. As such, WETF is in an area of generally higher potential for seismic surface rupture, relative to locations farther removed from the Pajarito fault zone. Probabilistic analyses of surface rupture potential at S-Site by Olig et al. (2001), however, indicate that, even in consideration of 1-in-10,000 year events, seismic surface rupture only becomes a significant hazard on the principal or main trace of the Pajarito fault.

## **VI. ACKNOWLEDGEMENTS**

The Nuclear Weapons Program Office has provided support for this project; in particular, we are grateful for the leadership and vision of Larry Goen, Scott Gibbs, Jim Holt, Carolyn Zerkle, Donna Richardson, and Craig Leasure and their recognition that Los Alamos National Laboratory needs a seismic hazards program. Additionally, we are grateful to Jim Aldrich who has provided unflagging line management support of our efforts. Without the help of Yolanda Frazier, Kathy Martinez, Bill McCormick, Joe Brophy, and Lou Horak at S-Site, this work would not have been possible. Cindy Werner, Lara Heister, Seth McMillan, and Mark Van Eeckhout assisted in various stages of the field work. Dave Broxton, Rick Warren, Ken Wohletz, and Dave Vaniman provided discussions and insights on issues regarding the stratigraphy of the Bandelier Tuff. Peg Snow, Amy Howard, Emily Kluk, Kellie Raven, and Destiny Baldonado provided dependable assistance with the geochemical analytical work. At the Laboratory's Facility for Information Management, Analysis, and Display, Marcia Jones, Kerry Cummings, Matt Rice, and Jeff Blossom contributed their expertise with data bases and helped with digitizing the geomorphic data. Eric McDonald contributed to interpretations of the soil stratigraphy in the western part of the map area. Anthony Garcia prepared the high quality illustrations in this report, Mable Amador gave the final manuscript a much-needed edit, and Lanny Piotrowski did another outstanding job putting the final production-ready paper together. Helpful reviews were provided by Dave Vaniman and Larry Goen.

## **VII. REFERENCES**

- Bailey, R. A., Smith, R. L., and Ross, C. S., 1969, Stratigraphic nomenclature of volcanic rocks in the Jemez Mountains, New Mexico; *U. S. Geological Survey Bulletin 1274-P*, 19 p.
- Baldrige, W. S., Dickerson, P. W., Riecker, R. E., and Zidek, J., (eds.), 1984, Rio Grande rift: Northern New Mexico; *New Mexico Geological Society Guidebook 35*, 379 p.
- Baldrige, W. S., Keller, G. R., Haak, V., Wendlandt, E., Jiracek, G. R., and Olsen, K. H., 1995, The Rio Grande rift; in *Continental Rifts: Evolution, Structure, Tectonics*, K. H. Olsen, Ed.; Elsevier, Amsterdam, Holland, 233-275.

- Brown, F., Purtymun, W. D., Stoker, A., and Barr, A., 1988, Site geology and hydrology of Technical Area 16, Area P; Los Alamos National Laboratory report LA-11209-MS, 8 p.
- Broxton, D.E. and Reneau, S.L., 1995, Stratigraphic Nomenclature of the Bandelier Tuff for the Environmental Restoration Project at Los Alamos National Laboratory; Los Alamos National Laboratory report LA-13010-MS, 21 p.
- Broxton, D.E., Rytli, R.T., Carlson, D., Warren, R.G., Kluk, E., and Chipera, S., 1996, Natural background geochemistry of the Bandelier Tuff at MDA P, Los Alamos National Laboratory; Los Alamos National Laboratory report LA-UR-96-1151, 42 p.
- Budding, A. J., and Purtymun, W. D., 1976, Seismicity of the Los Alamos area based on geologic data; Los Alamos Scientific Laboratory report LA-6278-MS, 9 p.
- Dransfield, B. J., and Gardner, J. N., 1985, Subsurface geology of the Pajarito Plateau, Espanola Basin, New Mexico; Los Alamos National Laboratory report LA-10455-MS, 15 p.
- Environmental Restoration Project, 1998, RFI Report for Potential Release Site; Los Alamos National Laboratory report LA-UR-98-4104, Volume 16-021 (c); report in three volumes.
- Environmental Restoration Project (in prep., draft dated 11-5-99) Interim completion report for characterization well R-25, Los Alamos National Laboratory Report, 80 p.
- Gardner, J. N. and Goff, F., 1984, Potassium-Argon dates from the Jemez volcanic field: Implications for tectonic activity in the north-central Rio Grande rift; *New Mexico Geological Society Guidebook* 35, 75-81.
- Gardner, J. N., Goff, F., Garcia, S., and Hagan, R. C., 1986, Stratigraphic relations and lithologic variations in the Jemez volcanic field, New Mexico; *Journal of Geophysical Research* 91, 1763-1778.
- Gardner, J. N., and House, L., 1987, Seismic Hazards Investigations at Los Alamos National Laboratory, 1984 to 1985; Los Alamos National Laboratory report LA-11072-MS, 76 p.
- Gardner, J. N., Baldrige, W. S., Gribble, R., Manley, K., Tanaka, K., Geissman, J. W., Gonzalez, M., and Baron, G., 1990, Results from Seismic Hazards Trench #1 (SHT-1), Los Alamos Seismic Hazards Investigations; Los Alamos National Laboratory unpublished report EES1-SH90-19, 57 p.
- Gardner, J. N., Kolbe, T., and Chang, S., 1993, Geology, drilling, and some hydrologic aspects of Seismic Hazards Program core holes, Los Alamos National Laboratory; Los Alamos National Laboratory report, LA-12460-MS, 19 p.
- Gardner, J. N., Lavine, A., Vaniman, D., and WoldeGabriel, G., 1998a, High-precision geologic mapping to evaluate the potential for seismic surface rupture at TA-55, Los Alamos National Laboratory; Los Alamos National Laboratory report LA-13456-MS, 13 p.
- Gardner, J. N., Lavine, A., WoldeGabriel, G., Krier, D. J., Vaniman, D., and McCalpin, J., 1998b, Evolution of the western boundary of the Rio Grande rift, northern New Mexico: *EOS, Trans. American Geophysical Union* 79 (45), F614.
- Gardner, J. N., Lavine, A., WoldeGabriel, G., Krier, D., Vaniman, D., Caporuscio, F., Lewis, C., Reneau, S., Kluk, E., and Snow, M., 1999, Structural geology of the northwestern portion of Los Alamos National Laboratory, Rio Grande rift, New Mexico: Implications for seismic surface rupture potential from TA-3 to TA-55; Los Alamos National Laboratory report LA-13589-MS, 112 p.
- Goff, F., Gardner, J. N., and Valentine, G., 1990, Geology of St. Peters Dome area, Jemez Mountains, New Mexico; *New Mexico Bureau of Mines and Mineral Resources, Geologic Map* 69, scale 1:24000.
- Goff, S., 1986, Curatorial policy guidelines and procedures for the Continental Scientific Drilling Program; Los Alamos National Laboratory report LA-10542-OBES, 23 p.
- Golombek, M. P., 1981, Structural analysis of the Pajarito fault zone in the Espanola Basin of the Rio Grande rift, New Mexico; Ph.D. dissertation, University of Massachusetts, 129 p.
- Griggs, R. L., 1964, Geology and ground water resources of the Los Alamos area, New Mexico; *U. S. Geological Survey, Water-Supply Paper* 1753, 107 p.
- Heiken, G., Goff, F., Stix, J., Tamanyu, G., Shafiqullah, M., Garcia, S., and Hagan, R., 1986, Intracaldera volcanic activity, Toledo caldera and embayment, Jemez Mountains, New Mexico; *Journal of Geophysical Research* 91, 1799-1815.
- Izett, G. A., and Obradovich, J. D., 1994,  $^{40}\text{Ar}/^{39}\text{Ar}$  age constraints for the Jaramillo Normal Subchron and the Matuyama-Brunhes geomagnetic boundary; *Journal of Geophysical Research* 99, 2925-2934.
- Keller, G. R., (ed.), 1986, Special section on the Rio Grande rift; *Journal of Geophysical Research* 91, 6142-6345.
- Kelson, K. I., Hemphill-Haley, M. A., Olig, S. S., Simpson, G. D., Gardner, J. N., Reneau, S. L., Kolbe, T. R., Forman, S. L., and Wong, I. G., 1996, Late-Pleistocene and Possibly Holocene Displacement along the Rendija Canyon fault, Los Alamos County, New Mexico; *New Mexico Geological Society Guidebook* 47, 153-160.



- Reneau, S. L., and Gardner, J. N., 1999, An evaluation of possible paleoseismic trench sites in the Pajarito fault system, Los Alamos County, New Mexico; unpublished Los Alamos National Laboratory report LA-UR-99-5943, 17 pp.
- Reneau, S. L., Kolbe, T., Simpson, D., Carney, J. S., Gardner, J. N., Olig, S. S., and Vaniman, D. T., 1995, Surficial materials and structure at Pajarito Mesa; in *Geological site characterization for the proposed Mixed Waste Disposal Facility, Los Alamos National Laboratory*, S. L. Reneau and R. Raymond, Eds.; Los Alamos National Laboratory report LA-13089-MS, Los Alamos, New Mexico, 31–69.
- Reneau, S. L., McDonald, E. V., Gardner, J. N., Kolbe, T. R., Carney, J. S., Watt, P. M., and Longmire, P. A., 1996a, Erosion and deposition on the Pajarito Plateau, New Mexico, and implications for geomorphic responses to late Quaternary climatic changes; *New Mexico Geological Society Guidebook* 47, 391–397.
- Reneau, S. L., Gardner, J. N., and Forman, S. L., 1996b, New evidence for the age of the youngest eruptions in the Valles caldera, New Mexico; *Geology* 24, 7–10.
- Riecker, R. E., (ed.), 1979, *Rio Grande rift: Tectonics and magmatism*; American Geophysical Union, Washington, D. C., 438 p.
- Rogers, M. A., 1995, Geologic map of Los Alamos National Laboratory reservation; publication of the State of New Mexico Environment Department, scale 1:400.
- Sanford, A. R., Jaksha, L. H., and Cash, D. J., 1991, Seismicity in the Rio Grande rift; in *Neotectonics of North America, Decade Map Volume 1*, D. B. Slemmons, E. R. Engdahl, M. D. Zoback, and D. D. Blackwell, Eds.; Geological Society of America, 229–244.
- Smith, R.L., and Bailey, R.A., 1966, The Bandelier Tuff: A study of ash-flow eruption cycles from zoned magma chambers; *Bulletin Volcanologique* 29, 83–103.
- Smith, R. L., Bailey, R. A., and Ross, C. S., 1970, Geologic map of the Jemez Mountains, New Mexico; *U. S. Geological Survey, Miscellaneous Investigations Map I-571*, scale 1:125000.
- Spell, T. L., and Harrison, T. M., 1993,  $^{40}\text{Ar}/^{39}\text{Ar}$  geochronology of post-Valles caldera rhyolites, Jemez volcanic field, New Mexico; *Journal of Geophysical Research* 98, 8031–8051.
- Spell, T. L., Kyle, P. R., and Baker, J., 1996, Geochronology and geochemistry of the Cerro Toledo Rhyolite; *New Mexico Geological Society Guidebook* 47, 263–268.
- Steck, L. K., Thurber, C. H., Fehler, M. C., Lutter, W. J., Roberts, P. M., Baldrige, W. S., Stafford, D. G., and Sessions, R., 1998, Crust and upper mantle P wave velocity structure beneath Valles caldera, New Mexico: Results from the Jemez teleseismic tomography experiment; *Journal of Geophysical Research* 103, 24301–24320.
- Stimac, J. A., Broxton, D. E., Kluk, E. C., and Chipera, S. J., 1998, Preliminary stratigraphy of tuffs from borehole 49-2-700-1 at Technical Area 49, Los Alamos National Laboratory unpublished report, 21 p.
- Toyoda, S., Goff, F., Ikeda, S., and Ikeya, M., 1995, ESR dating of quartz phenocrysts in the El Cajete and Battleship Rock Members of the Valles Rhyolite, Valles caldera, New Mexico; *Journal of Volcanology and Geothermal Research* 67, 29–40.
- Warren, R.G., McDonald, E.V., and Rytí, R.T., 1997, Baseline geochemistry of soil and bedrock Tshirege Member of the Bandelier Tuff; Los Alamos National Laboratory report LA-13330-MS, 69 p.
- Wolff, J. A., and Gardner, J. N., 1995, Is the Valles caldera entering a new cycle of activity?; *Geology* 23, 411–414.
- Wong, I., Kelson, K., Olig, S., Kolbe, T., Hemphill-Haley, M., Bott, J., Green, R., Kanakari, H., Sawyer, J., Silva, W., Stark, C., Haraden, C., Fenton, C., Unruh, J., Gardner, J., Reneau, S., and House, L., 1995, Seismic Hazards Evaluation of the Los Alamos National Laboratory: unpublished consulting report prepared for Los Alamos National Laboratory by Woodward-Clyde Federal Services, Oakland, California, 3 volumes.

# Appendix A: Sample Locations

## Legend for Sample Locations Figures

-  Borehole
-  Sample Locations
- Faults and Related Structures**
  -  fault
  -  fault zone
  -  fissure
  -  flexure
  -  queried fault
  -  scarp
- Surveyed Points**
  -  Unit 2-Unit 3 Contact
  -  Within Unit 2
  -  Unit 3-Unit 3T Contact
  -  Within Unit 3
  -  Unit 3T-Unit 4 Contact
  -  Within Unit 3T
  -  Within Unit 4
  -  Basal Unit 4 Coarse-grained Unit 4 Contact
  -  Coarse-grained Unit 4 Clot-rich Unit 4 Contact
  -  Big Block Slide
  -  Prominent Weathered Fracture
-  Surge within Unit 3
-  Surge at Unit 3-Unit 3T Contact
-  Surge within Unit 3T
-  Surge at Unit 3T-Unit 4 Contact
-  Surge within Unit 4
-  Bandelier Tuff-Mesa-top Alluvium Contact
-  Ground Surface
-  Closed Depression
-  Fissure
-  Scarp
-  Within Clot-rich Unit 4
-  Welding break with Clot-rich Unit 4
- Surveyed Points at TA-9 Pipeline Trench**
  -  Faults, Fissures, and Fractures
  -  Surge within Unit 4
  -  Trench
-  Faults (Gardner and Reneau, unpublished data)
-  Roads
-  Buildings
-  10-Foot Contour Lines
-  20-Foot Contour Lines
-  100-Foot Contour Lines

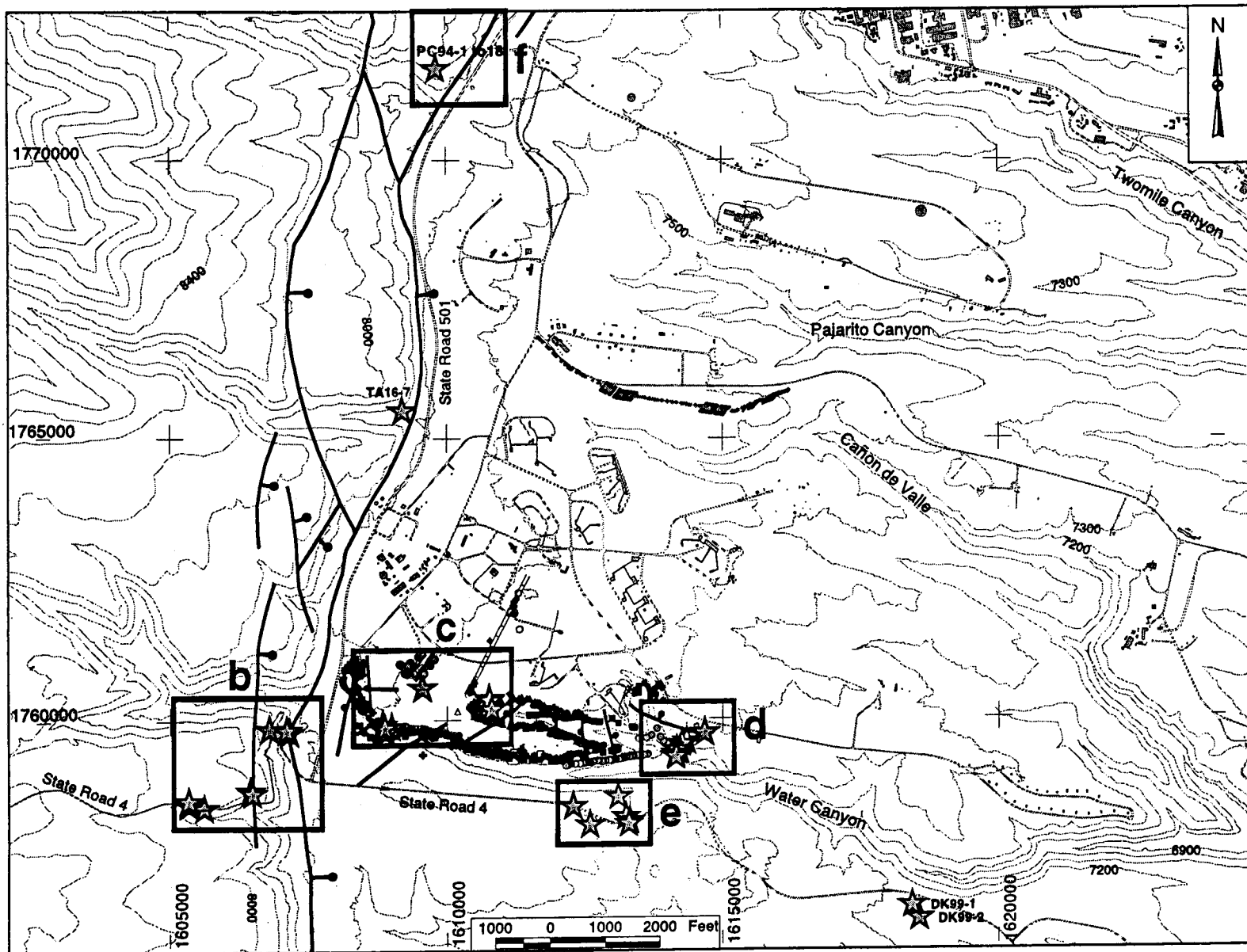


**Figure A-1a.** Map showing the location of samples taken for geochemical analyses. The locations of Figures A-1b through A-1f are shown by lettered boxes. The legend for Figures A-1a through A-1f precedes this map. The grid is in the State Plane Coordinate System (in feet), New Mexico Central Zone, 1983 North American Datum.

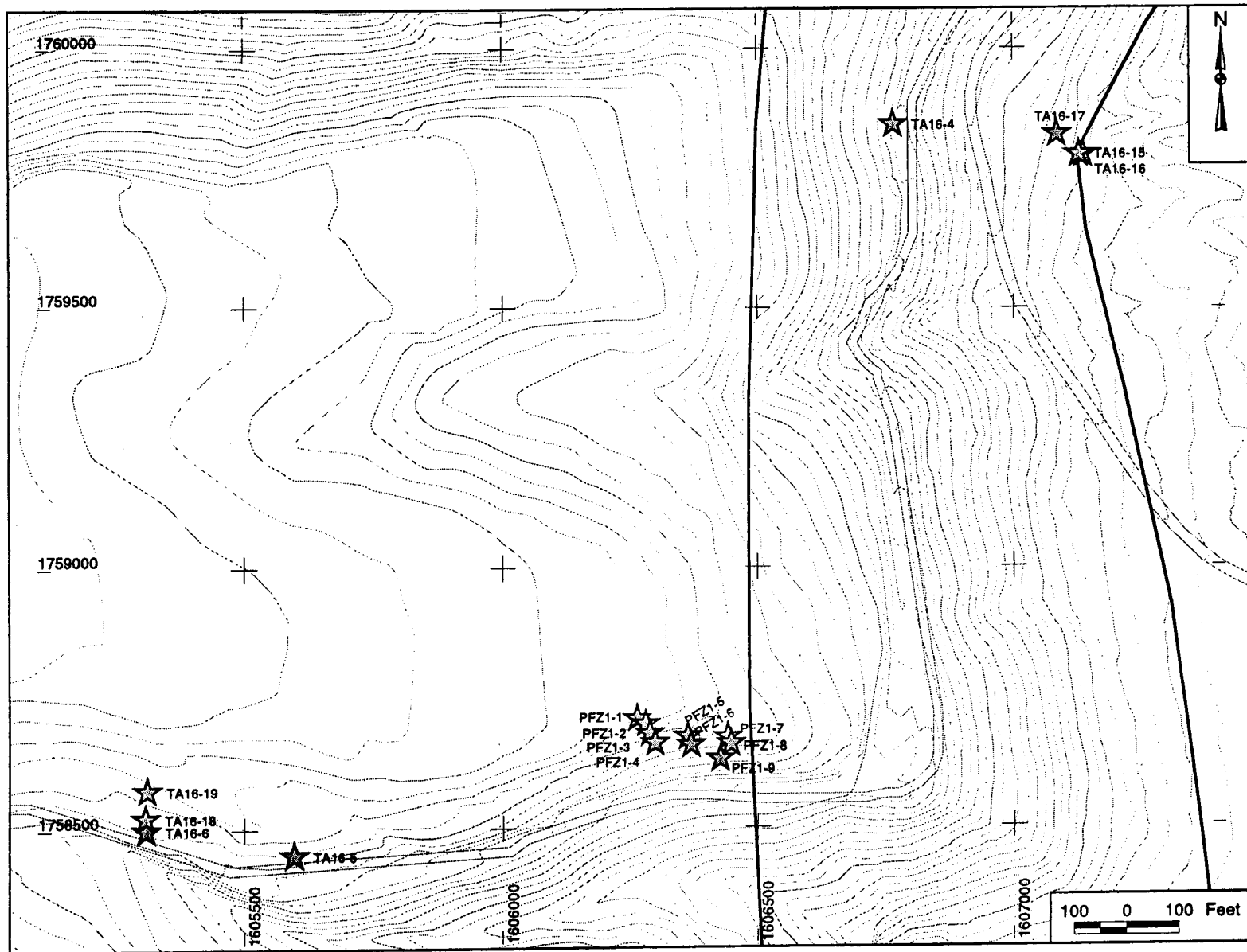


Figure A-1b. Map showing the location of samples TA16-4 through TA16-7, TA16-15 through TA16-19, and PFZ-1 through PFZ-9 on the Pajarito fault scarp near State Road 4. The grid is in the State Plane Coordinate System (in feet), New Mexico Central Zone, 1983 North American Datum.

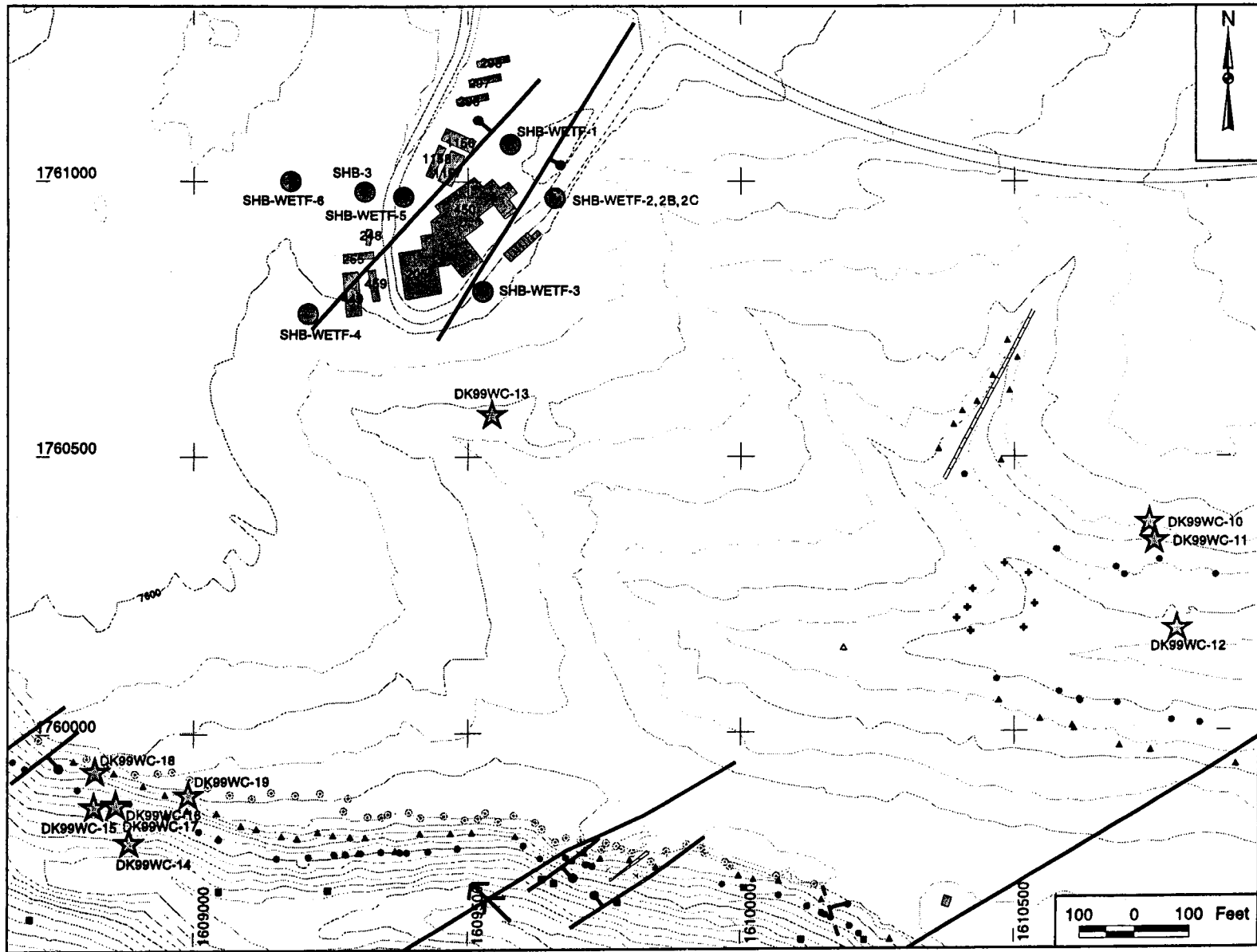


Figure A-1c. Map showing the location of samples DK99WC-10 through DK99WC-19, SHB-WETF-1 through 6, and SHB-3 near WETF and in Water Canyon and 430 Canyon. The grid is in the State Plane Coordinate System (in feet), New Mexico Central Zone, 1983 North American Datum.

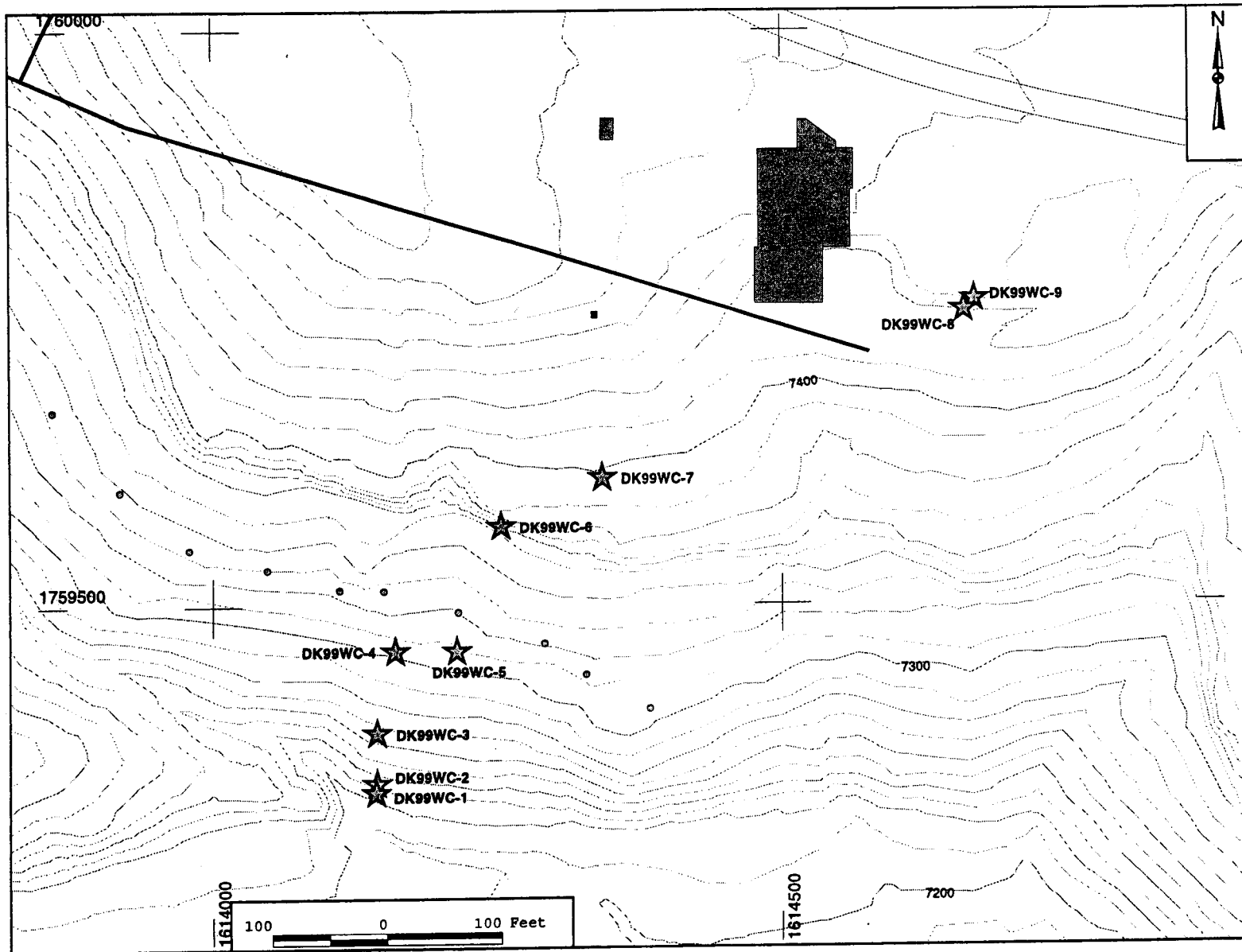


Figure A-1d. Map showing the location of samples DK99WC-1 through DK99WC-9 in Water Canyon near Building 370. The grid is in the State Plane Coordinate System (in feet), New Mexico Central Zone, 1983 North American Datum.

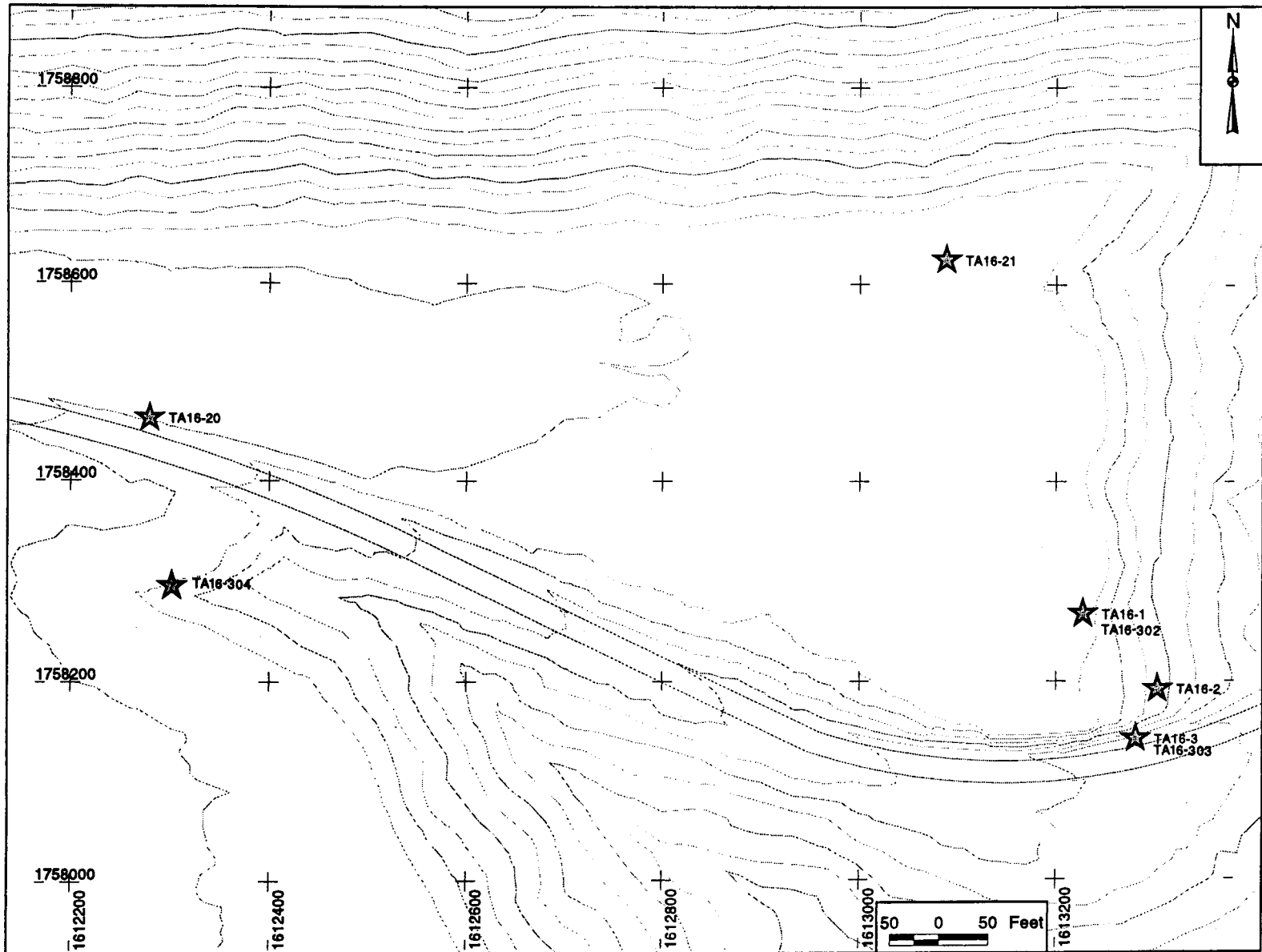


Figure A-1e. Map showing the location of samples TA16-1 through TA16-3, TA16-20, TA16-21, and TA16-302 through TA16-304 on Campground Mesa. The grid is in the State Plane Coordinate System (in feet), New Mexico Central Zone, 1983 North American Datum.

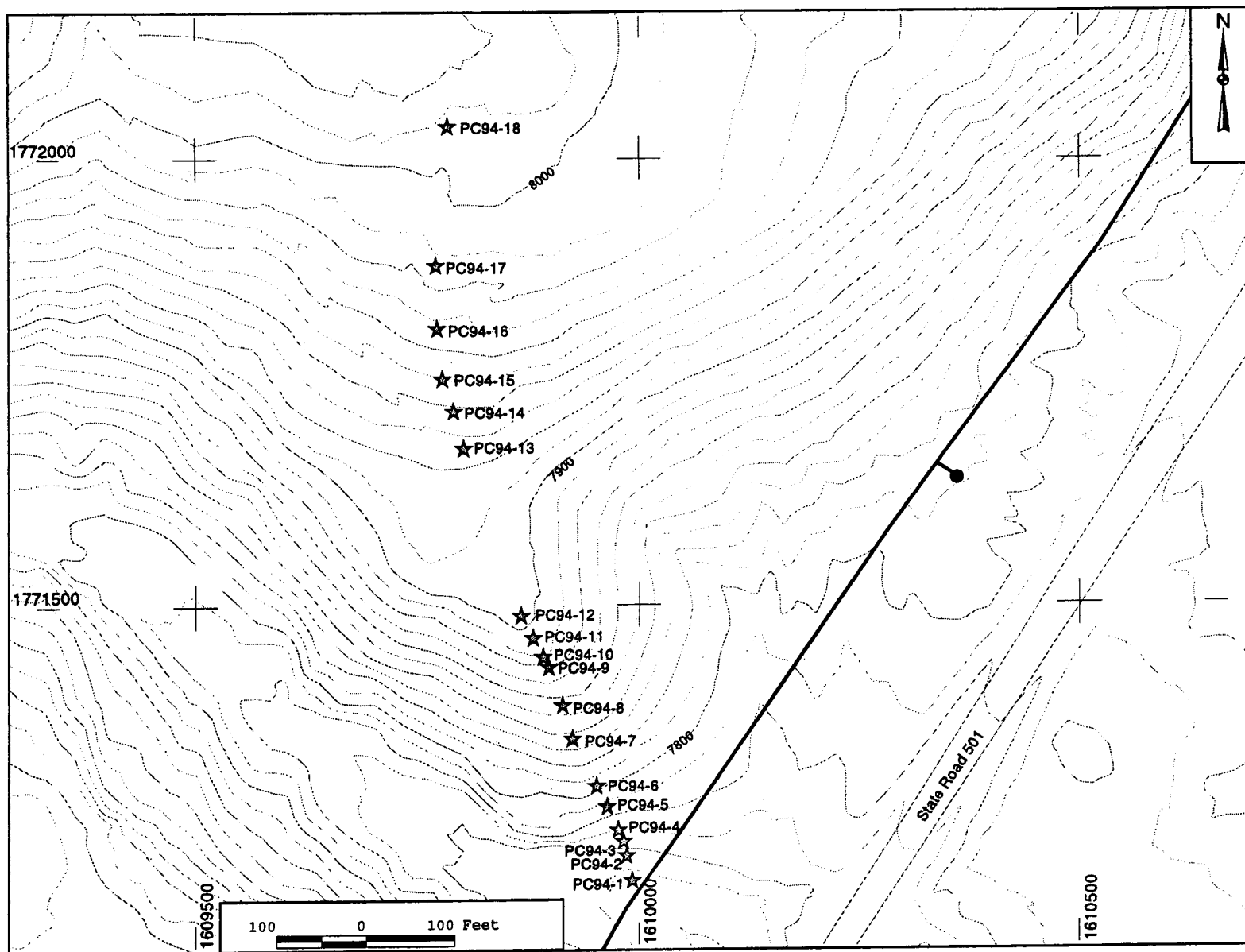


Figure A-1f. Map showing the location of samples PC94-1 through PC94-18 from Pajarito Canyon. The grid is in the State Plane Coordinate System (in feet), New Mexico Central Zone, 1983 North American Datum.

## Whole Rock Geochemistry

## Appendix B

Sample Number	TA16-5	TA16-6	TA16-18	TA16-19	TA16-4	TA16-15	TA16-16	TA16-17	TA16-7	PFZ1-1	PFZ1-2	PFZ1-3	PFZ1-4	PFZ1-5	PFZ1-6
Stratigraphic Unit	Qbt 3T	Qbt 4	Qbt 4	Qbt 4	Qbt 3T	Qbt 4	Qbt 4	Qbt 4	Qbt3T	Qbt 4					
Northing (ft)	1758451*	1758502	1758525	1758579	1759856	1759797	1759797	1759836	1765511	1758713	1758702	1758684	1758665	1758678	1758661
Easting (ft)	1605595	1605311	1605310	1605313	1606766	1607135	1607128	1607085	1609184	1606261	1606278	1606286	1606296	1606360	1606367
Elevation (ft)	8010	8013	8015	8025	7784	7654	7657	7673	7744	8031	8021	8014	7999	7994	7994
<b>Major Elements (wt %)</b>															
SiO <sub>2</sub>	75.46	68.57	73.87	73.65	75.91	73.56	73.89	73.47	75.60	72.77	73.94	73.12	69.91	70.52	70.70
TiO <sub>2</sub>	0.20	0.40	0.28	0.23	0.18	0.26	0.24	0.26	0.19	0.24	0.19	0.26	0.29	0.27	0.23
Al <sub>2</sub> O <sub>3</sub>	12.98	15.96	13.55	13.72	12.90	13.92	13.64	14.00	12.70	13.78	13.06	13.91	14.86	14.66	14.55
Fe <sub>2</sub> O <sub>3</sub> T	2.04	3.86	2.40	2.22	1.88	2.36	2.25	2.22	1.95	2.23	1.95	2.27	3.08	2.94	2.82
MnO	0.07	0.08	0.08	0.07	0.05	0.09	0.08	0.03	0.07	0.11	0.07	0.05	0.04	0.04	0.03
MgO	0.00	0.67	0.17	0.15	0.00	0.14	0.00	0.00	0.00	0.12	0.00	0.00	0.43	0.45	0.39
CaO	0.37	1.09	0.60	0.55	0.22	0.49	0.34	0.34	0.34	0.51	0.43	0.37	0.60	0.55	0.45
Na <sub>2</sub> O	4.39	3.65	4.57	4.58	4.33	4.55	4.51	4.39	4.48	4.45	4.63	4.60	4.02	4.05	3.98
K <sub>2</sub> O	4.76	4.02	4.63	4.83	4.87	4.65	4.77	4.71	4.75	4.83	4.71	4.70	4.20	4.34	4.36
P <sub>2</sub> O <sub>5</sub>	0.02	0.07	0.05	0.03	0.02	0.03	0.01	0.00	0.02	0.05	0.02	0.00	0.04	0.03	0.03
LOI %	0.26	2.38	0.36	0.89	0.24	0.56	0.47	0.72	0.27	0.57	0.09	0.48	2.29	1.72	1.87
Total	100.29	98.37	100.19	100.02	100.36	100.06	99.71	99.41	100.11	99.10	99.01	99.28	97.47	97.86	97.55
<b>Trace Elements (ppm)</b>															
Zn	52	97	49	55	57	73	69	43	68	46	51	58	80	81	74
Rb	96	107	78	74	107	86	87	83	101	85	90	85	94	95	109
Sr	33	130	81	65	26	69	49	62	32	72	40	70	79	72	47
Y	39	49	41	27	45	47	27	20	43	43	29	30	66	51	49
Zr	360	325	374	366	336	372	388	407	343	392	346	377	339	320	303
Nb	52	43	53	41	49	32	51	40	43	50	46	39	39	45	53
Ba	233	482	390	314	204	375	333	313	229	391	250	361	320	321	147

Notes: Analytical uncertainties are available on request from the authors.  
V, Cr, & Ni concentrations are below detection limits and therefore not reported.

Appendix B (cont.)

PFZ1-7 Qbt 4 1758676 1606439 7988	PFZ1-8 surge 1758663 1606445 7987	PFZ1-9 Qbt 3T 1758634 1606425 7981	DK99-2 Qbt 3 1758607 1618557 7240	DK99-1 Qbt 4 1758645 1618419 7280	TA16-3 Qbt 4 1758142 1613281 7481	TA16-20 Qbt4 1758465 1612279 7542	TA16-2 Qbt 4 1758193 1613303 7506	TA16-1 Qbt 5(?) 1758269 1613227 7533	TA16-21 Qbt4 1758627 1613088 7538	DK99WC-1 Qbt 2 1759339.84 1614140.59 7214.77	DK99WC-2 Qbt 2 1759347.88 1614141.39 7232.12	DK99WC-3 Qbt 2 1759391.26 1614141.39 7259.19	DK99WC-4 Qbt 2 1759461.96 1614157.46 7297.94	DK99WC-5 Qbt 2 1759461.96 1614211.29 7306.99	DK99WC-6 Qbt 3 1759568.82 1614249.85 7352.56
72.11	67.92	74.13	75.89	74.08	73.87	73.30	73.46	71.14	71.60	77.92	78.34	77.47	78.13	77.49	78.07
0.30	0.56	0.19	0.15	0.23	0.23	0.25	0.25	0.25	0.26	0.09	0.09	0.10	0.09	0.09	0.13
13.92	14.38	13.10	12.55	13.24	12.91	14.10	13.43	14.34	14.20	11.83	11.73	12.27	11.89	11.49	12.32
2.41	4.46	2.02	1.76	2.14	2.14	2.37	2.24	2.38	2.35	1.44	1.44	1.58	1.46	1.39	1.49
0.08	0.15	0.09	0.06	0.06	0.07	0.04	0.07	0.07	0.07	0.04	0.05	0.08	0.05	0.07	0.05
0.38	0.94	0.00	0.00	0.13	0.26	0.00	0.21	0.14	0.20	0.00	0.00	0.00	0.00	0.19	0.00
0.95	1.79	0.29	0.27	0.39	0.72	0.35	0.62	0.57	0.74	0.14	0.15	0.14	0.14	0.38	0.20
4.30	4.87	4.54	4.02	4.32	3.96	4.47	3.98	4.27	3.91	3.81	3.80	3.88	3.98	3.87	3.90
4.51	3.59	4.84	4.53	4.81	4.62	4.77	4.60	4.68	4.66	4.28	4.24	4.44	4.38	4.32	4.43
0.08	0.13	0.02	0.02	0.02	0.05	0.01	0.04	0.04	0.09	0.00	0.00	0.00	0.00	0.01	0.01
0.41	0.51	0.32	0.48	0.47	1.51	0.81	1.69	2.19	2.66	0.45	0.45	0.53	0.37	1.11	0.50
99.03	98.80	99.21	99.24	99.41	98.82	99.60	98.90	97.87	98.04	99.54	99.85	99.95	100.11	99.30	100.61
82	138	53	48	52	56	52	50	50	68	46	49	74	40	44	37
96	46	98	102	87	90	78	82	82	78	123	126	126	137	125	96
116	235	35	36	56	86	68	79	65	70	20	20	24	20	30	33
35	36	24	37	45	35	27	40	19	33	37	34	51	52	32	21
331	402	345	260	351	310	395	338	371	405	199	196	215	211	204	221
36	20	52	46	48	46	47	46	55	47	75	55	62	56	80	45
442	821	226	200	280	323	347	355	417	379	124	90	119	90	57	258

Appendix B (cont.)

DK99WC-7	DK99WC-8	DK99WC-9	DK99WC-14	DK99WC-15	DK99WC-12	DK99WC-16	DK99WC-17	DK99WC-11	DK99WC-18	DK99WC-10	DK99WC-19	DK99WC-13	SHB-WETF-1-34.0	SHB-WETF-1-39.9	SHB-WETF-1-42.4
Qbt 3	Qbt 3	Qbt 3T	Qbt 4	Qbt 4	Qbt 4										
1759610.59	1759756.81	1759765.65	1759805.86	1759870.40	1760187.61	1759872.91	1759874.75	1760349.20	1759934.30	1760382.57	1759890.86	1760576.21	1761069.31	1761069.31	1761069.31
1614339.83	1614660.39	1614669.23	1608881.82	1608818.55	1610794.72	1608858.84	1608857.60	1610753.74	1608820.12	1610744.49	1608989.16	1609543.30	1609576.52	1609576.52	1609576.52
7396.26	7419.14	7431.03	7465.73	7503.49	7515.39	7521.67	7518	7539.36	7549.74	7551.43	7553.24	7578	7568	7563	7560
76.80	76.25	75.50	75.89	75.72	75.83	75.43	69.12	74.32	73.12	73.52	73.68	73.10	72.74	70.76	72.41
0.13	0.15	0.19	0.18	0.19	0.18	0.20	0.55	0.24	0.25	0.26	0.26	0.26	0.24	0.24	0.27
12.35	12.64	13.08	12.80	12.96	13.16	12.96	15.00	13.53	13.91	14.03	13.88	13.90	13.61	14.47	13.58
1.57	1.72	2.05	1.94	2.01	1.93	1.94	3.78	2.28	2.47	2.34	2.40	2.40	2.29	2.50	2.50
0.05	0.06	0.06	0.06	0.07	0.07	0.07	0.10	0.04	0.07	0.08	0.09	0.07	0.07	0.05	0.07
0.00	0.00	0.00	0.00	0.00	0.00	0.00	1.00	0.00	0.20	0.00	0.00	0.00	0.00	0.24	0.35
0.20	0.36	0.25	0.30	0.31	0.27	0.28	1.48	0.27	0.47	0.38	0.44	0.42	0.37	0.48	0.67
4.08	4.25	4.36	4.48	4.48	4.42	4.54	4.32	4.42	4.48	4.68	4.74	4.78	4.63	4.55	4.11
4.55	4.62	4.80	4.70	4.83	4.87	4.74	4.21	4.74	4.65	4.85	4.86	4.85	4.62	4.54	4.20
0.00	0.01	0.01	0.02	0.03	0.02	0.02	0.15	0.03	0.04	0.03	0.03	0.03	0.03	0.03	0.05
0.35	0.29	0.48	0.18	0.21	0.29	0.21	1.13	0.47	0.61	0.38	0.30	0.41	0.52	1.25	1.11
99.73	100.06	100.29	100.39	100.59	100.77	100.19	99.71	99.86	99.68	100.16	100.38	99.82	98.62	97.84	98.18
45	38	37	40	55	57	44	111	58	46	42	42	87	61	58	59
103	96	94	97	103	92	88	82	78	90	81	85	77	85	87	89
24	46	37	34	34	35	35	212	64	64	63	36	70	65	73	99
36	26	33	35	36	30	41	36	35	39	38	37	54	34	35	45
251	260	357	350	354	334	331	350	393	364	366	411	408	384	344	293
54	59	48	51	45	51	46	34	45	49	42	39	41	44	33	38
124	229	194	204	195	229	199	651	342	351	347	304	318	384	416	421

Appendix B (cont.)

SHB-WETF- 1-43.0 Qbt 4	SHB-WETF- 1-43.7 Qbt 4	SHB-WETF- 1-45.0 Qbt 4	SHB-WETF- 1-46.9 Qbt 4	SHB-WETF- 1-48.0 Qbt 4	SHB-WETF- 1-48.8 Qbt 4	SHB-WETF- 1-50.0 Qbt 4	SHB-WETF- 1-50.5 Qbt 4	SHB-WETF- 1-51.5 Qbt 4	SHB-WETF- 1-51.8 Qbt 4	SHB-WETF- 1-52.0 Qbt 4	SHB-WETF- 1-52.2 Qbt 4	SHB-WETF- 1-52.5 Qbt 4	SHB-WETF- 1-54.9 Qbt 3T	SHB-WETF- 2C-37.5 Qbt 4	SHB-WETF- 3-45.9 Qbt 4
1761069.31	1761069.31	1761069.31	1761069.31	1761069.31	1761069.31	1761069.31	1761069.31	1761069.31	1761069.31	1761069.31	1761069.31	1761069.31	1761069.31	1760972.31	1760802.69
1609576.52	1609576.52	1609576.52	1609576.52	1609576.52	1609576.52	1609576.52	1609576.52	1609576.52	1609576.52	1609576.52	1609576.52	1609576.52	1609576.52	1609658.11	1609523.98
7559	7559	7557	7556	7554	7554	7552	7552	7551	7551	7550	7550	7550	7548	7564	7555
75.78	71.01	72.21	71.65	71.65	71.66	69.75	70.73	70.56	70.97	70.71	70.55	71.71	74.61	57.02	72.84
70.18	0.27	0.25	0.26	0.30	0.29	0.42	0.34	0.36	0.34	0.34	0.38	0.33	0.19	0.67	0.22
12.34	14.26	13.76	14.00	13.86	14.24	14.84	14.01	14.49	14.51	14.20	14.47	13.93	13.01	16.26	13.18
1.71	2.72	2.41	2.63	2.61	2.22	3.16	2.67	2.78	2.63	3.20	3.02	2.65	1.94	6.14	2.19
0.05	0.06	0.08	0.08	0.08	0.06	0.11	0.09	0.17	0.11	0.14	0.09	0.07	0.08	0.11	0.07
0.00	0.47	0.28	0.40	0.30	0.21	0.37	0.31	0.56	0.27	0.30	0.39	0.25	0.00	2.72	0.27
0.36	0.73	0.71	0.58	0.80	0.81	1.04	0.88	0.96	0.88	0.94	0.88	0.88	0.32	2.56	0.67
4.15	3.97	4.38	4.03	4.32	4.57	4.88	4.50	4.45	4.52	4.18	4.32	4.53	4.52	2.06	4.17
4.64	4.12	4.43	4.16	4.28	4.56	4.28	4.36	4.47	4.46	4.30	4.40	4.48	4.75	3.54	4.34
0.02	0.05	0.05	0.04	0.07	0.06	0.09	0.07	0.07	0.06	0.07	0.07	0.06	0.02	0.14	0.04
0.24	1.81	0.52	1.50	1.02	0.55	0.75	0.61	1.07	0.82	1.04	1.30	0.61	0.28	7.98	0.71
99.24	97.67	98.56	97.83	98.27	98.68	98.94	97.97	98.89	98.75	98.37	98.57	98.89	99.45	91.23	97.97
40	73	155	77	70	53	94	87	100	78	76	79	79	58	93	86
95	87	91	93	96	91	63	73	84	81	81	89	84	86	129	98
36	97	110	80	114	111	168	126	128	119	128	120	109	41	297	84
49	45	34	53	26	29	36	25	41	37	36	38	41	38	19	48
340	267	286	265	303	330	426	390	371	355	381	368	379	333	112	291
43	36	41	32	38	47	33	36	38	41	38	39	37	56	14	45
207	410	423	362	377	524	708	493	521	411	487	549	489	245	977	317

## Appendix B (cont.)

SHB-WETF- 3-48.1 Qbt 4	SHB-WETF- 3-49.0 Qbt 3T	SHB-WETF- 3-50.0 Qbt 3T	SHB-WETF- 3-54.2 Qbt 3T	SHB-WETF- 3-55.1 Qbt 3T	SHB-WETF- 3-56.6 Qbt 3T	SHB-WETF- 4-35.0 Qbt 4	SHB-WETF- 4-35.6 Qbt 4	SHB-WETF- 4-36.2 Qbt 4	SHB-WETF- 4-38.2 Qbt 4	SHB-WETF- 4-39.9 Qbt 4	SHB-WETF- 4-42.7 Qbt 4	SHB-WETF- 4-45.0 Qbt 3T	SHB-WETF- 4-45.5 Qbt 3T	SHB-WETF- 4-46.3 Qbt 3T	SHB-WETF- 5-47.8 Qbt 4
1760802.69	1760802.69	1760802.69	1760802.69	1760802.69	1760802.69	1760758.91	1760758.91	1760758.91	1760758.91	1760758.91	1760758.91	1760758.91	1760758.91	1760758.91	1760971.1
1609523.98	1609523.98	1609523.98	1609523.98	1609523.98	1609523.98	1609206.65	1609206.65	1609206.65	1609206.65	1609206.65	1609206.65	1609206.65	1609206.65	1609206.65	1609380.45
7553	7552	7551	7547	7546	7545	7560	7559	7559	7557	7555	7552	7550	7550	7549	7558
69.66	72.77	74.74	73.87	72.86	73.33	71.48	71.60	68.50	73.37	71.58	71.27	71.27	75.35	74.33	74.65
0.41	0.18	0.20	0.19	0.22	0.20	0.24	0.25	0.33	0.25	0.29	0.38	0.38	0.20	0.20	0.21
14.09	13.85	12.76	12.98	13.48	13.21	13.90	14.55	15.82	14.13	14.12	14.08	14.08	13.37	13.41	13.11
3.13	1.68	1.90	1.89	2.21	2.11	2.46	2.74	3.36	2.58	3.05	2.96	2.96	1.75	1.98	2.05
0.10	0.06	0.08	0.06	0.07	0.07	0.07	0.04	0.06	0.05	0.07	0.06	0.06	0.05	0.07	0.08
0.40	0.11	0.11	0.00	0.13	0.00	0.29	0.39	0.43	0.33	0.38	0.35	0.35	0.00	0.00	0.00
1.05	0.50	0.51	0.33	0.37	0.34	0.50	0.48	0.66	0.57	0.53	0.63	0.63	0.40	0.38	0.30
4.89	4.96	4.50	4.56	4.43	4.44	4.44	3.76	4.53	3.82	3.70	3.79	3.79	4.63	4.52	4.39
4.47	4.85	4.60	4.69	4.71	4.68	4.50	4.25	4.31	4.08	4.04	3.93	3.93	4.69	4.68	4.71
0.08	0.03	0.03	0.03	0.03	0.03	0.03	0.04	0.04	0.04	0.04	0.07	0.07	0.04	0.05	0.04
0.27	0.18	0.23	0.19	0.71	0.42	0.94	1.74	1.59	1.64	2.37	2.02	2.02	0.36	0.41	0.45
98.27	98.97	99.42	98.61	98.51	98.42	97.91	98.09	98.04	99.23	97.80	97.53	97.53	100.48	99.62	99.53
82	43	43	33	65	43	87	61	74	66	68	67	67	29	33	37
93	81	86	87	93	90	88	98	71	97	90	91	91	83	86	93
141	52	42	47	46	38	62	47	96	53	67	78	78	44	46	42
30	39	41	40	41	40	42	53	46	43	38	48	48	35	40	48
415	308	353	323	357	354	323	334	368	316	344	460	460	332	329	349
46	37	38	37	49	50	35	39	35	38	41	36	36	38	37	46
550	256	226	260	205	259	301	232	609	218	283	358	358	274	259	245

Appendix B (cont.)

SHB-WETF- 5-50.0 Qbt 4	SHB-WETF- 5-50.5 Qbt 4	SHB-WETF- 5-52.0 Qbt 4	SHB-WETF- 6-40 Qbt 4	SHB-WETF- 6-46.9 Qbt 4	SHB-WETF- 6-48.5 Qbt 4	SHB-WETF- 6-50.1 Qbt 4	SHB-WETF- 6-50.3 Qbt 4	SHB-WETF- 6-51.2 Qbt 3T	SHB-WETF- 6-51.5 Qbt 3T	SHB-WETF- 6-52.3 Qbt 3T	SHB-WETF- 6-54 Qbt 3T	SHB-WETF- 6-54.5 Qbt 3T	SHB-WETF- 6-55 Qbt 3T	SHB3-8.5 Qbt 4	SHB3-28 Qbt 4
1760971.1 1609380.45 7556	1760971.1 1609380.45 7556	1760971.1 1609380.45 7554	1761004.07 1609175.93 7565	1761004.07 1609175.93 7558	1761004.07 1609175.93 7557	1761004.07 1609175.93 7555	1761004.07 1609175.93 7555	1761004.07 1609175.93 7554	1761004.07 1609175.93 7554	1761004.07 1609175.93 7553	1761004.07 1609175.93 7551	1761004.07 1609175.93 7551	1761004.07 1609175.93 7550	1760990 1609310 7599	1760990 1609310 7579
70.22	70.34	70.22	71.71	69.90	73.99	72.21	71.78	73.12	74.28	73.97	72.61	74.13	74.26	73.00	72.94
0.34	0.29	0.34	0.25	0.30	0.23	0.26	0.31	0.27	0.20	0.20	0.24	0.21	0.19	0.24	0.25
14.19	14.61	14.19	13.82	14.57	13.15	14.05	13.89	13.25	13.05	13.05	13.60	13.07	12.99	13.40	13.65
2.76	3.20	2.76	2.38	3.30	2.10	2.15	2.43	2.21	1.82	2.02	2.26	2.14	1.98	2.26	2.32
0.77	0.13	0.77	0.08	0.08	0.07	0.06	0.08	0.07	0.06	0.07	0.07	0.09	0.11	0.07	0.07
0.79	0.54	0.79	0.18	0.58	0.26	0.26	0.35	0.22	0.00	0.12	0.15	0.12	0.00	0.09	0.10
0.90	0.65	0.90	0.58	0.83	0.76	0.86	1.02	0.55	0.44	0.45	0.56	0.42	0.41	0.46	0.44
4.16	3.42	4.16	4.74	3.85	4.40	4.65	4.62	4.15	4.51	4.56	4.55	4.57	4.57	4.60	4.63
4.30	3.90	4.30	4.68	4.05	4.38	4.59	4.54	4.53	4.63	4.77	4.78	4.73	4.84	4.76	4.72
0.07	0.04	0.07	0.04	0.06	0.04	0.06	0.07	0.03	0.02	0.03	0.09	0.03	0.02	0.04	0.04
1.33	2.93	1.33	0.34	1.86	0.21	0.27	0.20	0.71	0.18	0.35	0.56	0.18	0.17	0.32	0.52
98.51	97.12	98.51	98.46	97.52	99.37	99.15	99.10	98.40	99.02	99.23	98.91	99.51	99.38	98.90	99.16
228	77	228	50	106	63	45	62	50	41	45	60	54	53	43	50
103	115	103	80	96	89	99	94	96	80	83	87	87	95	79	85
129	70	129	70	87	88	92	118	52	38	34	67	35	41	64	61
67	57	67	34	55	24	35	29	38	26	27	25	34	35	46	35
319	281	319	364	318	299	327	340	348	333	329	357	352	347	376	373
39	49	39	43	46	43	43	47	44	47	42	47	44	44	43	42
672	435	672	369	362	313	376	493	271	260	163	320	172	216	349	318

## Appendix B (cont.)

SHB3-38 Qbt 4 1760990 1609310 7569	SHB3-45 Qbt 4 1760990 1609310 7562	SHB3-53 Qbt 4 1760990 1609310 7554	SHB3-58 Qbt 3T 1760990 1609310 7549	SHB3-79 Qbt 3T 1760990 1609310 7528	SHB3-99 Qbt 3T 1760990 1609310 7508	SHB3-102.75 Qbt 3T 1760990 1609310 7504	SHB3-109 Qbt 3T 1760990 1609310 7498	SHB3-119 Qbt 3T 1760990 1609310 7488	SHB3-130 Qbt 3T 1760990 1609310 7477	SHB3-140 Qbt 3T 1760990 1609310 7467	SHB3-151 Qbt 3T 1760990 1609310 7456	SHB3-158.5 Qbt 3 1760990 1609310 7449	SHB3-170 Qbt 3 1760990 1609310 7437	SHB3-178.5 Qbt 3 1760990 1609310 7429	SHB3-199 Qbt 3 1760990 1609310 7408
72.17	75.35	74.93	74.22	74.60	74.27	75.81	75.39	74.56	76.17	74.49	76.31	75.30	77.99	75.62	76.32
0.25	0.20	0.20	0.19	0.19	0.19	0.18	0.19	0.18	0.17	0.16	0.16	0.15	0.13	0.14	0.13
13.73	12.89	13.05	12.99	12.70	12.82	12.78	12.72	12.62	12.83	12.51	12.93	12.34	12.05	12.26	12.09
2.31	1.98	2.03	1.91	1.97	2.00	1.96	2.04	1.88	1.89	1.79	1.80	1.71	1.50	1.62	1.56
0.07	0.07	0.07	0.07	0.07	0.07	0.07	0.05	0.08	0.06	0.06	0.07	0.06	0.05	0.06	0.06
0.12	0.00	0.11	0.09	0.10	0.10	0.00	0.00	0.08	0.00	0.00	0.00	0.10	0.00	0.00	0.00
0.48	0.45	0.47	0.45	0.39	0.38	0.36	0.26	0.33	0.33	0.29	0.35	0.42	0.35	0.27	0.31
4.80	4.45	4.52	4.55	4.45	4.49	4.46	4.42	4.42	4.42	4.39	4.40	4.20	4.17	4.24	4.22
4.65	4.74	4.77	4.78	4.75	4.81	4.76	4.80	4.73	4.78	4.67	4.77	4.49	4.41	4.63	4.48
0.04	0.02	0.03	0.03	0.03	0.03	0.02	0.03	0.02	0.02	0.02	0.02	0.01	0.02	0.00	0.02
0.36	0.15	0.13	0.20	0.22	0.23	0.16	0.26	0.28	0.18	0.25	0.20	0.29	0.12	0.21	0.21
98.61	100.15	100.17	99.28	99.24	99.16	100.42	99.90	98.89	100.68	98.38	100.80	98.78	100.66	98.84	99.25
57	48	52	36	59	56	69	64	58	68	44	67	57	58	60	45
80	84	89	90	91	98	89	95	99	107	97	104	94	89	108	97
75	40	41	39	34	38	41	35	29	36	28	37	46	40	29	31
36	33	28	39	36	36	33	39	39	33	38	47	39	35	40	38
377	377	369	325	336	337	342	333	319	326	301	290	248	246	254	239
40	52	43	42	48	47	45	51	50	50	54	60	48	45	43	45
370	229	253	216	220	206	224	147	194	234	184	177	179	177	127	158

Appendix B (cont.)

SHB3-215	SHB3-223	SHB3-228.5	SHB3-233	SHB3-235	SHB3-255	SHB3-275	SHB3-295	SHB3-314	SHB3-321.5	SHB3-342.4	SHB3-423.5	SHB3-433.5	SHB3-499	SHB3-555.2	SHB3-600
Qbt 3	Qbt 3	Qbt 3	Qbt 3	Qbt 2	Tsankawi(?)	Cerro Toledo	Cerro Toledo	Qbo	Qbo	Qbo	Qbo				
1760990	1760990	1760990	1760990	1760990	1760990	1760990	1760990	1760990	1760990	1760990	1760990	1760990	1760990	1760990	1760990
1609310	1609310	1609310	1609310	1609310	1609310	1609310	1609310	1609310	1609310	1609310	1609310	1609310	1609310	1609310	1609310
7392	7384	7379	7374	7352	7352	7332	7312	7293	7286	7265	7184	7174	7108	7052	7007
75.98	78.26	78.71	77.53	77.30	77.32	77.21	77.68	77.63	78.28	70.69	77.24	77.05	76.31	76.44	76.04
0.14	0.12	0.11	0.15	0.09	0.09	0.09	0.09	0.09	0.13	0.57	0.12	0.12	0.16	0.16	0.13
11.89	11.79	11.56	11.71	11.43	11.38	11.34	11.34	11.50	11.57	14.08	12.17	12.13	12.49	12.20	11.93
1.50	1.39	1.30	1.63	1.33	1.35	1.31	1.36	1.40	1.60	3.53	1.44	1.44	1.67	1.58	1.44
0.05	0.05	0.04	0.06	0.05	0.05	0.05	0.06	0.06	0.06	0.12	0.04	0.04	0.08	0.06	0.06
0.00	0.00	0.00	0.15	0.00	0.00	0.00	0.00	0.00	0.11	0.98	0.00	0.00	0.13	0.15	0.12
0.33	0.33	0.29	0.31	0.20	0.19	0.22	0.22	0.22	0.42	0.90	0.20	0.18	0.51	0.52	0.48
4.09	4.10	3.98	3.97	3.94	3.97	3.93	4.02	3.99	3.88	1.63	4.03	4.27	4.25	3.94	3.30
4.38	4.30	4.26	4.31	4.31	4.31	4.26	4.24	4.23	4.05	2.92	4.67	4.72	4.33	4.36	4.78
0.00	0.01	0.01	0.03	0.00	0.00	0.00	0.00	0.00	0.02	0.03	0.00	0.00	0.03	0.03	0.02
0.15	0.14	0.18	0.25	0.23	0.15	0.20	0.22	0.23	0.32	4.35	0.42	0.20	0.37	0.62	1.71
98.37	100.35	100.27	99.85	98.64	98.67	98.40	99.06	99.12	100.11	95.44	99.91	99.96	99.97	99.44	98.30
43	43	44	74	59	51	50	52	74	63	85	50	52	89	47	62
92	78	80	101	121	126	116	120	118	117	180	103	118	119	92	124
42	39	32	35	19	18	25	23	24	57	178	8	0	69	61	47
28	27	31	39	44	38	47	40	47	39	53	30	26	38	32	34
218	201	205	214	190	189	189	191	188	196	325	250	251	213	213	172
43	40	46	49	51	53	56	50	54	63	47	45	53	53	61	45
170	163	139	152	95	107	128	101	91	172	600	0	0	229	215	162

## Appendix B (cont.)

SHB3-665	SHB3-703	SHB3-757	SHB3-798	SHB3-838.1	PC94-4	PC94-5	PC94-6	PC94-7	PC84-8	PC94-9	PC94-1	PC94-2	PC94-3	PC94-10	PC94-11
Qbo	Qbo	Qbo	Qbo	Guaje Pumice	Qbt 3	Qbt 3	Qbt 3	Qbt 3T	Qbt 3T	Qbt 3T	Qbt 3T	Qbt 4	Qbt 4	Qbt 4	Qbt 4
1760990	1760990	1760990	1760990	1760990	1771686	1771686	1771686	1771686	1771686	1771686	1771686	1771686	1771686	1771686	1771686
1609310	1609310	1609310	1609310	1609310	1609814	1609814	1609814	1609814	1609814	1609814	1609814	1609814	1609814	1609814	1609814
6942	6904	6850	6809	6769	7770	7787	7802	7837	7855	7879	7747	7757	7762	7885	7895
76.46	75.45	75.47	73.25	72.41	75.72	74.86	74.90	74.61	75.55	74.56	73.87	72.60	72.57	71.41	73.68
0.07	0.11	0.12	0.18	0.19	0.14	0.14	0.14	0.18	0.17	0.18	0.20	0.22	0.24	0.33	0.21
11.81	12.15	12.30	12.76	12.17	12.25	12.38	12.13	12.45	12.68	12.47	12.97	13.48	13.41	13.49	12.96
1.24	1.55	1.59	1.98	2.43	1.65	1.72	1.73	1.92	1.86	1.90	2.00	2.29	2.34	3.03	2.05
0.06	0.08	0.07	0.08	0.09	0.06	0.05	0.07	0.05	0.07	0.06	0.05	0.06	0.05	0.09	0.06
0.00	0.00	0.11	0.23	0.56	0.00	0.00	0.00	0.08	0.00	0.08	0.00	0.16	0.24	0.16	0.00
0.19	0.41	0.47	0.76	0.68	0.30	0.24	0.17	0.32	0.25	0.29	0.26	0.40	0.43	0.40	0.23
3.41	3.69	3.72	3.69	2.87	4.03	4.14	4.19	4.32	4.40	4.36	4.38	4.30	4.23	4.53	4.33
5.25	4.79	4.78	4.58	5.16	4.55	4.64	4.69	4.81	4.69	4.80	4.87	4.77	4.69	4.84	4.92
0.00	0.02	0.02	0.04	0.04	0.03	0.04	0.00	0.02	0.02	0.04	0.03	0.03	0.03	0.02	0.01
1.79	2.12	2.17	2.70	3.54	0.23	0.33	0.34	0.24	0.21	0.19	0.30	0.77	1.06	1.00	0.41
98.49	98.24	98.64	97.53	96.60	98.71	98.21	98.02	98.76	99.70	98.72	98.61	98.32	98.23	98.30	98.44
77	89	84	107	129	50	50	59	66	59	61	63	70	64	74	65
175	246	228	288	412	101	104	104	99	97	95	98	92	88	89	98
9	43	48	107	95	37	28	26	29	33	29	33	38	56	49	35
46	79	71	82	97	40	29	35	36	32	30	32	32	39	36	31
162	193	192	246	246	236	272	270	324	304	315	336	336	332	443	343
78	118	123	150	158	48	50	49	48	45	45	51	47	42	52	49
72	94	147	259	229	175	168	154	161	211	195	178	214	240	260	176

Appendix B (cont.)

PC94-12 Qbt 4 1771686 1609814 7902	PC94-13 Qbt 4 1771686 1609814 7924	PC94-14 Qbt 4 1771686 1609814 7937	PC94-15 Qbt 3T 1771686 1609814 7950	PC94-16 Qbt 3T 1771686 1609814 7968	PC94-17 Qbt 3T 1771686 1609814 7985	PC94-18 Qbt 3T 1771686 1609814 8008
74.09	70.13	74.87	75.11	74.93	75.27	74.20
0.21	0.32	0.17	0.17	0.18	0.18	0.20
12.92	14.38	12.53	12.62	12.68	12.77	13.12
2.05	3.27	1.87	1.87	1.92	1.94	2.05
0.03	0.06	0.07	0.05	0.06	0.05	0.07
0.00	0.39	0.00	0.00	0.00	0.00	0.00
0.23	0.42	0.27	0.20	0.22	0.20	0.24
4.35	3.88	4.33	4.32	4.42	4.27	4.28
4.82	4.31	4.76	4.73	4.78	4.83	4.89
0.00	0.00	0.02	0.00	0.02	0.00	0.02
0.39	2.16	0.22	0.29	0.26	0.35	0.50
98.70	97.17	98.90	99.08	99.22	99.50	99.07
42	87	46	62	65	57	58
99	92	98	92	98	104	98
37	50	30	30	30	29	36
20	31	36	32	45	34	34
338	390	315	310	314	319	355
53	47	50	47	48	46	48
221	288	172	183	174	165	240

## Electron Microprobe Analyses of Volcanic Glasses

Appendix C: Table 1. Otowi Member of the Bandelier Tuff

Sample	SiO <sub>2</sub>	Al <sub>2</sub> O <sub>3</sub>	MgO	Na <sub>2</sub> O	CaO	K <sub>2</sub> O	SrO	P <sub>2</sub> O <sub>5</sub>	TiO <sub>2</sub>	MnO	FeO	BAO	TOTAL
ss99btg_4	74.54	11.77	0.02	3.65	0.32	4.77	0.00	0.07	0.12	0.05	1.01	0.04	96.35
ss99btg_4	74.80	11.85	0.02	3.80	0.32	4.64	0.00	0.00	0.11	0.05	1.26	0.03	96.87
ss99btg_4	75.82	11.80	0.02	3.68	0.30	4.65	0.00	0.01	0.21	0.06	1.21	0.00	97.75
ss99btg_4	75.68	11.76	0.01	3.70	0.33	4.67	0.00	0.01	0.15	0.06	1.18	0.04	97.60
ss99btg_4	75.67	11.81	0.02	3.65	0.34	4.49	0.00	0.01	0.20	0.06	1.27	0.07	97.59
ss99btg_4	73.51	11.58	0.03	3.59	0.35	4.76	0.00	0.00	0.13	0.02	1.20	0.03	95.19
ss99btg_4	75.22	11.92	0.03	3.68	0.32	4.59	0.00	0.00	0.08	0.03	1.17	0.10	97.15
ss99btg_4	74.08	11.93	0.03	3.63	0.35	4.74	0.00	0.04	0.11	0.06	1.28	0.00	96.23
ss99btg_4	75.56	11.96	0.03	3.65	0.32	4.55	0.00	0.00	0.19	0.02	1.33	0.00	97.61
ss99btg_4	74.80	11.80	0.01	3.96	0.31	4.64	0.00	0.00	0.17	0.10	1.21	0.00	96.99
ss99btg_4	74.94	11.85	0.02	3.63	0.30	4.68	0.00	0.00	0.09	0.05	1.25	0.07	96.88
ss99btg_4	74.53	11.87	0.03	3.35	0.33	4.69	0.00	0.00	0.07	0.07	1.13	0.00	96.07
ss99btg_4	75.53	11.94	0.04	3.85	0.33	4.55	0.00	0.01	0.01	0.06	1.28	0.00	97.59
ss99btg_4	74.50	11.77	0.01	3.60	0.34	4.70	0.00	0.13	0.15	0.03	1.18	0.04	96.43
ss99btg_4	75.22	11.91	0.00	3.48	0.34	4.66	0.00	0.01	0.17	0.05	1.19	0.00	97.03
ss99btg_4	75.61	11.89	0.01	3.67	0.35	4.64	0.00	0.09	0.05	0.09	1.27	0.00	97.67
ss99btg_4	75.84	11.97	0.01	3.70	0.34	4.69	0.00	0.00	0.13	0.06	1.29	0.00	98.02
ss99btg_4	75.83	12.03	0.02	3.56	0.28	4.68	0.00	0.02	0.07	0.11	1.23	0.00	97.84
ss99btg_4	75.54	11.73	0.02	3.82	0.31	4.63	0.00	0.01	0.18	0.00	1.22	0.07	97.52
ss99btg_4	74.75	11.90	0.02	3.59	0.35	4.73	0.00	0.02	0.12	0.04	1.26	0.05	96.83
ss99btg_4	73.80	11.74	0.03	3.53	0.31	4.70	0.00	0.00	0.10	0.04	1.13	0.00	95.38
ss99btg_4	74.84	11.76	0.02	3.66	0.33	4.63	0.00	0.01	0.07	0.02	1.27	0.00	96.61
ss99btg_4	75.29	11.85	0.02	3.71	0.32	4.67	0.00	0.02	0.07	0.03	1.37	0.00	97.35
ss99btg_4	74.98	11.75	0.02	3.70	0.31	4.68	0.00	0.04	0.07	0.06	1.32	0.02	96.95
ss99btg_4	75.08	12.01	0.01	3.53	0.35	4.63	0.00	0.00	0.18	0.08	1.27	0.03	97.17
ss99btg_4	75.13	11.81	0.03	3.80	0.31	4.47	0.00	0.00	0.13	0.07	1.25	0.03	97.02
ss99btg_4	75.28	11.93	0.02	3.64	0.31	4.54	0.00	0.01	0.11	0.06	1.26	0.00	97.16
ss99btg_4	75.26	11.98	0.01	3.63	0.33	4.70	0.00	0.00	0.14	0.03	1.20	0.00	97.28
ss99btg_4	75.89	11.85	0.03	3.81	0.35	4.62	0.00	0.00	0.12	0.03	1.20	0.03	97.93

Appendix C: Table 1. Otowi Member of the Bandelier Tuff (cont.)

Sample	SiO <sub>2</sub>	Al <sub>2</sub> O <sub>3</sub>	MgO	Na <sub>2</sub> O	CaO	K <sub>2</sub> O	SPD	P <sub>2</sub> O <sub>5</sub>	TiO <sub>2</sub>	MnO	FeO	BAO	TOTAL
ss99btg_13	74.39	11.86	0.00	3.50	0.24	3.33	0.00	0.00	0.06	0.04	1.31	0.03	94.76
ss99btg_13	74.12	11.83	0.00	3.60	0.24	3.68	0.00	0.03	0.05	0.05	1.31	0.00	94.91
ss99btg_13	72.77	11.60	0.00	3.55	0.24	3.67	0.00	0.00	0.03	0.09	1.28	0.00	93.22
ss99btg_13	71.73	11.25	0.00	3.52	0.24	3.60	0.00	0.00	0.05	0.10	1.18	0.00	91.66
ss99btg_13	72.65	11.50	0.00	3.69	0.23	3.65	0.00	0.03	0.00	0.08	1.18	0.00	93.00
ss99btg_13	75.09	11.81	0.00	3.46	0.26	3.17	0.00	0.00	0.04	0.11	1.26	0.03	95.22
ss99btg_13	74.22	11.84	0.00	3.69	0.25	3.65	0.00	0.00	0.08	0.08	1.25	0.09	95.15
ss99btg_13	71.45	11.07	0.00	3.62	0.22	3.37	0.01	0.00	0.05	0.10	1.05	0.00	90.93
ss99btg_13	72.07	11.42	0.00	3.49	0.23	3.10	0.00	0.00	0.02	0.08	1.15	0.00	91.56
ss99btg_13	74.84	11.83	0.00	3.48	0.24	3.77	0.00	0.00	0.04	0.08	1.32	0.00	95.61
ss99btg_13	73.82	11.75	0.00	3.72	0.22	3.48	0.00	0.00	0.05	0.06	1.33	0.01	94.43
ss99btg_13	73.25	11.65	0.00	3.60	0.23	3.93	0.00	0.00	0.09	0.10	1.38	0.00	94.21
ss99btg_13	74.02	11.73	0.00	3.61	0.25	3.67	0.00	0.00	0.04	0.05	1.29	0.06	94.71
ss99btg_13	75.17	11.76	0.00	3.65	0.25	3.31	0.00	0.01	0.08	0.05	1.31	0.02	95.59
ss99btg_13	73.92	11.72	0.00	3.35	0.25	3.25	0.00	0.00	0.00	0.08	1.31	0.00	93.88
ss99btg_13	75.42	11.89	0.00	3.68	0.26	3.64	0.00	0.02	0.00	0.10	1.30	0.00	96.31
ss99btg_13	74.33	11.84	0.00	3.41	0.22	4.24	0.00	0.00	0.00	0.08	1.32	0.04	95.47
ss99btg_13	74.13	11.72	0.00	3.74	0.27	3.63	0.00	0.01	0.06	0.09	1.31	0.00	94.95
ss99btg_13	70.82	11.14	0.00	3.47	0.21	3.18	0.00	0.02	0.04	0.10	1.12	0.03	90.13
ss99btg_13	71.13	11.13	0.00	3.47	0.24	2.94	0.00	0.01	0.00	0.05	1.03	0.00	90.01

Appendix C: Table 1. Otowi Member of the Bandelier Tuff (cont.)

Sample	SiO <sub>2</sub>	TiO <sub>2</sub>	Al <sub>2</sub> O <sub>3</sub>	FeO	MnO	MgO	CaO	Na <sub>2</sub> O	K <sub>2</sub> O	P <sub>2</sub> O <sub>5</sub>	SrO	BAO	TOTAL
shb3_600	75.49	0.00	11.98	1.19	0.05	0.00	0.21	3.50	4.99	0.00	0.01	0.01	97.43
shb3_600	75.60	0.13	12.04	1.30	0.02	0.01	0.24	3.59	4.98	0.00	0.03	0.01	97.93
shb3_600	76.21	0.12	11.97	1.17	0.04	0.01	0.23	3.44	5.08	0.02	0.00	0.00	98.29
shb3_600	75.54	0.00	11.98	1.25	0.00	0.00	0.22	3.55	5.04	0.00	0.01	0.00	97.59
shb3_600	75.92	0.14	11.94	1.04	0.06	0.00	0.21	3.42	5.10	0.01	0.00	0.00	97.84
shb3_600	75.41	0.13	11.94	1.22	0.04	0.01	0.24	3.42	5.07	0.00	0.03	0.00	97.51
shb3_600	75.36	0.06	11.92	1.26	0.02	0.00	0.23	3.35	5.05	0.03	0.00	0.00	97.27
shb3_600	75.21	0.11	11.93	1.27	0.03	0.01	0.20	3.50	5.03	0.01	0.00	0.00	97.31
shb3_600	75.55	0.06	11.84	1.30	0.00	0.01	0.24	3.45	5.00	0.03	0.04	0.00	97.53
shb3_600	75.72	0.13	11.98	0.75	0.05	0.00	0.20	3.32	5.32	0.00	0.03	0.04	97.55
shb3_600	75.72	0.07	11.96	1.01	0.06	0.00	0.21	3.41	5.06	0.02	0.00	0.02	97.55
shb3_600	75.87	0.12	11.93	0.21	0.02	0.00	0.19	2.61	6.02	0.00	0.02	0.02	97.00
shb3_600	76.04	0.05	11.99	0.83	0.06	0.00	0.27	3.49	4.94	0.02	0.02	0.01	97.74
shb3_600	75.07	0.08	11.83	1.23	0.06	0.00	0.18	3.56	5.03	0.00	0.01	0.00	97.06
shb3_600	75.16	0.08	12.00	1.25	0.09	0.01	0.20	3.62	5.06	0.03	0.05	0.00	97.53
shb3_600	75.51	0.04	11.95	1.06	0.08	0.01	0.21	3.46	5.03	0.00	0.02	0.02	97.38
shb3_600	75.91	0.00	11.89	1.12	0.01	0.00	0.22	3.44	5.13	0.00	0.00	0.00	97.73
shb3_600	76.79	0.13	12.09	0.45	0.03	0.00	0.17	3.41	5.38	0.00	0.00	0.09	98.54
shb3_600	76.19	0.21	11.98	1.20	0.03	0.01	0.23	3.42	4.98	0.00	0.01	0.00	98.26
shb3_600	75.73	0.05	12.02	1.01	0.06	0.00	0.21	3.52	5.08	0.02	0.02	0.00	97.74
shb3_600	75.15	0.13	11.97	1.29	0.07	0.00	0.20	3.46	4.98	0.00	0.03	0.00	97.28
shb3_600	75.15	0.06	11.98	1.20	0.04	0.01	0.17	3.50	5.20	0.00	0.02	0.04	97.35
shb3_600	76.11	0.14	11.97	1.24	0.04	0.02	0.20	3.61	4.96	0.00	0.00	0.00	98.28
shb3_600	76.50	0.07	12.02	1.12	0.02	0.01	0.24	3.48	4.93	0.02	0.00	0.06	98.47
shb3_600	75.50	0.01	11.90	1.22	0.06	0.00	0.20	3.30	5.02	0.00	0.04	0.00	97.23
shb3_600	74.46	0.06	11.85	1.22	0.01	0.01	0.19	3.55	5.05	0.00	0.05	0.00	96.43
shb3_600	75.72	0.02	11.97	1.19	0.08	0.01	0.23	3.38	5.05	0.00	0.05	0.00	97.69
shb3_600	75.24	0.10	12.01	1.09	0.04	0.01	0.21	3.40	5.08	0.02	0.02	0.02	97.21
shb3_600	75.46	0.14	11.89	1.16	0.06	0.01	0.20	3.46	5.07	0.01	0.01	0.02	97.51
shb3_600	75.46	0.02	11.88	1.25	0.08	0.02	0.20	3.29	5.06	0.00	0.03	0.00	97.29
shb3_600	75.72	0.08	11.96	1.28	0.02	0.00	0.19	3.59	4.92	0.00	0.07	0.02	97.86
shb3_600	75.29	0.05	11.88	1.21	0.06	0.01	0.21	3.47	5.00	0.00	0.04	0.01	97.24
shb3_600	75.22	0.08	11.81	1.22	0.01	0.00	0.21	3.52	5.06	0.00	0.00	0.09	97.23
shb3_600	75.46	0.16	12.04	1.13	0.05	0.02	0.22	3.64	4.94	0.00	0.00	0.03	97.70
shb3_600	75.46	0.16	12.04	1.13	0.05	0.02	0.22	3.64	4.94	0.00	0.00	0.03	97.70
shb3_600	75.18	0.08	12.02	1.03	0.08	0.00	0.21	3.61	5.01	0.01	0.00	0.07	97.31
shb3_600	75.18	0.08	12.02	1.03	0.08	0.00	0.21	3.61	5.01	0.01	0.00	0.07	97.31
shb3_600	74.78	0.13	11.92	1.27	0.02	0.01	0.21	3.34	5.06	0.00	0.00	0.00	96.73
shb3_600	74.78	0.13	11.92	1.27	0.02	0.01	0.21	3.34	5.06	0.00	0.00	0.00	96.73
shb3_600	75.26	0.05	11.87	1.24	0.04	0.01	0.20	3.38	4.97	0.01	0.00	0.03	97.06
shb3_600	75.26	0.05	11.87	1.24	0.04	0.01	0.20	3.38	4.97	0.01	0.00	0.03	97.06
shb3_600	75.46	0.06	11.85	1.22	0.04	0.00	0.21	3.40	5.02	0.00	0.02	0.01	97.28
shb3_600	75.46	0.06	11.85	1.22	0.04	0.00	0.21	3.40	5.02	0.00	0.02	0.01	97.28
shb3_600	74.96	0.11	11.84	1.26	0.03	0.01	0.22	3.44	4.94	0.00	0.00	0.00	96.83

Appendix C: Table 1. Otowi Member of the Bandelier Tuff (cont.)

Sample	SiO <sub>2</sub>	Al <sub>2</sub> O <sub>3</sub>	MgO	Na <sub>2</sub> O	CaO	K <sub>2</sub> O	SrO	P <sub>2</sub> O <sub>5</sub>	TiO <sub>2</sub>	MnO	FeO	BAO	TOTAL
shb3_665	74.69	11.75	0.00	4.10	0.08	4.56	0.02	0.02	0.08	0.01	1.21	0.00	96.52
shb3_665	73.40	11.77	0.01	4.00	0.08	4.90	0.03	0.00	0.07	0.03	0.97	0.00	95.27
shb3_665	73.47	11.65	0.00	4.15	0.09	4.52	0.00	0.00	0.10	0.01	1.21	0.00	95.20
shb3_665	65.69	18.65	0.00	6.55	0.23	6.99	0.08	0.00	0.01	0.00	0.14	0.00	98.34
shb3_665	73.63	11.77	0.00	3.95	0.09	4.73	0.00	0.02	0.02	0.04	1.12	0.01	95.36
shb3_665	72.66	11.76	0.00	4.04	0.07	4.70	0.03	0.00	0.05	0.02	1.13	0.03	94.48
shb3_665	73.30	11.65	0.00	3.99	0.10	4.57	0.02	0.00	0.02	0.05	1.21	0.02	94.91
shb3_665	74.17	11.77	0.00	4.07	0.11	4.57	0.00	0.00	0.07	0.01	1.24	0.00	95.99
shb3_665	73.37	11.71	0.01	4.13	0.09	4.54	0.05	0.05	0.12	0.04	1.20	0.04	95.32
shb3_665	73.24	11.74	0.00	3.95	0.10	4.64	0.00	0.00	0.17	0.06	1.13	0.00	95.03
shb3_665	74.21	11.74	0.01	4.12	0.08	4.62	0.01	0.00	0.10	0.09	1.19	0.00	96.16
shb3_665	74.86	11.82	0.00	4.10	0.10	4.52	0.02	0.07	0.19	0.07	1.28	0.04	97.06
shb3_665	73.34	11.71	0.00	4.19	0.10	4.55	0.01	0.01	0.11	0.04	1.29	0.00	95.36
shb3_665	74.72	11.60	0.00	3.87	0.08	4.55	0.03	0.02	0.06	0.08	1.23	0.00	96.25
shb3_665	73.18	11.73	0.02	3.98	0.07	4.58	0.00	0.01	0.08	0.05	1.29	0.00	94.98
shb3_665	73.80	11.71	0.01	4.11	0.11	4.55	0.03	0.00	0.09	0.09	1.27	0.02	95.79
shb3_665	73.47	11.70	0.00	4.01	0.10	4.55	0.06	0.04	0.08	0.06	1.24	0.01	95.30
shb3_665	73.87	11.44	0.00	3.82	0.07	4.58	0.04	0.00	0.11	0.07	1.20	0.00	95.19
shb3_665	74.33	11.77	0.00	4.15	0.10	4.56	0.04	0.02	0.00	0.09	1.17	0.06	96.27
shb3_665	73.99	11.82	0.01	4.11	0.10	4.57	0.00	0.00	0.05	0.04	1.31	0.00	95.99
shb3_665	74.43	11.70	0.00	4.06	0.11	4.49	0.00	0.03	0.06	0.03	1.19	0.00	96.11
shb3_665	74.67	11.81	0.00	4.07	0.10	4.51	0.00	0.00	0.08	0.09	1.22	0.00	96.55
shb3_665	74.60	11.88	0.02	4.03	0.09	4.49	0.00	0.01	0.11	0.09	1.22	0.00	96.53
shb3_665	73.61	11.76	0.00	4.05	0.11	4.45	0.03	0.00	0.03	0.05	1.24	0.00	95.33
shb3_665	73.71	11.83	0.00	4.05	0.08	4.51	0.00	0.00	0.05	0.06	1.31	0.00	95.59
shb3_665	73.53	11.68	0.00	3.96	0.09	4.57	0.04	0.00	0.10	0.06	1.15	0.00	95.19
shb3_665	73.61	11.71	0.00	4.16	0.09	4.61	0.00	0.02	0.00	0.07	1.29	0.00	95.54
shb3_665	73.61	11.71	0.00	4.16	0.09	4.61	0.00	0.02	0.05	0.09	1.25	0.00	95.75
shb3_665	73.99	11.73	0.01	3.90	0.09	4.60	0.04	0.02	0.05	0.09	1.25	0.00	95.75
shb3_665	73.99	11.73	0.01	3.90	0.09	4.60	0.04	0.02	0.05	0.09	1.25	0.00	95.75
shb3_665	73.70	11.58	0.00	4.03	0.10	4.58	0.00	0.00	0.09	0.08	1.26	0.00	95.42
shb3_665	73.70	11.58	0.00	4.03	0.10	4.58	0.00	0.00	0.09	0.08	1.26	0.00	95.42
shb3_665	74.11	11.69	0.00	3.86	0.10	4.68	0.05	0.00	0.06	0.01	1.18	0.02	95.76
shb3_665	74.11	11.69	0.00	3.86	0.10	4.68	0.05	0.00	0.06	0.01	1.18	0.02	95.76
shb3_665	73.94	11.80	0.00	4.05	0.10	4.65	0.01	0.00	0.13	0.00	1.22	0.01	95.90
shb3_665	73.94	11.80	0.00	4.05	0.10	4.65	0.01	0.00	0.13	0.00	1.22	0.01	95.90
shb3_665	73.48	11.61	0.00	4.02	0.12	4.56	0.01	0.00	0.05	0.05	1.28	0.02	95.20
shb3_665	73.48	11.61	0.00	4.02	0.12	4.56	0.01	0.00	0.05	0.05	1.28	0.02	95.20
shb3_665	73.96	11.70	0.00	3.95	0.08	4.61	0.00	0.00	0.11	0.00	1.24	0.01	95.65

Appendix C: Table 1. Otowi Member of the Bandelier Tuff (cont.)

Sample	SiO <sub>2</sub>	Al <sub>2</sub> O <sub>3</sub>	MgO	Na <sub>2</sub> O	CaO	K <sub>2</sub> O	SrO	P <sub>2</sub> O <sub>5</sub>	TiO <sub>2</sub>	MnO	FeO	BAO	TOTAL
shb3_703	74.07	11.85	0.00	3.96	0.25	4.49	0.02	0.00	0.00	0.02	1.26	0.12	96.04
shb3_703	73.01	11.81	0.00	4.22	0.26	4.45	0.00	0.00	0.10	0.06	1.23	0.00	95.14
shb3_703	74.50	11.85	0.00	4.13	0.28	4.51	0.00	0.01	0.01	0.08	1.37	0.00	96.72
shb3_703	73.78	11.72	0.01	4.05	0.25	4.52	0.00	0.05	0.10	0.10	1.23	0.00	95.81
shb3_703	73.84	11.81	0.00	4.07	0.25	4.51	0.00	0.00	0.01	0.16	1.26	0.00	95.91
shb3_703	73.57	11.70	0.00	4.03	0.23	4.48	0.01	0.01	0.01	0.08	1.23	0.08	95.43
shb3_703	73.99	11.81	0.00	3.96	0.28	4.54	0.00	0.04	0.08	0.04	1.16	0.00	95.90
shb3_703	73.23	11.66	0.00	4.03	0.26	4.50	0.04	0.00	0.05	0.11	1.39	0.00	95.26
shb3_703	74.24	11.86	0.01	4.02	0.26	4.56	0.02	0.01	0.03	0.04	1.22	0.02	96.31
shb3_703	73.64	11.83	0.00	4.16	0.28	4.47	0.03	0.02	0.07	0.07	1.28	0.00	95.85
shb3_703	73.52	11.83	0.00	4.03	0.23	4.45	0.03	0.02	0.08	0.05	1.27	0.02	95.52
shb3_703	73.50	11.71	0.00	4.18	0.25	4.41	0.03	0.00	0.00	0.08	1.33	0.02	95.52
shb3_703	74.74	11.98	0.00	4.06	0.29	4.51	0.01	0.00	0.13	0.14	1.18	0.00	97.03
shb3_703	73.43	11.76	0.00	3.93	0.28	4.53	0.00	0.00	0.00	0.08	1.18	0.00	95.19
shb3_703	74.75	11.94	0.01	4.07	0.26	4.51	0.02	0.01	0.07	0.09	1.23	0.00	96.95
shb3_703	73.64	11.75	0.00	3.99	0.24	4.46	0.03	0.06	0.04	0.05	1.24	0.00	95.51
shb3_703	73.71	11.77	0.00	4.08	0.29	4.49	0.00	0.00	0.01	0.07	1.22	0.08	95.72
shb3_703	73.55	11.80	0.00	3.89	0.22	4.71	0.02	0.01	0.07	0.07	1.19	0.00	95.53
shb3_703	73.89	11.76	0.00	3.98	0.24	4.56	0.00	0.05	0.00	0.10	1.26	0.00	95.86
shb3_703	74.22	11.81	0.00	4.01	0.26	4.36	0.04	0.04	0.09	0.10	1.24	0.04	96.20
shb3_703	74.06	11.87	0.01	4.12	0.24	4.45	0.02	0.01	0.00	0.11	1.37	0.03	96.31
shb3_703	74.12	11.85	0.00	4.12	0.27	4.40	0.00	0.02	0.06	0.09	1.43	0.07	96.43
shb3_703	73.56	11.86	0.01	3.86	0.28	4.45	0.00	0.02	0.11	0.06	1.21	0.00	95.41
shb3_703	73.89	11.76	0.00	3.97	0.25	4.41	0.03	0.00	0.00	0.08	1.20	0.00	95.59
shb3_703	72.59	11.58	0.00	4.03	0.24	4.59	0.00	0.02	0.04	0.08	1.12	0.00	94.28
shb3_703	73.85	11.73	0.00	4.08	0.28	4.54	0.04	0.01	0.10	0.06	1.22	0.04	95.95
shb3_703	73.74	11.55	0.00	4.09	0.25	4.49	0.00	0.00	0.12	0.08	1.23	0.00	95.54
shb3_703	73.13	11.80	0.00	4.21	0.25	4.44	0.03	0.00	0.01	0.07	1.26	0.00	95.21
shb3_703	73.19	11.91	0.00	3.99	0.22	4.54	0.01	0.01	0.14	0.06	1.19	0.05	95.31
shb3_703	73.88	11.74	0.00	4.12	0.27	4.41	0.00	0.00	0.00	0.12	1.21	0.00	95.75
shb3_703	73.51	11.96	0.00	4.00	0.26	4.57	0.01	0.00	0.04	0.03	1.22	0.02	95.61
shb3_703	73.40	11.76	0.00	4.01	0.26	4.44	0.05	0.00	0.00	0.03	1.27	0.00	95.22
shb3_703	73.61	11.80	0.01	4.07	0.24	4.46	0.04	0.02	0.11	0.10	1.22	0.00	95.68
shb3_703	74.79	11.93	0.00	3.98	0.27	4.49	0.01	0.00	0.10	0.08	1.21	0.09	96.96
shb3_703	73.98	11.83	0.01	4.15	0.23	4.38	0.05	0.01	0.00	0.01	1.26	0.00	95.90

Appendix C: Table 1. Otowi Member of the Bandelier Tuff (cont.)

Sample	SiO <sub>2</sub>	Al <sub>2</sub> O <sub>3</sub>	MgO	Na <sub>2</sub> O	CaO	K <sub>2</sub> O	SrO	P <sub>2</sub> O <sub>5</sub>	TiO <sub>2</sub>	MnO	FeO	BAO	TOTAL
SHB3-757	75.28	11.93	0.00	4.13	0.26	4.35	0.00	0.00	0.12	0.08	1.12	0.01	97.28
SHB3-757	73.46	11.77	0.01	4.12	0.27	4.39	0.01	0.03	0.07	0.03	1.21	0.01	95.37
SHB3-757	73.78	11.73	0.00	4.13	0.27	4.42	0.02	0.00	0.04	0.11	1.28	0.03	95.81
SHB3-757	75.22	11.86	0.01	4.15	0.27	4.40	0.00	0.02	0.06	0.09	1.42	0.00	97.49
SHB3-757	74.50	11.81	0.00	4.10	0.28	4.40	0.02	0.00	0.00	0.04	1.25	0.00	96.39
SHB3-757	74.12	11.78	0.00	4.18	0.23	4.42	0.03	0.00	0.09	0.08	1.35	0.01	96.28
SHB3-757	74.31	11.88	0.00	3.95	0.27	4.41	0.00	0.00	0.09	0.00	1.20	0.00	96.11
SHB3-757	74.11	11.77	0.00	4.00	0.27	4.48	0.03	0.00	0.07	0.11	1.26	0.00	96.10
SHB3-757	73.49	11.81	0.00	4.00	0.29	4.43	0.02	0.00	0.05	0.08	1.24	0.00	95.40
SHB3-757	74.09	11.92	0.00	4.12	0.28	4.37	0.02	0.02	0.13	0.10	1.25	0.00	96.30
SHB3-757	74.10	11.89	0.00	4.22	0.27	4.48	0.02	0.00	0.03	0.11	1.26	0.01	96.39
SHB3-757	74.80	11.94	0.00	4.13	0.27	4.38	0.00	0.00	0.12	0.09	1.29	0.00	97.02
SHB3-757	75.87	11.94	0.00	3.88	0.27	4.49	0.01	0.00	0.08	0.05	1.29	0.03	97.90
SHB3-757	75.02	11.90	0.00	4.02	0.29	4.44	0.00	0.00	0.05	0.03	1.32	0.00	97.06
SHB3-757	74.05	11.89	0.00	4.22	0.26	4.46	0.02	0.02	0.05	0.07	1.27	0.03	96.31
SHB3-757	74.92	12.06	0.01	4.16	0.28	4.38	0.02	0.03	0.10	0.08	1.26	0.03	97.32
SHB3-757	74.40	11.89	0.00	4.17	0.27	4.33	0.00	0.02	0.12	0.07	1.32	0.02	96.61
SHB3-757	73.93	11.96	0.00	4.03	0.26	4.43	0.02	0.02	0.09	0.12	1.17	0.00	96.04
SHB3-757	74.30	11.89	0.01	3.96	0.30	4.34	0.01	0.00	0.05	0.06	1.31	0.00	96.22
SHB3-757	74.71	12.03	0.00	3.99	0.27	4.44	0.00	0.00	0.08	0.08	1.28	0.01	96.90
SHB3-757	75.05	11.96	0.00	4.02	0.29	4.51	0.00	0.00	0.10	0.09	1.22	0.05	97.30
SHB3-757	74.21	11.92	0.01	3.91	0.26	4.53	0.00	0.00	0.08	0.12	1.27	0.00	96.32
SHB3-757	73.48	11.84	0.00	3.91	0.29	4.44	0.00	0.00	0.03	0.09	1.29	0.00	95.36
SHB3-757	74.45	11.97	0.00	4.06	0.27	4.34	0.00	0.00	0.10	0.06	1.27	0.00	96.50
SHB3-757	74.74	12.03	0.00	4.20	0.26	4.50	0.01	0.00	0.00	0.11	1.27	0.00	97.11
SHB3-757	74.42	11.87	0.01	4.07	0.27	4.40	0.01	0.00	0.07	0.09	1.27	0.00	96.49
SHB3-757	74.28	11.93	0.00	4.11	0.29	4.42	0.01	0.00	0.05	0.12	1.28	0.01	96.50
SHB3-757	74.10	11.91	0.00	4.16	0.27	4.44	0.04	0.00	0.05	0.06	1.22	0.03	96.28
SHB3-757	73.64	11.86	0.00	4.17	0.25	4.35	0.01	0.00	0.00	0.08	1.23	0.03	95.61
SHB3-757	73.63	11.96	0.01	4.03	0.27	4.42	0.03	0.00	0.04	0.10	1.18	0.02	95.69
SHB3-757	74.11	11.88	0.00	4.12	0.28	4.39	0.03	0.02	0.12	0.09	1.23	0.04	96.31
SHB3-757	55.43	27.21	0.02	5.57	9.87	0.38	0.20	0.08	0.06	0.03	0.52	0.09	99.47

Appendix C: Table 1. Otowi Member of the Bandelier Tuff (cont.)

Sample	SiO <sub>2</sub>	Al <sub>2</sub> O <sub>3</sub>	MgO	Na <sub>2</sub> O	CaO	K <sub>2</sub> O	SrO	P <sub>2</sub> O <sub>5</sub>	TiO <sub>2</sub>	MnO	FeO	BAO	TOTAL
SHB3_798	73.29	11.73	0.00	3.94	0.24	4.48	0.01	0.04	0.10	0.07	1.20	0.00	95.11
SHB3_798	72.28	11.66	0.00	4.37	0.26	4.19	0.03	0.01	0.03	0.09	1.29	0.00	94.20
SHB3_798	72.45	12.23	0.00	4.49	0.23	4.39	0.01	0.00	0.03	0.06	1.17	0.00	95.07
SHB3_798	72.56	11.87	0.00	4.18	0.23	4.15	0.02	0.05	0.04	0.09	1.34	0.00	94.53
SHB3_798	73.64	11.95	0.00	4.24	0.24	4.18	0.00	0.00	0.03	0.12	1.28	0.00	95.67
SHB3_798	72.76	11.89	0.00	4.28	0.23	4.17	0.03	0.00	0.08	0.12	1.19	0.04	94.79
SHB3_798	73.09	11.72	0.00	4.12	0.24	4.25	0.00	0.00	0.10	0.10	1.28	0.06	94.94
SHB3_798	72.73	11.85	0.00	4.17	0.25	4.28	0.01	0.02	0.06	0.06	1.19	0.08	94.69
SHB3_798	73.72	11.80	0.00	4.19	0.23	4.22	0.00	0.04	0.04	0.09	1.28	0.00	95.60
SHB3_798	75.17	11.85	0.00	4.31	0.23	4.27	0.01	0.00	0.07	0.03	1.28	0.00	97.20
SHB3_798	73.85	11.84	0.00	4.02	0.26	4.24	0.02	0.03	0.09	0.08	1.25	0.00	95.66
SHB3_798	73.42	11.65	0.00	4.15	0.25	4.27	0.00	0.06	0.04	0.08	1.26	0.00	95.17
SHB3_798	72.97	11.91	0.00	4.09	0.26	4.25	0.00	0.02	0.09	0.07	1.34	0.07	95.08
SHB3_798	73.44	11.89	0.00	4.07	0.26	4.44	0.02	0.00	0.01	0.04	1.35	0.02	95.53
SHB3_798	73.42	11.71	0.00	4.10	0.24	4.25	0.03	0.00	0.09	0.08	1.26	0.02	95.20
SHB3_798	72.80	11.80	0.00	4.09	0.27	4.28	0.03	0.00	0.08	0.08	1.31	0.04	94.78
SHB3_798	72.67	11.56	0.00	3.88	0.24	4.41	0.01	0.01	0.06	0.10	1.24	0.02	94.19
SHB3_798	72.80	11.74	0.00	4.02	0.27	4.30	0.04	0.01	0.05	0.11	1.36	0.00	94.70
SHB3_798	73.20	11.86	0.00	4.22	0.23	4.28	0.05	0.00	0.07	0.13	1.30	0.00	95.34
SHB3_798	73.11	11.77	0.00	4.05	0.25	4.48	0.00	0.02	0.03	0.09	1.28	0.03	95.10
SHB3_798	73.43	11.75	0.00	3.92	0.25	4.29	0.01	0.00	0.08	0.06	1.32	0.01	95.12
SHB3_798	71.39	11.47	0.00	3.45	0.38	5.00	0.02	0.00	0.04	0.12	1.20	0.00	93.07
SHB3_798	73.28	11.96	0.00	3.97	0.25	4.46	0.02	0.01	0.03	0.08	1.30	0.00	95.36
SHB3_798	72.91	11.87	0.00	4.29	0.23	4.10	0.00	0.00	0.07	0.10	1.33	0.04	94.95
SHB3_798	73.05	11.83	0.00	4.16	0.24	4.43	0.00	0.03	0.09	0.09	1.29	0.01	95.22
SHB3_798	72.75	11.74	0.00	4.18	0.26	4.27	0.00	0.00	0.04	0.10	1.30	0.06	94.71
SHB3_798	72.39	11.70	0.00	4.15	0.26	4.22	0.02	0.00	0.01	0.06	1.27	0.00	94.09
SHB3_798	72.44	11.87	0.00	4.14	0.24	4.26	0.04	0.01	0.05	0.10	1.27	0.00	94.39
SHB3_798	71.12	11.70	0.00	4.07	0.25	4.20	0.03	0.03	0.00	0.10	1.32	0.00	92.81
SHB3_798	73.74	11.88	0.00	4.14	0.26	4.27	0.00	0.04	0.12	0.09	1.32	0.03	95.89

Appendix C: Table 2. Cerro Toledo Rhyolite

Sample	SiO <sub>2</sub>	Al <sub>2</sub> O <sub>3</sub>	MgO	Na <sub>2</sub> O	CaO	K <sub>2</sub> O	SP0	P <sub>2</sub> O <sub>5</sub>	TiO <sub>2</sub>	MNO	FeO	BAO	TOTAL
ss99btg_5	72.79	12.18	0.02	3.50	0.33	5.08	0.00	0.00	0.04	0.00	1.17	0.04	95.15
ss99btg_5	74.49	11.50	0.03	3.32	0.29	5.01	0.00	0.03	0.04	0.02	1.26	0.02	96.00
ss99btg_5	73.81	11.50	0.02	3.23	0.40	5.11	0.02	0.02	0.12	0.06	1.19	0.04	95.50
ss99btg_5	74.86	11.70	0.02	3.42	0.31	5.02	0.01	0.03	0.15	0.02	1.23	0.00	96.76
ss99btg_5	74.03	11.62	0.02	3.19	0.30	5.14	0.00	0.03	0.09	0.05	1.23	0.03	95.72
ss99btg_5	75.06	11.75	0.02	3.12	0.29	5.04	0.00	0.00	0.18	0.01	1.22	0.00	96.69
ss99btg_5	75.41	11.69	0.03	3.35	0.29	4.97	0.00	0.00	0.13	0.00	1.27	0.04	97.17
ss99btg_5	74.18	11.67	0.02	3.26	0.31	5.16	0.00	0.00	0.10	0.02	1.26	0.00	95.98
ss99btg_5	73.53	11.56	0.02	3.25	0.28	5.13	0.00	0.00	0.10	0.05	1.23	0.02	95.16
ss99btg_5	74.17	11.79	0.01	3.38	0.28	5.04	0.00	0.00	0.14	0.07	1.26	0.02	96.15
ss99btg_5	74.75	11.76	0.01	3.53	0.30	4.73	0.00	0.03	0.16	0.06	1.20	0.01	96.53
ss99btg_5	74.05	11.64	0.01	3.16	0.30	5.10	0.00	0.00	0.16	0.10	1.18	0.02	95.71
ss99btg_5	74.78	11.76	0.03	3.42	0.28	4.90	0.00	0.00	0.12	0.05	1.23	0.01	96.58
ss99btg_5	73.44	11.87	0.02	3.59	0.31	4.81	0.00	0.00	0.06	0.02	1.28	0.00	95.38
ss99btg_5	73.84	12.16	0.02	3.47	0.33	4.92	0.00	0.00	0.16	0.10	1.25	0.00	96.23
ss99btg_5	74.16	11.75	0.01	3.28	0.30	5.02	0.00	0.02	0.13	0.04	1.26	0.00	95.98
ss99btg_5	74.26	11.61	0.01	3.11	0.35	5.18	0.00	0.00	0.15	0.08	1.24	0.00	95.98
ss99btg_5	74.99	11.71	0.01	3.21	0.29	5.15	0.00	0.02	0.19	0.09	1.22	0.08	96.96
ss99btg_5	72.47	11.23	0.03	3.40	0.31	4.73	0.00	0.01	0.10	0.06	1.09	0.01	93.43
ss99btg_5	73.34	11.60	0.02	3.14	0.34	5.25	0.00	0.01	0.14	0.07	1.24	0.07	95.21
ss99btg_5	76.97	11.76	0.03	3.32	0.33	5.06	0.00	0.00	0.04	0.05	1.21	0.00	98.76
ss99btg_5	75.40	11.69	0.02	3.47	0.29	4.88	0.00	0.03	0.08	0.05	1.21	0.00	97.11
ss99btg_5	75.10	11.67	0.02	3.39	0.34	4.91	0.01	0.00	0.09	0.02	1.23	0.00	96.76
ss99btg_5	75.70	11.65	0.03	3.44	0.34	5.04	0.00	0.02	0.21	0.04	1.26	0.02	97.72
ss99btg_5	75.44	11.76	0.02	3.63	0.30	4.72	0.00	0.02	0.10	0.00	1.41	0.07	97.48
ss99btg_5	75.86	11.80	0.02	3.22	0.37	4.84	0.00	0.02	0.10	0.03	1.19	0.00	97.45
ss99btg_5	76.63	11.88	0.00	3.42	0.35	4.94	0.00	0.03	0.07	0.07	1.20	0.00	98.59
ss99btg_5	75.54	11.37	0.02	3.44	0.37	4.60	0.00	0.00	0.09	0.05	1.31	0.00	96.79
ss99btg_5	74.15	11.67	0.03	3.50	0.34	4.62	0.00	0.00	0.12	0.04	1.22	0.02	95.70
ss99btg_5	75.59	11.81	0.00	1.47	0.36	4.27	0.00	0.05	0.11	0.05	1.23	0.00	94.93

Appendix C: Table 2. Cerro Toledo Rhyolite (cont.)

Sample	SiO <sub>2</sub>	Al <sub>2</sub> O <sub>3</sub>	MgO	Na <sub>2</sub> O	CaO	K <sub>2</sub> O	SrO	P <sub>2</sub> O <sub>5</sub>	TiO <sub>2</sub>	MnO	FeO	BAO	TOTAL
SSBTG_6	73.68	11.74	0.03	3.38	0.25	4.83	0.00	0.01	0.17	0.05	1.36	0.05	95.55
SSBTG_6	73.72	11.80	0.02	3.27	0.27	4.95	0.00	0.06	0.12	0.00	1.35	0.03	95.59
SSBTG_6	72.37	11.73	0.01	3.39	0.26	4.70	0.00	0.00	0.10	0.05	1.32	0.00	93.93
SSBTG_6	73.91	11.84	0.01	3.47	0.26	4.65	0.00	0.01	0.09	0.07	1.24	0.00	95.55
SSBTG_6	74.12	11.77	0.00	3.40	0.27	4.90	0.01	0.00	0.14	0.04	1.40	0.00	96.05
SSBTG_6	73.23	11.68	0.02	3.44	0.23	4.89	0.00	0.07	0.10	0.07	1.31	0.00	95.03
SSBTG_6	74.02	11.64	0.02	3.23	0.27	4.71	0.01	0.04	0.16	0.08	1.31	0.01	95.48
SSBTG_6	74.49	11.85	0.02	3.29	0.24	4.98	0.01	0.02	0.05	0.00	1.24	0.00	96.20
SSBTG_6	75.31	11.82	0.02	3.03	0.31	5.09	0.00	0.00	0.07	0.05	1.28	0.08	97.06
SSBTG_6	74.62	11.84	0.02	3.51	0.26	4.79	0.00	0.00	0.14	0.00	1.44	0.00	96.61
SSBTG_6	74.25	11.88	0.00	3.45	0.27	4.57	0.00	0.00	0.10	0.02	1.19	0.07	95.80
SSBTG_6	73.26	11.83	0.01	3.37	0.25	4.67	0.00	0.00	0.10	0.06	1.26	0.00	94.80
SSBTG_6	74.38	11.83	0.03	3.20	0.28	4.98	0.00	0.00	0.07	0.03	1.35	0.01	96.16
SSBTG_6	73.56	11.81	0.02	3.31	0.26	4.80	0.00	0.00	0.13	0.04	1.33	0.00	95.25
SSBTG_6	74.60	11.92	0.02	3.19	0.24	5.14	0.00	0.02	0.14	0.04	1.26	0.00	96.56
SSBTG_6	74.34	12.23	0.03	3.36	0.33	4.97	0.00	0.03	0.14	0.10	1.28	0.05	96.85
SSBTG_6	74.34	11.75	0.08	3.04	0.29	4.76	0.00	0.00	0.04	0.03	1.28	0.02	95.63
SSBTG_6	73.81	11.67	0.03	3.04	0.28	4.88	0.00	0.00	0.11	0.04	1.22	0.00	95.09
SSBTG_6	74.37	11.89	0.01	3.55	0.26	4.64	0.00	0.00	0.13	0.05	1.36	0.02	96.27
SSBTG_6	74.20	11.80	0.02	3.40	0.25	4.60	0.00	0.01	0.04	0.02	1.38	0.00	95.72
SSBTG_6	74.40	12.10	0.05	3.25	0.32	4.88	0.00	0.00	0.14	0.06	1.23	0.00	96.41
SSBTG_6	74.14	11.74	0.02	3.26	0.28	4.60	0.00	0.00	0.12	0.05	1.13	0.01	95.34
SSBTG_6	74.55	11.84	0.00	3.02	0.20	5.00	0.00	0.04	0.14	0.02	0.94	0.04	95.78
SSBTG_6	75.33	11.79	0.02	3.12	0.28	4.80	0.00	0.00	0.11	0.05	1.27	0.05	96.82
SSBTG_6	75.05	11.77	0.03	3.42	0.25	4.47	0.00	0.04	0.07	0.07	1.36	0.00	96.52
SSBTG_6	74.28	11.69	0.02	3.37	0.28	4.62	0.00	0.05	0.16	0.05	1.29	0.05	95.84
SSBTG_6	75.21	11.88	0.03	3.24	0.27	5.00	0.02	0.00	0.04	0.03	1.22	0.03	96.97
SSBTG_6	74.96	11.78	0.01	3.21	0.32	4.82	0.00	0.01	0.08	0.03	1.24	0.04	96.50

Appendix C: Table 2. Cerro Toledo Rhyolite (cont.)

Sample	SiO <sub>2</sub>	Al <sub>2</sub> O <sub>3</sub>	MgO	Na <sub>2</sub> O	CaO	K <sub>2</sub> O	SrO	P <sub>2</sub> O <sub>5</sub>	TiO <sub>2</sub>	MnO	FeO	BAO	TOTAL
ss99btg_7	74.91	11.87	0.03	3.22	0.32	4.23	0.00	0.00	0.09	0.07	0.89	0.00	95.62
ss99btg_7	74.87	11.77	0.03	3.34	0.33	4.34	0.00	0.01	0.08	0.05	0.98	0.00	95.79
ss99btg_7	75.22	11.65	0.02	3.26	0.31	4.31	0.00	0.05	0.03	0.05	0.85	0.00	95.74
ss99btg_7	75.51	11.66	0.03	3.28	0.31	4.32	0.00	0.00	0.00	0.07	0.89	0.00	96.07
ss99btg_7	75.35	11.65	0.03	3.35	0.32	4.35	0.00	0.02	0.09	0.04	0.91	0.00	96.10
ss99btg_7	74.78	11.70	0.02	3.31	0.29	4.28	0.00	0.02	0.08	0.01	0.88	0.00	95.36
ss99btg_7	75.03	11.73	0.02	3.48	0.33	4.21	0.00	0.03	0.10	0.13	0.96	0.00	96.01
ss99btg_7	75.10	11.73	0.02	3.37	0.31	4.32	0.03	0.00	0.00	0.03	0.93	0.00	95.84
ss99btg_7	75.66	11.82	0.03	3.37	0.29	4.40	0.00	0.03	0.08	0.05	1.00	0.00	96.74
ss99btg_7	75.53	11.80	0.02	3.38	0.33	4.37	0.00	0.06	0.11	0.03	0.97	0.03	96.62
ss99btg_7	75.09	11.70	0.02	3.41	0.33	4.40	0.00	0.00	0.14	0.07	0.94	0.00	96.09
ss99btg_7	76.59	11.81	0.02	3.32	0.32	4.39	0.00	0.00	0.05	0.06	0.85	0.00	97.40
ss99btg_7	75.58	11.77	0.02	3.47	0.34	4.40	0.00	0.00	0.13	0.07	0.84	0.00	96.62
ss99btg_7	75.73	11.73	0.03	3.19	0.32	4.35	0.00	0.00	0.07	0.07	0.95	0.03	96.47
ss99btg_7	75.58	11.85	0.03	3.40	0.30	4.37	0.00	0.00	0.08	0.06	0.88	0.00	96.56
ss99btg_7	75.92	11.87	0.03	3.55	0.31	4.27	0.01	0.00	0.13	0.04	0.92	0.04	97.07
ss99btg_7	75.56	11.78	0.03	3.37	0.31	4.33	0.02	0.02	0.09	0.04	0.93	0.00	96.48
ss99btg_7	75.90	11.81	0.03	3.38	0.32	4.37	0.00	0.04	0.00	0.06	0.89	0.02	96.81
ss99btg_7	75.44	11.71	0.03	3.42	0.30	4.32	0.00	0.00	0.02	0.03	0.90	0.00	96.16
ss99btg_7	74.55	11.93	0.03	3.33	0.31	4.33	0.00	0.02	0.04	0.06	0.95	0.00	95.54
ss99btg_7	75.81	11.84	0.03	3.34	0.33	4.26	0.00	0.01	0.06	0.02	0.76	0.00	96.45
ss99btg_7	75.82	11.79	0.02	3.43	0.29	4.34	0.00	0.01	0.04	0.02	0.90	0.07	96.71
ss99btg_7	75.26	11.83	0.02	3.30	0.31	4.31	0.00	0.00	0.11	0.05	0.90	0.02	96.11
ss99btg_7	75.01	11.83	0.02	3.39	0.30	4.24	0.00	0.02	0.11	0.01	0.94	0.00	95.89
ss99btg_7	75.20	11.81	0.02	3.26	0.31	4.16	0.00	0.00	0.14	0.02	0.92	0.00	95.82
ss99btg_7	75.60	11.88	0.03	3.14	0.30	4.34	0.02	0.00	0.06	0.10	0.90	0.00	96.36
ss99btg_7	74.97	11.83	0.02	3.34	0.30	4.30	0.00	0.01	0.09	0.05	0.89	0.01	95.80

Appendix C: Table 2. Cerro Toledo Rhyolite (cont.)

Sample	SiO <sub>2</sub>	Al <sub>2</sub> O <sub>3</sub>	MgO	Na <sub>2</sub> O	CaO	K <sub>2</sub> O	FeO	P <sub>2</sub> O <sub>5</sub>	TiO <sub>2</sub>	MnO	FeO	BAO	TOTAL
SSBTG_8	74.28	11.95	0.02	3.34	0.35	4.99	0.00	0.00	0.08	0.07	0.76	0.00	95.83
SSBTG_8	75.36	11.94	0.02	3.20	0.33	4.86	0.00	0.00	0.17	0.06	0.81	0.01	96.76
SSBTG_8	72.55	11.67	0.00	3.44	0.35	4.72	0.00	0.04	0.08	0.04	0.74	0.00	93.62
SSBTG_8	74.12	11.78	0.03	3.28	0.37	4.89	0.00	0.03	0.12	0.10	0.86	0.00	95.58
SSBTG_8	75.36	11.91	0.04	3.29	0.35	4.89	0.00	0.00	0.10	0.08	0.84	0.06	96.91
SSBTG_8	75.78	12.00	0.03	3.11	0.37	4.91	0.00	0.00	0.06	0.06	0.77	0.00	97.10
SSBTG_8	74.08	11.85	0.00	3.10	0.37	4.92	0.00	0.00	0.11	0.01	0.80	0.01	95.24
SSBTG_8	75.46	12.03	0.02	3.28	0.34	4.90	0.00	0.00	0.10	0.10	0.81	0.00	97.03
SSBTG_8	75.32	11.92	0.01	3.10	0.35	5.02	0.00	0.00	0.10	0.05	0.78	0.00	96.65
SSBTG_8	75.27	12.06	0.04	3.39	0.36	4.95	0.00	0.00	0.14	0.00	0.81	0.00	97.01
SSBTG_8	74.56	11.97	0.02	3.32	0.35	4.78	0.00	0.00	0.06	0.03	0.83	0.02	95.93
SSBTG_8	75.70	12.02	0.02	3.20	0.35	4.98	0.00	0.00	0.06	0.01	0.88	0.03	97.24
SSBTG_8	70.40	10.94	0.02	3.00	0.35	4.88	0.00	0.01	0.10	0.05	0.83	0.00	90.58
SSBTG_8	74.77	11.87	0.02	3.24	0.37	4.94	0.01	0.00	0.06	0.09	0.79	0.03	96.18
SSBTG_8	73.25	11.55	0.03	3.18	0.33	4.67	0.00	0.00	0.08	0.06	0.75	0.00	93.91
SSBTG_8	74.17	12.06	0.01	3.35	0.36	4.87	0.00	0.03	0.11	0.09	0.73	0.00	95.77
SSBTG_8	74.55	12.05	0.02	3.40	0.36	4.82	0.00	0.02	0.08	0.08	0.75	0.08	96.21
SSBTG_8	70.87	12.02	0.02	3.51	0.39	4.70	0.00	0.00	0.10	0.05	0.72	0.00	92.38
SSBTG_8	75.40	11.99	0.01	3.51	0.33	4.64	0.02	0.06	0.09	0.06	0.79	0.03	96.93
SSBTG_8	74.99	11.90	0.01	3.31	0.33	4.84	0.00	0.01	0.09	0.02	0.79	0.00	96.29
SSBTG_8	74.09	11.91	0.03	3.53	0.36	4.77	0.00	0.04	0.06	0.03	0.79	0.00	95.61
SSBTG_8	75.08	11.93	0.03	3.29	0.35	4.85	0.00	0.02	0.13	0.08	0.74	0.00	96.49
SSBTG_8	75.34	11.92	0.03	3.12	0.36	4.92	0.00	0.02	0.10	0.05	0.78	0.06	96.69
SSBTG_8	75.08	11.95	0.03	3.34	0.36	4.81	0.00	0.01	0.08	0.07	0.77	0.00	96.50
SSBTG_8	75.21	12.03	0.02	3.44	0.34	4.77	0.01	0.00	0.02	0.04	0.78	0.06	96.71
SSBTG_8	74.68	11.89	0.03	3.34	0.37	4.83	0.00	0.00	0.08	0.04	0.79	0.00	96.04
SSBTG_8	74.21	12.01	0.02	3.25	0.38	4.83	0.00	0.00	0.11	0.09	0.80	0.04	95.73
SSBTG_8	75.39	12.02	0.03	3.38	0.37	4.83	0.00	0.00	0.07	0.04	0.75	0.01	96.88
SSBTG_8	75.20	11.96	0.02	3.31	0.37	4.86	0.00	0.00	0.11	0.08	0.78	0.00	96.70
SSBTG_8	74.38	11.93	0.04	3.34	0.36	4.80	0.00	0.00	0.16	0.03	0.77	0.00	95.79
SSBTG_8	75.85	11.94	0.05	3.33	0.36	4.85	0.00	0.02	0.05	0.07	0.76	0.00	97.26
SSBTG_8	74.78	11.94	0.03	3.32	0.35	4.89	0.00	0.07	0.05	0.03	0.84	0.04	96.34
SSBTG_8	74.13	11.89	0.02	3.37	0.34	4.83	0.00	0.00	0.06	0.12	0.74	0.00	95.51
SSBTG_8	74.78	11.95	0.03	3.28	0.33	4.96	0.00	0.04	0.13	0.03	0.77	0.00	96.30

Appendix C: Table 2. Cerro Toledo Rhyolite (cont.)

Sample	SiO <sub>2</sub>	Al <sub>2</sub> O <sub>3</sub>	MgO	Na <sub>2</sub> O	CaO	K <sub>2</sub> O	SrO	P <sub>2</sub> O <sub>5</sub>	TiO <sub>2</sub>	MnO	FeO	BAO	TOTAL
ss99btg_9	74.65	11.62	0.00	3.81	0.24	4.18	0.00	0.02	0.02	0.11	1.49	0.00	96.14
ss99btg_9	72.98	11.34	0.00	3.52	0.26	4.30	0.00	0.00	0.05	0.10	1.48	0.00	94.02
ss99btg_9	74.86	11.66	0.00	3.75	0.22	4.13	0.00	0.00	0.09	0.09	1.42	0.00	96.22
ss99btg_9	74.30	11.56	0.00	3.66	0.23	4.13	0.00	0.05	0.12	0.07	1.52	0.01	95.65
ss99btg_9	73.35	11.22	0.00	3.59	0.23	4.14	0.00	0.00	0.05	0.14	1.34	0.00	94.06
ss99btg_9	75.45	11.57	0.00	3.59	0.24	4.41	0.00	0.01	0.04	0.09	1.42	0.00	96.82
ss99btg_9	72.94	11.28	0.00	3.64	0.24	4.08	0.00	0.00	0.04	0.12	1.31	0.00	93.64
ss99btg_9	75.38	11.76	0.00	3.85	0.23	4.09	0.00	0.04	0.00	0.11	1.46	0.00	96.91
ss99btg_9	74.66	11.44	0.00	3.68	0.24	4.07	0.00	0.02	0.04	0.10	1.56	0.00	95.80
ss99btg_9	74.32	11.66	0.00	3.53	0.27	4.24	0.00	0.00	0.04	0.12	1.45	0.03	95.66
ss99btg_9	71.75	11.19	0.00	3.36	0.23	3.87	0.00	0.01	0.05	0.08	1.52	0.00	92.05
ss99btg_9	72.69	11.24	0.00	3.48	0.26	4.04	0.00	0.05	0.04	0.11	1.36	0.00	93.27
ss99btg_9	74.68	11.47	0.00	3.72	0.25	4.11	0.00	0.00	0.02	0.17	1.95	0.00	96.37
ss99btg_9	71.49	10.95	0.00	3.15	0.24	3.86	0.00	0.00	0.01	0.10	1.47	0.02	91.30
ss99btg_9	75.39	11.59	0.00	3.89	0.22	4.08	0.00	0.03	0.09	0.06	1.50	0.00	96.86
ss99btg_9	73.63	11.32	0.00	3.49	0.26	4.08	0.00	0.01	0.04	0.11	1.38	0.00	94.33
ss99btg_9	74.26	11.30	0.00	3.70	0.24	4.07	0.00	0.01	0.01	0.13	1.42	0.00	95.14
ss99btg_9	75.16	11.60	0.00	3.73	0.22	4.26	0.00	0.02	0.06	0.08	1.44	0.00	96.56
ss99btg_9	73.84	11.40	0.00	3.66	0.24	4.11	0.00	0.00	0.04	0.06	1.43	0.00	94.78
ss99btg_9	75.47	11.62	0.00	3.63	0.24	4.18	0.00	0.00	0.10	0.06	1.45	0.00	96.74

Appendix C: Table 3. Tshirege Member of the Bandelier Tuff (cont.)

Sample	SiO <sub>2</sub>	Al <sub>2</sub> O <sub>3</sub>	MgO	Na <sub>2</sub> O	CaO	K <sub>2</sub> O	SrO	P <sub>2</sub> O <sub>5</sub>	TiO <sub>2</sub>	MnO	FeO	BaO	TOTAL
ss99btg_11	73.87	11.73	0.00	3.94	0.26	4.05	0.00	0.00	0.10	0.09	1.49	0.03	95.56
ss99btg_11	74.32	11.76	0.00	3.97	0.24	4.11	0.00	0.02	0.10	0.08	1.56	0.00	96.16
ss99btg_11	73.38	11.79	0.00	3.85	0.25	4.09	0.00	0.02	0.14	0.13	1.56	0.05	95.26
ss99btg_11	73.94	11.73	0.00	3.79	0.23	4.05	0.00	0.01	0.02	0.14	1.47	0.00	95.38
ss99btg_11	74.46	11.83	0.00	3.89	0.26	4.09	0.00	0.02	0.02	0.09	1.56	0.04	96.26
ss99btg_11	75.48	11.76	0.00	3.95	0.26	4.09	0.00	0.04	0.05	0.08	1.46	0.03	97.19
ss99btg_11	75.17	11.88	0.00	3.91	0.26	4.09	0.00	0.00	0.06	0.09	1.58	0.08	97.12
ss99btg_11	75.28	11.88	0.00	3.68	0.26	4.06	0.00	0.02	0.05	0.16	1.56	0.00	96.95
ss99btg_11	76.81	11.85	0.00	3.86	0.26	4.06	0.00	0.00	0.03	0.05	1.57	0.00	98.49
ss99btg_11	75.89	11.94	0.00	3.79	0.27	4.14	0.00	0.00	0.07	0.07	1.49	0.00	97.66
ss99btg_11	75.89	11.78	0.00	3.87	0.25	4.12	0.00	0.04	0.07	0.10	1.61	0.01	97.75
ss99btg_11	75.96	11.88	0.00	3.85	0.22	4.11	0.00	0.07	0.16	0.14	1.54	0.00	97.93
ss99btg_11	74.26	11.68	0.00	3.87	0.21	4.12	0.00	0.02	0.03	0.11	1.51	0.02	95.84
ss99btg_11	76.18	11.89	0.00	3.75	0.27	4.24	0.00	0.03	0.10	0.08	1.63	0.00	98.17
ss99btg_11	75.90	11.83	0.00	3.87	0.27	4.14	0.00	0.03	0.15	0.10	1.61	0.00	97.90
ss99btg_11	74.59	11.68	0.00	3.81	0.26	4.05	0.00	0.00	0.06	0.12	1.55	0.01	96.12
ss99btg_11	74.75	11.74	0.00	3.85	0.25	4.12	0.00	0.02	0.05	0.09	1.51	0.06	96.45
ss99btg_11	74.89	11.78	0.00	3.83	0.24	4.16	0.00	0.04	0.06	0.12	1.58	0.00	96.68
ss99btg_11	74.74	11.88	0.00	3.84	0.27	4.06	0.00	0.01	0.00	0.09	1.58	0.00	96.46
ss99btg_11	74.62	11.81	0.00	3.82	0.25	4.03	0.00	0.02	0.05	0.10	1.60	0.00	96.29
ss99btg_11	74.50	11.83	0.01	4.00	0.25	4.11	0.00	0.00	0.03	0.06	1.56	0.00	96.34
ss99btg_11	73.79	11.48	0.00	3.96	0.22	3.88	0.00	0.00	0.06	0.10	1.40	0.02	94.90
ss99btg_11	76.01	11.76	0.00	3.85	0.25	4.09	0.00	0.00	0.08	0.11	1.50	0.00	97.63
ss99btg_11	75.49	11.83	0.00	3.97	0.25	4.12	0.00	0.00	0.03	0.12	1.56	0.03	97.42
ss99btg_11	75.47	11.84	0.00	3.86	0.24	4.18	0.00	0.00	0.02	0.17	1.51	0.00	97.28
ss99btg_11	75.17	11.78	0.00	3.85	0.23	4.14	0.00	0.01	0.00	0.09	1.46	0.00	96.73
ss99btg_11	75.67	11.85	0.00	3.86	0.24	4.01	0.00	0.01	0.06	0.09	1.56	0.01	97.34
ss99btg_11	74.32	11.70	0.00	3.89	0.22	4.15	0.00	0.00	0.00	0.09	1.62	0.00	95.98

Appendix C: Table 3. Tshirege Member of the Bandelier Tuff (cont.)

Sample	SiO <sub>2</sub>	Al <sub>2</sub> O <sub>3</sub>	MgO	Na <sub>2</sub> O	CaO	K <sub>2</sub> O	SP0	P <sub>2</sub> O <sub>5</sub>	TiO <sub>2</sub>	MNO	FeO	BAO	TOTAL
ta16_302	76.07	11.91	0.02	3.60	5.28	0.20	0.00	0.04	0.03	0.08	1.07	0.00	98.28
ta16_302	75.23	11.94	0.01	3.46	5.22	0.19	0.04	0.04	0.18	0.04	0.83	0.00	97.15
ta16_302	75.45	11.94	0.01	3.41	5.28	0.14	0.03	0.00	0.16	0.00	1.08	0.00	97.50
ta16_302	75.52	12.02	0.02	3.54	5.22	0.15	0.00	0.02	0.18	0.03	1.13	0.01	97.83
ta16_302	75.85	11.87	0.02	3.48	5.20	0.16	0.05	0.00	0.09	0.01	0.98	0.02	97.72
ta16_302	75.82	11.87	0.02	3.54	5.20	0.16	0.02	0.00	0.19	0.08	1.27	0.05	98.22
ta16_302	76.14	12.08	0.00	3.68	5.15	0.15	0.01	0.05	0.09	0.06	1.05	0.02	98.49
ta16_302	75.31	11.87	0.05	3.57	5.20	0.20	0.03	0.00	0.11	0.02	1.03	0.00	97.37
ta16_302	76.02	11.95	0.04	3.66	5.21	0.15	0.03	0.02	0.16	0.05	1.24	0.05	98.58
ta16_302	75.13	12.08	0.03	3.53	5.20	0.17	0.04	0.01	0.11	0.07	1.30	0.00	97.67
ta16_302	75.36	11.85	0.01	3.66	5.20	0.12	0.01	0.03	0.00	0.06	1.09	0.08	97.48
ta16_302	74.93	11.95	0.04	3.60	5.21	0.17	0.03	0.00	0.15	0.07	1.18	0.03	97.37
ta16_302	76.32	12.00	0.00	3.51	5.15	0.13	0.00	0.01	0.17	0.04	0.84	0.04	98.22
ta16_302	75.41	11.98	0.02	3.50	5.17	0.13	0.01	0.01	0.05	0.04	1.14	0.02	97.47
ta16_302	75.55	11.82	0.03	3.68	5.11	0.13	0.02	0.00	0.11	0.02	1.12	0.00	97.59
ta16_302	75.20	11.97	0.08	3.56	5.11	0.32	0.03	0.02	0.25	0.05	1.57	0.00	98.16
ta16_302	75.49	12.03	0.03	3.66	5.21	0.15	0.01	0.04	0.11	0.01	0.95	0.07	97.74
ta16_302	75.32	11.92	0.00	3.53	5.25	0.12	0.00	0.07	0.17	0.02	0.95	0.00	97.34
ta16_302	75.55	12.01	0.00	3.53	5.37	0.09	0.00	0.00	0.18	0.05	0.47	0.00	97.26
ta16_302	75.83	11.87	0.01	3.55	5.16	0.15	0.02	0.00	0.14	0.04	1.13	0.00	97.90
ta16_302	75.54	11.96	0.03	3.70	5.18	0.18	0.00	0.00	0.10	0.00	1.29	0.00	97.97
ta16_302	75.11	11.98	0.02	3.48	5.22	0.16	0.04	0.00	0.08	0.06	1.04	0.01	97.18
ta16_302	75.66	12.01	0.03	3.74	5.13	0.20	0.00	0.00	0.06	0.06	1.25	0.01	98.14
ta16_302	76.00	12.05	0.00	3.45	5.28	0.11	0.01	0.05	0.16	0.03	0.53	0.00	97.67
ta16_302	75.63	11.93	0.02	3.51	5.18	0.17	0.02	0.04	0.18	0.02	1.09	0.00	97.79
ta16_302	74.86	11.98	0.02	3.54	5.17	0.16	0.02	0.04	0.16	0.00	1.05	0.00	97.00
ta16_302	75.31	11.87	0.04	3.74	5.08	0.25	0.04	0.05	0.12	0.02	1.17	0.00	97.68
ta16_302	75.89	12.02	0.01	3.53	5.19	0.14	0.07	0.04	0.12	0.01	1.02	0.00	98.04
ta16_302	75.69	12.09	0.00	3.57	5.36	0.11	0.00	0.00	0.09	0.03	0.70	0.00	97.62
ta16_302	75.15	12.02	0.02	3.62	5.25	0.17	0.02	0.05	0.13	0.02	1.11	0.02	97.58

Appendix C: Table 3. Tshirege Member of the Bandelier Tuff (cont.)

Sample	SiO <sub>2</sub>	Al <sub>2</sub> O <sub>3</sub>	MgO	Na <sub>2</sub> O	CaO	K <sub>2</sub> O	SrO	P <sub>2</sub> O <sub>5</sub>	TiO <sub>2</sub>	MnO	FeO	BAO	TOTAL
ta16_300	70.04	15.49	0.00	5.95	4.53	0.36	0.00	0.00	0.06	0.01	0.62	0.05	97.10
ta16_303	74.18	11.72	0.01	3.13	5.29	0.08	0.00	0.02	0.16	0.07	1.28	0.00	95.94
ta16_303	75.37	11.77	0.00	3.27	5.41	0.10	0.07	0.00	0.03	0.02	1.17	0.02	97.23
ta16_303	74.56	11.80	0.00	3.20	5.40	0.09	0.00	0.00	0.05	0.02	0.98	0.00	96.09
ta16_303	74.74	11.67	0.03	3.15	5.25	0.12	0.02	0.00	0.11	0.03	1.26	0.00	96.39
ta16_303	74.92	11.83	0.00	3.12	5.33	0.09	0.05	0.07	0.18	0.01	1.30	0.01	96.91
ta16_303	72.98	11.56	0.01	2.98	5.31	0.08	0.03	0.01	0.13	0.01	1.23	0.00	94.31
ta16_303	74.50	11.78	0.00	3.22	5.25	0.10	0.02	0.00	0.05	0.00	1.31	0.06	96.28
ta16_303	74.08	11.55	0.01	3.18	5.28	0.11	0.00	0.02	0.20	0.00	1.36	0.08	95.87
ta16_303	74.63	11.69	0.01	3.20	5.21	0.11	0.01	0.02	0.09	0.03	1.34	0.04	96.39
ta16_303	74.63	11.61	0.00	3.22	5.47	0.12	0.03	0.00	0.08	0.00	1.15	0.00	96.31
ta16_303	74.84	11.69	0.02	3.12	5.22	0.08	0.02	0.00	0.14	0.03	1.26	0.00	96.42
ta16_303	74.67	11.70	0.01	3.17	5.28	0.12	0.00	0.00	0.14	0.00	1.15	0.01	96.25
ta16_303	74.65	11.82	0.00	3.28	5.38	0.10	0.03	0.01	0.11	0.00	0.91	0.02	96.30
ta16_303	75.15	11.70	0.01	3.41	5.27	0.10	0.00	0.02	0.22	0.06	1.39	0.00	97.32
ta16_303	73.80	11.67	0.00	3.17	5.32	0.09	0.00	0.00	0.09	0.05	1.15	0.00	95.34
ta16_303	74.61	11.75	0.01	3.16	5.34	0.09	0.00	0.00	0.18	0.00	1.13	0.00	96.27
ta16_303	74.05	11.63	0.00	3.28	5.32	0.08	0.04	0.00	0.03	0.03	1.17	0.09	95.73
ta16_303	73.80	12.14	0.01	3.35	5.34	0.11	0.05	0.00	0.15	0.00	1.16	0.00	96.11
ta16_303	74.80	11.73	0.00	3.07	5.42	0.09	0.03	0.02	0.10	0.02	0.88	0.03	96.19
ta16_303	75.34	11.80	0.00	3.45	5.29	0.10	0.03	0.05	0.14	0.00	1.26	0.03	97.48
ta16_303	74.53	11.87	0.00	3.19	5.35	0.11	0.06	0.00	0.11	0.01	0.98	0.00	96.20
ta16_303	73.93	11.64	0.00	3.28	5.20	0.12	0.06	0.00	0.18	0.04	1.31	0.02	95.78
ta16_303	74.49	11.65	0.01	3.15	5.25	0.09	0.04	0.04	0.09	0.04	1.23	0.00	96.07
ta16_303	73.74	11.65	0.00	3.25	5.29	0.09	0.00	0.03	0.18	0.01	1.12	0.05	95.42
ta16_303	74.13	11.78	0.02	3.22	5.21	0.13	0.03	0.02	0.09	0.00	1.26	0.00	95.90
ta16_303	74.18	11.75	0.02	3.17	5.16	0.12	0.00	0.00	0.17	0.00	1.28	0.02	95.88
ta16_303	75.27	11.82	0.00	2.81	5.53	0.12	0.08	0.05	0.12	0.02	0.37	0.08	96.26
ta16_303	73.55	11.67	0.00	3.17	5.31	0.15	0.01	0.01	0.17	0.04	1.12	0.06	95.24
ta16_303	73.58	11.73	0.00	3.13	5.50	0.14	0.01	0.03	0.13	0.01	0.51	0.00	94.76
ta16_303	72.88	11.53	0.00	3.20	5.36	0.15	0.00	0.01	0.10	0.03	0.81	0.05	94.12

Appendix C: Table 3. Tshirege Member of the Bandelier Tuff (cont.)

Sample	SiO <sub>2</sub>	Al <sub>2</sub> O <sub>3</sub>	MgO	Na <sub>2</sub> O	CaO	K <sub>2</sub> O	SrO	P <sub>2</sub> O <sub>5</sub>	TiO <sub>2</sub>	MnO	FeO	BAO	TOTAL
ta16_304	74.88	11.90	0.04	2.93	4.44	0.22	0.01	0.02	0.15	0.01	1.22	0.06	95.87
ta16_304	74.64	11.85	0.05	2.88	4.46	0.26	0.00	0.00	0.12	0.07	1.33	0.12	95.79
ta16_304	73.76	11.82	0.01	2.88	4.76	0.17	0.08	0.02	0.21	0.01	0.79	0.00	94.50
ta16_304	74.19	11.84	0.02	2.83	4.41	0.19	0.00	0.00	0.07	0.05	1.12	0.11	94.83
ta16_304	74.14	11.93	0.02	2.98	4.61	0.22	0.00	0.00	0.15	0.08	0.82	0.10	95.05
ta16_304	72.63	11.81	0.04	3.28	4.69	0.33	0.00	0.03	0.13	0.07	1.61	0.02	94.64
ta16_304	74.26	12.39	0.04	3.26	4.61	0.32	0.01	0.05	0.09	0.06	1.18	0.06	96.34
ta16_304	73.54	12.34	0.02	3.04	4.50	0.26	0.01	0.02	0.20	0.07	1.07	0.04	95.10
ta16_304	73.68	12.05	0.04	3.11	4.66	0.25	0.00	0.04	0.17	0.03	1.10	0.00	95.11
ta16_304	74.17	11.95	0.04	2.52	4.46	0.25	0.00	0.01	0.08	0.05	1.63	0.00	95.15
ta16_304	75.54	11.96	0.04	2.78	4.18	0.26	0.03	0.05	0.09	0.05	1.21	0.03	96.19
ta16_304	72.74	11.85	0.00	2.94	4.74	0.17	0.00	0.04	0.25	0.04	0.76	0.00	93.52
ta16_304	73.55	11.83	0.05	2.86	4.38	0.24	0.00	0.00	0.15	0.06	1.41	0.02	94.55
ta16_304	73.69	11.83	0.01	2.97	4.62	0.20	0.03	0.04	0.20	0.02	0.86	0.05	94.51
ta16_304	73.23	11.82	0.02	2.81	4.44	0.17	0.02	0.00	0.07	0.04	1.11	0.01	93.75
ta16_304	72.64	11.73	0.05	2.82	4.54	0.28	0.02	0.02	0.10	0.04	1.26	0.00	93.51
ta16_304	73.41	11.79	0.04	2.91	4.60	0.23	0.03	0.02	0.18	0.08	1.10	0.00	94.40
ta16_304	73.17	11.82	0.04	2.95	4.51	0.24	0.00	0.00	0.11	0.05	1.33	0.13	94.35
ta16_304	72.29	11.96	0.04	2.93	4.51	0.26	0.03	0.09	0.18	0.03	1.24	0.00	93.55
ta16_304	73.21	11.93	0.02	2.85	4.57	0.20	0.00	0.03	0.16	0.05	1.03	0.00	94.03
ta16_304	73.79	11.88	0.04	2.77	4.46	0.26	0.04	0.04	0.17	0.08	1.25	0.03	94.80
ta16_304	72.79	11.78	0.04	2.73	4.47	0.22	0.02	0.00	0.12	0.00	1.24	0.02	93.42
ta16_304	73.48	11.78	0.05	2.94	4.49	0.26	0.00	0.05	0.11	0.06	1.22	0.00	94.44
ta16_304	74.19	12.06	0.04	2.92	4.50	0.29	0.00	0.02	0.04	0.01	1.33	0.00	95.40
ta16_304	74.70	11.88	0.05	2.89	4.51	0.28	0.00	0.02	0.09	0.06	1.33	0.01	95.81
ta16_304	74.09	11.83	0.04	2.82	4.55	0.26	0.00	0.02	0.10	0.05	1.34	0.05	95.14
ta16_304	74.09	11.83	0.04	2.82	4.55	0.26	0.00	0.02	0.10	0.05	1.34	0.05	95.14
ta16_304	71.68	11.60	0.04	2.80	4.59	0.25	0.05	0.00	0.07	0.00	1.29	0.08	92.44
ta16_304	74.33	11.91	0.01	2.80	4.50	0.18	0.02	0.03	0.13	0.01	0.96	0.00	94.87
ta16_304	74.63	12.12	0.04	2.94	4.52	0.28	0.04	0.00	0.15	0.02	1.21	0.00	95.95
ta16_304	73.53	11.94	0.02	2.77	4.57	0.22	0.04	0.00	0.15	0.07	1.03	0.00	94.34
ta16_304	75.20	11.86	0.00	2.82	4.65	0.19	0.01	0.00	0.14	0.04	0.92	0.04	95.87

**Total Station Survey Data**

**Appendix D: Explanation of Mapped Contact Codes**

- |   |   |
|---|---|
| 2 = Within Unit 2                               | S4= Surge within Unit 4   |
| 2-3 = Unit 2-Unit 3 Contact                     | 4-4G = Basal ignimbrite of Unit 4-Fines-depleted Unit 4 Contact |
| 3 = Within Unit 3                               | 4G-4C = Fines-depleted unit 4- Clot-rich Unit 4 Contact         |
| S3 = Surge within Unit 3                        | 4CN-W= Welding break within Clot-rich Unit 4                    |
| 3-3T = Unit 3-Unit 3T Contact                   | T-A = Bandelier Tuff - Qoal or Qc Contact                       |
| S3-3T = Base of surge at Unit 3-Unit 3T Contact | TOPO = Ground Surface   |
| S3T = Surge within Unit 3T                      | BS = Block Slide  |
| 3T = Within Unit 3T                             | SCARP = Fault Scarp   |
| 3T-4 = Unit 3T-Unit 4 Contact                   | CD = Closed Depression  |
| S3T-4 = Base of surge at Unit 3T-Unit 4 Contact | FISSURE = Open Fissure  |

<u>Mapped Contact</u>	<u>Northing</u>	<u>Easting</u>	<u>Elevation</u>	<u>Mapped Contact</u>	<u>Northing</u>	<u>Easting</u>	<u>Elevation</u>
2-3	1759409.91	1614382.14	7304.61	2	1759219.99	1612584.38	7356.32
2-3	1759439.92	1614325.29	7309.26	2	1759201.74	1612395.65	7352.38
2-3	1759466.83	1614288.22	7312.59	2	1759194.88	1612311.72	7360.81
2-3	1759493.98	1614212.65	7317.59	3	1759205.19	1612241.46	7365.65
2-3	1759512.61	1614147.75	7321.86	S3	1760025.41	1612336.40	7472.40
2-3	1759530.85	1614046.25	7324.32	3-3T	1759751.64	1614334.01	7446.39
2-3	1759513.75	1614108.94	7322.63	3-3T	1759827.80	1613397.84	7476.51
2-3	1759548.39	1613979.13	7328.31	3-3T	1759844.39	1613353.29	7479.52
2-3	1759598.52	1613919.20	7331.50	3-3T	1759912.16	1613103.70	7483.70
2-3	1759667.03	1613861.31	7333.35	3-3T	1759936.06	1612763.36	7488.50
2-3	1759821.57	1613806.07	7340.85	3-3T	1759995.11	1612981.12	7482.86
2-3	1759698.58	1613708.12	7336.24	3-3T	1760442.14	1613482.89	7455.99
2-3	1759655.49	1613618.39	7335.14	3-3T	1760551.52	1613485.17	7458.97
2-3	1759641.14	1613467.77	7339.63	3-3T	1760390.57	1613689.16	7457.14
2-3	1759361.66	1613636.30	7329.72	3-3T	1759450.58	1613098.08	7481.48
2-3	1759274.08	1613052.66	7344.17	3-3T	1759434.79	1613064.34	7481.10
2-3	1759260.98	1612986.71	7351.25	3-3T	1759427.60	1613004.86	7483.12
2-3	1759248.03	1612856.96	7353.58	3-3T	1759415.53	1612967.21	7484.35
2-3	1759362.87	1613635.85	7329.82	3-3T	1759389.68	1612815.18	7486.43
2-3	1759346.91	1613574.09	7328.55	3-3T	1759313.87	1612456.00	7484.59
2-3	1759340.05	1613478.56	7333.94	3-3T	1759330.53	1612229.47	7486.02
2-3	1759336.93	1613498.31	7332.78	3-3T	1759313.33	1612166.00	7488.68
2-3	1759331.56	1613413.15	7337.45	3-3T	1759247.13	1612084.81	7486.96
2-3	1759342.63	1613446.32	7335.43	3-3T	1759248.67	1611980.35	7492.01
2-3	1759327.10	1613372.00	7336.91	3-3T	1759251.85	1611888.94	7495.41
2-3	1759328.06	1613344.17	7337.82	3-3T	1759287.78	1611662.41	7498.71
2-3	1759321.37	1613301.42	7337.82	3-3T	1759290.62	1611530.94	7496.24
2-3	1759301.66	1613204.10	7340.95	3-3T	1759280.96	1611368.79	7494.95
2-3	1759297.97	1613178.20	7343.17	3-3T	1759483.71	1613073.65	7477.90
2-3	1759287.16	1613140.08	7342.88	3-3T	1759933.57	1612747.56	7490.08
2-3	1759278.18	1613108.45	7343.60	3-3T	1759947.10	1612650.93	7488.28
2-3	1759275.72	1613045.57	7344.15	3-3T	1759970.02	1612535.54	7484.72
2-3	1759270.72	1613025.88	7346.07	3-3T	1760011.72	1612482.71	7485.09
2-3	1759258.58	1612960.96	7352.04	3-3T	1760048.33	1612417.67	7482.56
2-3	1759249.11	1612857.13	7353.77	3-3T	1760033.36	1612344.83	7479.96
2-3	1759239.29	1612801.79	7352.18	3-3T	1760003.88	1612178.58	7480.83
2-3	1759248.25	1612728.81	7354.78	3-3T	1760014.24	1612244.46	7478.65
2-3	1759236.10	1612644.74	7358.39	3-3T	1759308.39	1611105.00	7498.91

**Appendix D: Explanation of Mapped Contact Codes (cont.)**

<u>Mapped Contact</u>	<u>Northing</u>	<u>Easting</u>	<u>Elevation</u>	<u>Mapped Contact</u>	<u>Northing</u>	<u>Easting</u>	<u>Elevation</u>
2-3	1759217.70	1612506.27	7357.11	3-3T	1759333.06	1611056.37	7495.60
2-3	1759214.49	1612480.76	7358.14	3-3T	1759331.34	1611028.21	7494.88
2-3	1759209.61	1612449.13	7356.06	3-3T	1759374.93	1610949.79	7498.81
2-3	1759176.16	1612196.03	7364.17	3-3T	1759364.79	1610933.97	7496.25
2-3	1759169.08	1612180.58	7364.01	3-3T	1759365.10	1610802.06	7497.78
2-3	1759167.91	1612142.82	7367.45	3-3T	1759395.47	1610711.93	7496.23
2	1759321.89	1613304.81	7337.99	3-3T	1759410.94	1610657.70	7498.56
2	1759288.14	1613140.53	7343.06	3-3T	1759436.09	1610559.08	7496.02
2	1759307.31	1613240.76	7339.96	3-3T	1759431.58	1610523.50	7495.71
2	1759256.00	1612927.33	7350.86	3-3T	1759434.85	1610517.86	7496.10
3-3T	1759435.97	1610503.07	7498.46	S3-3T	1760283.35	1613843.88	7455.92
3-3T	1759443.83	1610479.47	7496.97	S3-3T	1760525.75	1613588.58	7452.49
3-3T	1759474.59	1610390.17	7495.99	S3-3T	1760576.85	1613561.07	7452.54
3-3T	1759498.95	1610346.19	7492.96	S3-3T	1759401.26	1612899.12	7484.69
3-3T	1759536.32	1610271.41	7490.00	S3-3T	1759403.09	1612747.71	7488.22
3-3T	1759579.39	1610204.79	7488.47	S3-3T	1759368.02	1612668.43	7487.85
3-3T	1759604.70	1610171.98	7489.57	S3-3T	1759357.07	1612599.85	7486.50
3-3T	1759624.31	1610112.04	7485.96	S3-3T	1759340.30	1612516.46	7484.22
3-3T	1759602.45	1610184.87	7491.41	S3-3T	1759322.35	1612427.32	7485.24
3-3T	1759692.78	1609774.06	7477.49	S3-3T	1759340.09	1612325.09	7486.63
3-3T	1759728.14	1609657.62	7475.32	S3-3T	1759281.73	1612014.48	7490.20
3-3T	1760010.11	1612122.03	7483.86	S3-3T	1759288.74	1611714.66	7497.71
3-3T	1760038.69	1612030.86	7487.78	S3-3T	1760025.99	1612902.45	7483.24
3-3T	1760049.34	1611964.72	7483.19	S3-3T	1760035.53	1612877.58	7482.80
3-3T	1760073.75	1611825.13	7484.07	S3-3T	1759386.86	1610867.88	7496.54
3-3T	1760085.80	1611721.12	7479.98	S3-3T	1759648.16	1610028.21	7479.78
3-3T	1760064.35	1611609.68	7480.69	S3-3T	1759655.35	1609988.83	7479.31
3-3T	1760064.52	1611609.73	7480.68	3T	1759538.73	1610372.37	7529.42
3-3T	1760064.95	1611485.47	7481.77	3T	1759559.69	1610339.92	7530.09
3-3T	1759735.14	1609635.59	7472.97	3T	1759622.50	1610225.55	7523.70
3-3T	1759715.24	1609045.53	7453.39	3T	1759718.42	1610006.56	7523.75
3-3T	1759716.99	1609243.90	7456.41	3T	1760227.53	1611591.92	7524.90
S3-3T	1760239.73	1613862.73	7456.23	3T	1759905.00	1611624.07	7518.95
S3-3T	1760181.73	1613890.48	7455.37	3T	1760167.71	1608465.11	7521.60
S3-3T	1760068.68	1613906.36	7458.60	3T	1760183.29	1608446.91	7521.57
S3-3T	1760030.22	1613921.05	7459.33	3T	1760054.98	1608571.14	7523.57
S3-3T	1759940.41	1613987.64	7460.75	3T	1759946.49	1610983.48	7527.67
S3-3T	1759907.33	1614011.65	7461.50	3T	1759912.37	1608417.70	7528.88
S3-3T	1759839.99	1614058.01	7465.83	3T	1759698.36	1608605.85	7528.38
S3-3T	1759815.51	1614074.98	7463.10	3T	1759666.09	1608704.35	7525.24
S3-3T	1759776.65	1614115.88	7462.07	S3T	1760035.08	1612898.25	7487.13
S3-3T	1759768.80	1614161.08	7461.60	S3T	1759501.54	1610366.79	7505.11
S3-3T	1759756.32	1614264.69	7453.91	3T-4	1760313.66	1613913.94	7476.84
S3-3T	1759761.58	1614635.84	7424.81	3T-4	1760496.82	1613658.98	7478.40
S3-3T	1759753.51	1614705.64	7421.84	3T-4	1760564.49	1613639.91	7474.97
S3-3T	1759944.31	1613489.52	7478.97	3T-4	1760615.25	1613579.43	7470.18
S3-3T	1759848.43	1613476.10	7477.44	3T-4	1760505.78	1613420.56	7483.45
S3-3T	1759836.20	1613462.90	7473.78	3T-4	1760419.01	1613389.35	7484.69
S3-3T	1759897.84	1613181.04	7483.86	3T-4	1759523.53	1612793.15	7514.46
S3-3T	1759928.69	1613071.46	7482.67	3T-4	1759525.72	1612828.51	7511.92
S3-3T	1760018.01	1612957.79	7487.16	3T-4	1759536.33	1612702.74	7515.01

Appendix D: Explanation of Mapped Contact Codes (cont.)

<u>Mapped Contact</u>	<u>Northing</u>	<u>Easting</u>	<u>Elevation</u>	<u>Mapped Contact</u>	<u>Northing</u>	<u>Easting</u>	<u>Elevation</u>
S3-3T	1759942.23	1613488.64	7479.30	3T-4	1759440.42	1612726.01	7511.17
S3-3T	1760001.58	1613492.46	7479.04	3T-4	1759415.57	1612670.98	7511.51
S3-3T	1760071.29	1613504.90	7477.88	3T-4	1759383.77	1612503.41	7509.28
S3-3T	1760335.60	1613457.18	7460.44	3T-4	1759384.33	1612399.21	7506.05
S3-3T	1760453.72	1613625.73	7452.84	3T-4	1759364.56	1612275.42	7508.20
S3-3T	1760359.80	1613754.80	7457.31	3T-4	1759372.59	1612194.08	7507.53
S3-3T	1760317.69	1613816.96	7455.21	3T-4	1759324.67	1612119.94	7508.42
3T-4	1759296.76	1611970.54	7514.91	3T-4	1760137.21	1612062.02	7519.51
3T-4	1759318.40	1611850.95	7518.80	3T-4	1760169.55	1611974.87	7519.63
3T-4	1759330.98	1611800.92	7519.84	3T-4	1760171.18	1611933.27	7517.30
3T-4	1759342.83	1611737.64	7520.93	3T-4	1760188.95	1611855.42	7519.74
3T-4	1759321.12	1611704.29	7521.84	3T-4	1760193.07	1611796.66	7519.89
3T-4	1759355.69	1611609.55	7523.43	3T-4	1760203.04	1611708.74	7522.23
3T-4	1759351.06	1611557.09	7524.36	3T-4	1760215.33	1611659.94	7523.35
3T-4	1759356.68	1611386.41	7526.24	3T-4	1759785.67	1609387.74	7499.83
3T-4	1759329.41	1611258.65	7529.41	3T-4	1759786.27	1609375.26	7499.03
3T-4	1759357.95	1611417.54	7523.79	3T-4	1759786.62	1609341.05	7501.32
3T-4	1759332.92	1611262.18	7528.13	3T-4	1759784.25	1609304.46	7502.06
3T-4	1759370.54	1611189.06	7529.51	3T-4	1759782.71	1609276.05	7501.99
3T-4	1759366.13	1611108.48	7530.54	3T-4	1759782.23	1609255.48	7501.57
3T-4	1759393.31	1611034.62	7530.93	3T-4	1759777.49	1609207.90	7502.64
3T-4	1759396.09	1611006.13	7526.69	3T-4	1759775.30	1609149.60	7503.68
3T-4	1759418.47	1610904.03	7526.18	3T-4	1759809.44	1609044.87	7508.08
3T-4	1759436.65	1610865.40	7527.97	3T-4	1759823.86	1609008.75	7510.18
3T-4	1759436.41	1610824.60	7530.06	3T-4	1759851.81	1608952.73	7513.83
3T-4	1759440.35	1610760.51	7528.24	3T-4	1759875.37	1608883.46	7523.82
3T-4	1759457.21	1610713.54	7529.28	3T-4	1760195.05	1611725.10	7520.45
3T-4	1759466.01	1610684.53	7530.27	3T-4	1760230.24	1611531.45	7522.42
3T-4	1759471.48	1610646.25	7529.49	3T-4	1760294.32	1611359.36	7520.19
3T-4	1759491.88	1610581.10	7530.72	3T-4	1760333.35	1611256.79	7526.88
3T-4	1759489.37	1610547.16	7530.43	3T-4	1760366.70	1611177.58	7531.84
3T-4	1759512.43	1610457.84	7529.89	3T-4	1760288.45	1611108.75	7528.64
3T-4	1759511.71	1610461.36	7530.80	3T-4	1760290.15	1610958.50	7530.00
3T-4	1759520.40	1610445.55	7531.42	3T-4	1760283.59	1610865.69	7529.32
3T-4	1759504.48	1610479.73	7530.71	3T-4	1760311.86	1610763.73	7531.18
3T-4	1759523.90	1610405.01	7530.39	3T-4	1759894.96	1611369.69	7523.06
3T-4	1759489.11	1610547.22	7529.71	3T-4	1759874.80	1611446.44	7522.21
3T-4	1759634.90	1610215.55	7524.31	3T-4	1759768.81	1609691.10	7516.87
3T-4	1759648.22	1610198.31	7525.35	3T-4	1760284.65	1610699.47	7528.79
3T-4	1759663.89	1610164.93	7524.30	3T-4	1760297.98	1610685.02	7530.56
3T-4	1759668.87	1610154.63	7525.54	3T-4	1760331.28	1610576.38	7529.06
3T-4	1759671.85	1610148.04	7526.01	3T-4	1760331.50	1610576.07	7529.08
3T-4	1759684.10	1610121.64	7526.11	3T-4	1760466.60	1610408.18	7526.81
3T-4	1759704.66	1610069.26	7523.85	3T-4	1760017.06	1610786.42	7523.07
3T-4	1759725.11	1609965.71	7521.88	3T-4	1760056.01	1610617.37	7521.11
3T-4	1759761.84	1609715.31	7517.88	3T-4	1760070.73	1610581.52	7520.54
3T-4	1759758.75	1609727.95	7518.92	3T-4	1760094.20	1610466.53	7520.29
3T-4	1759774.72	1609679.00	7517.37	3T-4	1759899.82	1608789.08	7525.72
3T-4	1759796.87	1609601.86	7504.23	3T-4	1759938.45	1608694.24	7531.66
3T-4	1759773.37	1609632.11	7506.68	3T-4	1759950.85	1608672.44	7529.93
3T-4	1759792.20	1609480.39	7497.86	3T-4	1759988.76	1608631.97	7526.17

Appendix D: Explanation of Mapped Contact Codes (cont.)

<u>Mapped Contact</u>	<u>Northing</u>	<u>Easting</u>	<u>Elevation</u>	<u>Mapped Contact</u>	<u>Northing</u>	<u>Easting</u>	<u>Elevation</u>
3T-4	1759786.75	1609426.54	7498.11	3T-4	1760151.30	1608482.75	7522.63
3T-4	1760103.82	1612319.58	7515.43	3T-4	1759882.82	1611635.09	7521.93
3T-4	1760110.58	1612371.12	7513.50	3T-4	1759875.61	1611541.33	7523.08
3T-4	1760102.77	1612167.53	7514.99	3T-4	1759843.78	1611773.82	7524.09
3T-4	1759893.24	1611313.41	7525.32	4G-4C	1759829.71	1609113.28	7540.45
3T-4	1759893.78	1611262.69	7524.63	4G-4C	1759834.95	1609085.34	7542.81
3T-4	1759739.85	1611967.49	7524.26	4G-4C	1759857.53	1609040.95	7545.82
3T-4	1760221.00	1608413.27	7518.55	4G-4C	1759862.58	1608988.12	7549.47
3T-4	1760247.44	1608391.39	7514.78	4G-4C	1759892.20	1608947.27	7554.10
3T-4	1760257.60	1608375.82	7512.94	4G-4C	1759907.85	1608907.78	7558.17
3T-4	1760280.24	1608342.56	7512.15	4G-4C	1759930.92	1608855.30	7563.59
3T-4	1760293.59	1608326.70	7510.94	4G-4C	1759951.96	1608782.78	7564.07
3T-4	1760052.93	1610618.99	7521.60	4G-4C	1760258.03	1611750.46	7538.87
3T-4	1760049.27	1610687.73	7521.11	4G-4C	1760274.15	1611702.67	7540.21
3T-4	1760011.78	1610837.38	7522.83	4G-4C	1760298.58	1611667.92	7544.23
3T-4	1759901.13	1611145.54	7525.56	4G-4C	1760300.85	1611645.57	7544.48
3T-4	1759882.26	1611278.28	7523.87	4G-4C	1760306.55	1611623.01	7543.51
3T-4	1759552.10	1612663.10	7512.90	4G-4C	1760319.72	1611577.90	7545.90
3T-4	1759568.99	1612612.59	7512.40	4G-4C	1760354.11	1611499.97	7547.46
3T-4	1759579.29	1612516.51	7512.92	4G-4C	1760367.42	1611479.62	7547.63
3T-4	1759602.22	1612458.73	7510.65	4G-4C	1760398.81	1611338.51	7545.12
3T-4	1759619.61	1612421.75	7510.20	4G-4C	1760380.67	1611287.61	7542.26
3T-4	1759642.92	1612350.34	7512.31	4G-4C	1760406.42	1611192.00	7545.02
3T-4	1759669.63	1612288.10	7515.81	4G-4C	1760405.06	1611155.77	7544.68
3T-4	1759687.48	1612244.43	7517.02	4G-4C	1759820.19	1609412.34	7517.98
3T-4	1759705.56	1612202.85	7519.56	4G-4C	1759820.42	1609467.68	7515.14
3T-4	1759731.78	1612124.81	7519.94	4G-4C	1759821.18	1609506.44	7514.15
3T-4	1759748.93	1612065.16	7520.12	4G-4C	1759814.40	1609586.38	7513.42
3T-4	1759767.61	1612026.70	7519.21	4G-4C	1759774.30	1609742.52	7534.35
3T-4	1759809.42	1611929.77	7517.86	4G-4C	1759783.66	1609713.04	7533.42
3T-4	1759801.67	1611895.33	7521.36	4G-4C	1760322.93	1610977.46	7537.88
3T-4	1759811.32	1608470.40	7530.42	4G-4C	1760348.51	1610754.75	7540.03
3T-4	1759782.94	1608488.67	7529.92	4G-4C	1760004.76	1610608.64	7530.82
3T-4	1759348.92	1611743.90	7521.23	4G-4C	1760598.87	1610431.29	7544.64
S3T-4	1760436.49	1613724.87	7478.81	4G-4C	1760646.68	1610459.66	7544.96
S3T-4	1760436.88	1613713.40	7479.08	4G-4C	1760582.10	1610404.59	7544.42
S3T-4	1760644.52	1613520.22	7473.31	4G-4C	1760710.21	1610486.15	7550.28
S3T-4	1759738.56	1609824.72	7519.91	4G-4C	1760558.09	1610388.46	7541.86
S3T-4	1759741.20	1609808.47	7520.40	4G-4C	1760513.87	1610361.69	7538.73
S3T-4	1759753.44	1609756.47	7520.51	4G-4C	1760678.90	1610505.30	7545.66
S3T-4	1759763.35	1609714.98	7519.00	4G-4C	1760618.69	1610490.63	7547.54
4-4G	1759789.31	1609366.39	7501.46	4G-4C	1760493.37	1610474.48	7542.37
4-4G	1759786.17	1609299.30	7503.52	4G-4C	1759850.51	1611218.45	7535.54
4-4G	1759783.74	1609275.89	7502.93	4G-4C	1759738.70	1611933.13	7534.30
4-4G	1759812.45	1609044.93	7509.30	4G-4C	1759748.54	1611880.75	7534.98
4G-4C	1759813.28	1609312.18	7523.59	4G-4C	1759762.26	1611859.70	7536.11
4G-4C	1759814.70	1609284.37	7523.21	4G-4C	1759834.48	1611662.45	7532.45
4G-4C	1759817.53	1609253.10	7525.93	4G-4C	1759848.00	1611523.17	7529.09
4G-4C	1759823.01	1609225.17	7528.00	4G-4C	1759846.01	1611410.12	7529.42
4G-4C	1759811.64	1609187.25	7532.15	4G-4C	1760251.35	1608470.42	7566.69
4G-4C	1759816.12	1609158.77	7535.01	4G-4C	1760265.68	1608463.60	7567.46

Appendix D: Explanation of Mapped Contact Codes (cont.)

<u>Mapped Contact</u>	<u>Northing</u>	<u>Easting</u>	<u>Elevation</u>	<u>Mapped Contact</u>	<u>Northing</u>	<u>Easting</u>	<u>Elevation</u>
4G-4C	1760322.00	1608400.38	7562.29	4CN-W	1759375.94	1611386.86	7546.71
4G-4C	1760362.18	1608361.44	7562.44	4CN-W	1759372.32	1611563.30	7535.60
4G-4C	1760367.79	1608345.93	7562.83	4CN-W	1759356.88	1611739.80	7525.11
4G-4C	1759771.12	1609795.96	7535.84	4CN-W	1759331.53	1611862.05	7529.52
4G-4C	1759757.71	1609844.29	7531.88	4CN-W	1759306.33	1611922.99	7522.64
4G-4C	1759742.31	1609996.56	7535.96	4CN-W	1759320.21	1612047.12	7519.48
4G-4C	1759735.25	1610022.73	7537.21	4CN-W	1759313.33	1612077.80	7515.97
4G-4C	1759731.87	1610069.11	7537.39	4CN-W	1759341.40	1612121.61	7517.45
4G-4C	1759696.95	1610148.68	7537.66	4CN-W	1759384.68	1612180.63	7516.63
4G-4C	1759625.31	1610272.01	7539.72	4CN-W	1759393.16	1612232.44	7516.87
4G-4C	1759574.07	1610372.05	7544.86	4CN-W	1759386.73	1612260.20	7519.05
4G-4C	1759550.53	1610408.16	7543.52	4CN-W	1759385.95	1612294.79	7517.78
4G-4C	1759473.97	1610729.89	7539.10	4CN-W	1759391.38	1612331.69	7514.49
4G-4C	1759459.09	1610839.66	7541.27	4CN-W	1759403.56	1612370.70	7518.73
4G-4C	1759455.68	1610911.69	7541.14	4CN-W	1759399.93	1612418.39	7518.34
4G-4C	1759433.94	1610988.37	7539.55	4CN-W	1759387.70	1612433.13	7515.92
4G-4C	1759416.55	1611019.90	7538.56	4CN-W	1759382.34	1612471.68	7515.48
4G-4C	1759397.17	1611078.53	7540.07	4CN-W	1759387.05	1612489.08	7522.03
4G-4C	1759395.63	1611109.86	7540.24	4CN-W	1759415.51	1612522.24	7522.01
4G-4C	1759973.08	1610691.46	7531.78	4CN-W	1759416.95	1612546.27	7519.95
4G-4C	1759964.62	1610747.98	7530.61	4CN-W	1759446.64	1612661.75	7522.23
4G-4C	1760009.67	1610604.79	7530.24	4CN-W	1759466.87	1612690.73	7526.86
4G-4C	1760022.12	1610546.65	7529.06	S4	1760549.81	1613314.42	7511.98
4G-4C	1760055.91	1610470.75	7526.39	S4	1760531.34	1613307.82	7512.57
4G-4C	1759938.21	1610903.08	7534.72	S4	1760526.53	1613305.42	7512.13
4G-4C	1759876.42	1611116.70	7532.32	S4	1760481.13	1613277.87	7514.63
4G-4C	1759849.72	1611160.20	7535.30	S4	1760415.09	1613238.93	7517.18
4G-4C	1759767.61	1611849.91	7536.14	S4	1760496.87	1613931.71	7514.47
4G-4C	1759358.40	1611328.99	7536.44	S4	1760524.63	1613906.01	7514.50
4G-4C	1759374.89	1611387.48	7536.15	S4	1760502.33	1613927.17	7514.06
4G-4C	1760278.51	1608442.29	7564.93	S4	1760507.47	1613921.65	7513.59
4CN-W	1759696.05	1612088.61	7533.14	S4	1760519.24	1613911.34	7514.11
4CN-W	1759481.45	1612774.81	7523.90	S4	1760523.67	1613907.01	7514.43
4CN-W	1759476.15	1612772.30	7525.85	S4	1760530.35	1613900.14	7513.45
4CN-W	1759475.95	1612751.32	7525.44	S4	1760544.35	1613886.91	7513.91
4CN-W	1759477.85	1612732.17	7527.53	S4	1760545.70	1613884.88	7513.40
4CN-W	1759491.40	1612753.09	7527.15	S4	1760556.44	1613875.14	7514.29
4CN-W	1759492.10	1612727.89	7529.19	S4	1760572.27	1613861.44	7514.95
4CN-W	1759511.07	1612590.54	7530.41	S4	1760585.51	1613848.71	7515.26
4CN-W	1759521.84	1612525.74	7531.58	S4	1760599.40	1613835.41	7514.87
4CN-W	1759551.44	1612423.94	7529.61	S4	1760600.54	1613833.48	7514.40
4CN-W	1759572.72	1612377.91	7529.83	S4	1760604.18	1613830.73	7515.02
4CN-W	1759593.42	1612324.41	7531.01	S4	1760610.55	1613824.78	7515.10
4CN-W	1759666.85	1612156.96	7536.26	S4	1760621.90	1613814.61	7515.69
4CN-W	1759692.93	1612047.35	7538.91	S4	1760625.23	1613810.65	7515.46
4CN-W	1759704.57	1611985.45	7540.02	S4	1759489.62	1610548.92	7530.97
4CN-W	1759734.40	1611910.88	7540.66	S4	1759526.30	1610402.78	7532.18
4CN-W	1759371.48	1611338.88	7549.34	S4	1759763.25	1609715.00	7518.90
S4	1759760.91	1609726.67	7519.76	T-A	1760670.33	1608112.53	7557.93
T-A	1759432.95	1611363.18	7559.79	T-A	1760633.12	1608121.19	7557.67
T-A	1759442.36	1611335.94	7560.43	T-A	1760593.90	1608138.47	7557.11

Appendix D: Explanation of Mapped Contact Codes (cont.)

<u>Mapped Contact</u>	<u>Northing</u>	<u>Easting</u>	<u>Elevation</u>	<u>Mapped Contact</u>	<u>Northing</u>	<u>Easting</u>	<u>Elevation</u>
T-A	1759469.63	1611317.74	7561.41	T-A	1760559.90	1608296.85	7569.44
T-A	1759480.27	1610902.41	7566.27	T-A	1760547.58	1608176.44	7555.75
T-A	1759375.39	1609551.06	7577.69	T-A	1760506.52	1608276.27	7558.53
T-A	1760258.64	1610422.83	7530.94	T-A	1760514.73	1608214.22	7553.79
T-A	1760224.06	1610412.86	7523.00	T-A	1760496.42	1608253.16	7554.90
T-A	1760204.84	1610394.02	7522.61	TOPO	1759849.22	1609341.59	7549.77
T-A	1760181.83	1610419.52	7518.24	TOPO	1759857.68	1609391.70	7551.02
T-A	1760186.96	1610516.69	7514.86	TOPO	1759847.41	1609413.24	7549.40
T-A	1760231.32	1610536.19	7516.10	TOPO	1759850.93	1609455.31	7551.48
T-A	1760287.43	1610525.28	7517.93	TOPO	1759843.52	1609493.30	7549.63
T-A	1760305.74	1610480.42	7520.79	TOPO	1759845.30	1609517.83	7550.15
T-A	1761992.78	1611194.04	7590.35	TOPO	1759855.75	1609531.73	7551.81
T-A	1762006.61	1611193.23	7590.59	TOPO	1759840.28	1609554.91	7548.40
T-A	1761882.54	1611197.37	7587.12	TOPO	1759851.12	1609583.23	7551.19
T-A	1762010.76	1611199.98	7591.30	TOPO	1759838.10	1609623.20	7549.69
T-A	1762077.09	1611204.68	7592.48	TOPO	1759826.71	1609635.04	7551.84
T-A	1762119.12	1611234.10	7594.27	TOPO	1759802.84	1609659.89	7555.76
T-A	1762079.80	1611204.48	7592.51	TOPO	1759810.69	1609679.64	7554.90
T-A	1760133.38	1608658.35	7591.43	TOPO	1759806.95	1609706.63	7557.91
T-A	1760165.88	1608623.49	7591.48	TOPO	1759791.82	1609713.85	7560.73
T-A	1760200.65	1608563.86	7591.65	TOPO	1759789.45	1609744.56	7566.96
T-A	1760242.37	1608568.98	7592.49	TOPO	1759800.78	1609752.62	7565.58
T-A	1760271.98	1608556.79	7592.26	TOPO	1759795.07	1609771.55	7567.00
T-A	1760291.05	1608536.62	7591.69	TOPO	1759789.64	1609781.11	7568.85
T-A	1760307.97	1608477.56	7587.35	TOPO	1759782.28	1609801.08	7566.96
T-A	1760351.95	1608459.42	7586.14	TOPO	1759767.28	1609835.10	7565.06
T-A	1760374.56	1608436.81	7583.68	TOPO	1759785.35	1609863.13	7565.26
T-A	1760410.11	1608446.23	7586.29	TOPO	1759797.46	1609900.44	7567.24
T-A	1760463.65	1608402.76	7585.71	TOPO	1759791.04	1609926.77	7570.48
T-A	1760488.32	1608383.61	7584.94	TOPO	1759781.67	1609933.82	7570.07
T-A	1760540.94	1608373.39	7583.32	TOPO	1759765.59	1609971.08	7570.18
T-A	1760555.25	1608393.00	7586.46	TOPO	1759758.24	1609980.04	7569.68
T-A	1760561.68	1608413.14	7588.85	TOPO	1759739.78	1610064.51	7569.09
T-A	1761028.52	1608484.73	7597.20	TOPO	1759724.63	1610134.87	7569.07
T-A	1761009.76	1608452.38	7594.92	TOPO	1759854.41	1609353.09	7550.31
T-A	1760975.45	1608454.42	7595.88	TOPO	1759850.06	1609316.17	7552.10
T-A	1760918.77	1608457.46	7596.18	TOPO	1759860.85	1609271.93	7554.36
T-A	1760874.54	1608451.33	7595.28	TOPO	1759883.47	1609280.34	7558.43
T-A	1760590.97	1608377.41	7586.24	TOPO	1759892.38	1609228.97	7562.17
T-A	1760819.59	1608460.50	7595.06	TOPO	1759889.01	1609182.96	7562.25
T-A	1760790.18	1608464.22	7595.71	TOPO	1759893.78	1609140.27	7563.88
T-A	1760769.01	1608418.47	7593.25	TOPO	1759883.44	1609104.55	7561.25
T-A	1760584.58	1608322.14	7578.34	TOPO	1759890.38	1609064.58	7562.48
T-A	1760758.62	1608125.23	7563.06	TOPO	1759903.94	1609025.35	7566.47
T-A	1760719.18	1608110.86	7560.47	TOPO	1759918.43	1608992.06	7568.76
TOPO	1759932.21	1608960.55	7571.60	CD	1761392.49	1610771.73	7579.89
TOPO	1759929.64	1608934.63	7572.19	CD	1761390.77	1610765.51	7580.14
TOPO	1759927.99	1608892.68	7574.10	CD	1761392.45	1610771.74	7579.88
TOPO	1759943.16	1608843.83	7572.75	BS	1759380.79	1611678.30	7550.48
TOPO	1759956.21	1608806.31	7580.03	BS	1759397.36	1611224.55	7561.94
TOPO	1759989.77	1608718.61	7585.74	BS	1759413.61	1611198.68	7562.86

2025 RELEASE UNDER E.O. 14176

Appendix D: Explanation of Mapped Contact Codes (cont.)

<u>Mapped Contact</u>	<u>Northing</u>	<u>Easting</u>	<u>Elevation</u>
BS	1759505.48	1610715.16	7564.87
BS	1759508.43	1610661.27	7565.52
FISSURE	1761870.42	1611208.75	7586.88
FISSURE	1761894.08	1611209.82	7586.56
FISSURE	1761592.34	1611303.76	7589.24
FISSURE	1761922.76	1611149.50	7587.50
FISSURE	1761918.39	1611156.62	7587.18
FISSURE	1761903.01	1611147.18	7587.05
FISSURE	1762234.65	1611281.79	7594.12
FISSURE	1762232.14	1611277.40	7594.31
FISSURE	1762237.02	1611276.72	7594.61
FISSURE	1762238.52	1611281.39	7594.15
SCARP	1761127.95	1608374.07	7580.35
SCARP	1761096.16	1608379.56	7582.18
SCARP	1761040.02	1608384.97	7584.35
SCARP	1760972.48	1608379.84	7585.52
SCARP	1760930.06	1608378.62	7586.20
SCARP	1760871.96	1608400.98	7586.47
SCARP	1760815.23	1608397.71	7589.09
SCARP	1760773.76	1608400.80	7590.85